COPPE
Instituto Alberto Luiz Coimbra de Pós-Graduação e Pesquisa de Engenharia
UFRJ

DEVELOPMENT OF A MESO-SCALE FLOW LOOP FACILITY TO INVESTIGATE SCALE DEPOSITION PHENOMENA IN PIPES

Victor Manuel Palma Contreras

Tese de Doutorado apresentada ao Programa de Pós-graduação em Engenharia Oceânica, COPPE, da Universidade Federal do Rio de Janeiro, como parte dos requisitos necessários à obtenção do título de Doutor em Engenharia Oceânica.

Orientador: Theodoro Antoun Netto

Rio de Janeiro
Outubro de 2019

DEVELOPMENT OF A MESO-SCALE FLOW LOOP FACILITY TO INVESTIGATE SCALE DEPOSITION PHENOMENA IN PIPES

Victor Manuel Palma Contreras

TESE SUBMETIDA AO CORPO DOCENTE DO INSTITUTO ALBERTO LUIZ COIMBRA DE PÓS-GRADUAÇÃO E PESQUISA DE ENGENHARIA (COPPE) DA UNIVERSIDADE FEDERAL DO RIO DE JANEIRO COMO PARTE DOS REQUISITOS NECESSÁRIOS PARA A OBTENÇÃO DO GRAU DE DOUTOR EM CIÊNCIAS EM ENGENHARIA OCEÂNICA.

Examinada por:

Prof. Theodoro Antoun Netto, Ph.D.

Prof. Rafael Mengotti Charin, D.Sc.

Prof. Luciana Loureiro da Silva Monteiro, D.Sc.

Prof. Ilson Paranhos Pasqualino, D.Sc.

Prof. Marcelo Igor Lourenço de Souza , D.Sc.

RIO DE JANEIRO, RJ – BRASIL
OUTUBRO DE 2019

Palma Contreras, Victor Manuel

Development of a meso-scale flow loop facility to investigate scale deposition phenomena in pipes/Victor Manuel Palma Contreras. – Rio de Janeiro: UFRJ/COPPE, 2019.

XVIII, 125 p.: il.; 29, 7cm.

Orientador: Theodoro Antoun Netto

Tese (doutorado) – UFRJ/COPPE/Programa de Engenharia Oceânica, 2019.

Referências Bibliográficas: p. 106 – 117.

1. Scale build-up. 2. Experimental flow loop. 3. IR analysis. 4. Prediction models. I. Antoun Netto, Theodoro. II. Universidade Federal do Rio de Janeiro, COPPE, Programa de Engenharia Oceânica. III. Título.

Acknowledges

La cantidad de personas e instituciones a las que tengo que agradecer es directamente proporsional a las horas invertidas para el aprimoramiento y realizacion de estos experimentos, pero resumiendo me gustaría agradecer al programa PRH-03 de Petrobras por el soporte económico. Al pueblo Brasilero del cual me siento como uno más y del cual estaré por siempre agradecido, cabe en mi corazón un gran espacio para todas las personas que conocí durante estos ocho años de los cuales tuve la fortuna de vivir procesos históricos indelebles, tanto para bien como para mal.

Agradecer al estimado profesor Theodoro por su apoyo en estos años de doctorado, jamás olvidaré sus consejos. Agradecer a los profesores que conforman la banca por su interés en revisar mi tesis.

Al excelente personal técnico del laboratorio de tecnología submarina, sin ellos no sería posible alcanzar las metas y premios que el laboratorio ha ganado al cumplir treinta años de existencia, sería un desconsiderado si no los nombro: A mi estimado amigo Wulf, aleman-mozambicano radicado en Brazil, por su ayuda y soporte técnico en la elaboracion del sistema electrónico y eléctrico del sistema experimental.A Renan y Latino por la ayuda en la construción del loop, por fin Renan podrá descansar de mi.A Luciano Crespo por la ayuda y consejos en la programación del sistema Labview. A Marcelão, Marcelino e don Elias por la ayuda en las panes emergenciales.A las queridas secretarias del laboratorio Dani y Cris, por el soporte en compras e impresiones.A Lucianita por estar siempre disponible para auxiliarme con mis problemas burocráticos y de matricula atrazada . Al estimado José Carlos por el café de todos los dias.

A los compañeros del laboratorio por los tips y pequeños consejos ; Katherin, Eldrede y Paulo.

A los amigos que conocí acá y a aquellos que siguen junto a mí desde chile y el extranjero, que pueden ser considerados mi segunda familia, una familia global, la gente que me aconsejó y me ayudó en los momentos amargos,ellos saben quienes son, en especial queria agradecer a Victoria Santos por el empújón para empezar la larga jornada de DsC. a mi compay Ernesto Molinas por los tips de programación, las caronas y por soportarme.A mi cubana favorita Anilé Ossorio por su compañía y amistad. A Vicente Magalhaes por la ayuda en los últimos años.A los amigos del

bloco Besame mucho por hacer mas llevadera la vida de un latino en Rio de Janeiro en especial a Bianca por su compañia y cariño en estos momentos tan tensos.

Por ultimo a mi amada familia, mi madre Silvia por su cariño y apoyo , a mi padre por alentarme a continuar mi doctorado. A mi madrina Margarita por siempre preguntar por mi estado y enviarme fotos del oceano Pacífico, al Toño y la Yaya por preparar esos ajies y platos siempre que vuelvo a Chile.A mis hermanas Andrea, Monserrat y Millaray por alegrarme la vida. A mi amado sobrino Alén por mostrarme que en lo simple está la felicidad.A mis abuelos que me aconsejan en sueños.

Dedicado a mi madre y a mi
padre..."Yeah I'm a lucky man
To count on both hands
The ones I love
Some folks just have one
Yeah others they got none"
Just Breathe-Pearl Jam.

Resumo da Tese apresentada à COPPE/UFRJ como parte dos requisitos necessários para a obtenção do grau de Doutor em Ciências (D.Sc.)

DESENVOLVIMENTO DE UMA INSTALAÇÃO DE LOOP DE FLUXO EM ESCALA MESO PARA INVESTIGAR FENÔMENOS DE DEPOSIÇÃO DE INCRUSTAÇÕES EM TUBULAÇÕES

Victor Manuel Palma Contreras

Outubro/2019

Orientador: Theodoro Antoun Netto

Programa: Engenharia Oceânica

Fenômenos de incrustação inorganica ou "*scale*" podem ser encontrados em vários sistemas de produção de petróleo e gás, incluindo oleodutos onshore e offshore, equipamentos complexos como válvulas de segurança, árvores de Natal e outros tipos de equipamentos de produção submarinos. A fim de estudar o mecanismo de deposição de incrustações em tubos, um loop experimental foi desenvolvido para gerar deposição de sais inorgânicos em um tubo de 27,3 mm de diâmetro. A água pré-aquecida contendo íons de cálcio e carbonato vem de um tanque de mistura que passa por uma seção aquecida do tubo para acelerar a precipitação e a deposição na parede interna do tubo. Uma seção de teste foi projetada para ser removida sem interromper o restante do experimento para estudar o aumento da escala ao longo do tempo. O sistema experimental permite realizar diversas experiências com diferentes geometrias, materiais tratados com revestimentos, inibidores mecânicos (indutores de campo magnético) e químicos. Experimentos controlados e seus resultados, comparando imagens de infravermelho e incrustação, são apresentados neste trabalho. Um algoritmo de previsão de escala foi desenvolvido usando diferentes modelos analíticos disponíveis na literatura. Esses modelos analíticos são avaliados à luz dos resultados experimentais.

Abstract of Thesis presented to COPPE/UFRJ as a partial fulfillment of the requirements for the degree of Doctor of Science (D.Sc.)

DEVELOPMENT OF A MESO-SCALE FLOW LOOP FACILITY TO INVESTIGATE SCALE DEPOSITION PHENOMENA IN PIPES

Victor Manuel Palma Contreras

October/2019

Advisor: Theodoro Antoun Netto

Department: Ocean Engineering

Scale deposition phenomena can be encountered in various oil and gas production systems, including onshore and offshore pipelines, complex equipment like safety valves, Christmas trees and other subsea production equipment. In order to study the mechanism of scale deposition in pipes, an experimental loop was developed to generate inorganic salt deposition in a one-inch diameter pipe.Pre-heated water containing calcium and carbonate ions comes from a mixture tank and passes through a heated section of the pipe to accelerate scale precipitation and deposition to the pipe inner wall. A test section was designed to be removed to study the scale build-up over time. The experimental system allows conducting diverse experiments with different geometries, surface-treated materials, mechanical (magnetic field inductors) and chemical scale inhibitors. Controlled experiments and their results, comparing IR images and scale build-up are presented in this work. A scale prediction algorithm was developed using different analytical models available in the literature. These analytical models are assessed in light of experimental results.

Contents

List of Figures

List of Tables

Nomenclature

β mass transfer coefficient m/s

λ_f heat conductivity of the test tube

ρ_f Scale formation density(kg/m^3)

ρ_p particle density kg/m^3

$\triangle c_p$ difference of heat capacity of calcite

$\triangle H_o$ Solution enthalpy stated as -81 3

$\triangle T$ Temperature gradient

$\triangle_C$ Total concentration difference difference(kg/m^3)

A surface area(m^2)

$ANNs$ Artificial Neural Networks

API American Petroleum Institute

C_F Bulk concentration Kg/m^3

C_p particle concentration ($kg/m3$)

c_p Heat transfer coefficient

C_s Saturation concentration(kg/m^3)

$CAPEX$ Capital Parameters Expenditure

CFD Computer Fluid Dynamics

D_i Internal pipeline diameter in meters

d_p particle hydrodynamic diameter

D_{coef} Diffusion coefficient

dm/dt Mass rate per unit time(kg/s)

dm_d/dt Deposited mass rate per unit time(kg/s)

dm_r/dt Removed mass rate per unit time(kg/s)

f Friction factor

$FPSO$ Floating Production Storage and Offloading

g Gravitational acceleration (m^2/s)

h heat transfer coefficient

$ICDs$ Inflow Control Devices

$ICVs$ Inflow Control Valves

IR Infra Red

K heat conductivity of pipe material(W/mk)

K^{eq} Chateliers equilibrium constant

K_B Boltzmann constant

K_d transport coefficient

K_r Surface reaction rate constant m^4kg/s

K_{spb} solubility product of $CaCO_3$

$K_{spb}A$ solubility product of Aragonite $CaCO_3$ crystals

$K_{spb}C$ solubility product of Calcite $CaCO_3$ crystals

$K_{spb}V$ solubility product of Varetite $CaCO_3$ crystals

N_0 particle deposition rate

Nu Nusselt number

$OPEX$ Operational Parameters Expenditure

P Crystaline action force

R Molar gas constant

R_f Fouling resistance m^2K/W

R_f Fouling resistance

R_o heat resistance without fouling m^2K/W

R_{Tot} total heat resistance of the system m^2K/W

Re Reynolds number

S_p Particle stopping distance

Sb Super saturation degree

Sc Schmidt number

Sh Sherwood number

SI Solubility Index

SP Sticking probability

SR Saturation Ratio

t_e lifetime of the near wall eddies

T_f surface temperature of the scaling layer (K)

t_p particle relaxation time

t_s^+ adimentional particle deposition time

T_{Bulk} Bulk temperature

T_{bulk} Bulk temperature $/circC$

T_{wall} Wall temperature $/circC$

U overall heat transfer coefficient(W/m^2K)

V_d particle deposion rate (m/s)

V_{avg} Flow velocity lt/min

$X-tree$ Crhistmass Tree

X_f Scale thickness(m)

Chapter 1

Introduction

One of the most severe operational hazards of offshore pipelines ans subsea production is the risk associated with the transportation of multi-phase fluids.Several complex equipment and structures operate in subsea systems ,such as risers, umbilical systems, Christmas trees, manifolds, well valves, among these, valve applications and tubular are strongly affected by solid deposition problems influencing the oil and gas production [10].In some cases, like production tubing, inflow control devices(ICDs) and inflow control valves(ICVs) Choke and down hole valves, the selection of appropriates down hole materials its critical to their operation over the well life. Among many criteria for selection, strength and corrosion resistance are primary considerations [11]. Sudden changes in temperature and pressure promote scale forming, which can even hamper the operation of actuators in the valves generating operational risks in emergency cases[12].The practice of identifying, quantifying, and mitigating all the flow risks associated with offshore pipelines and sub-sea systems is called flow assurance[8].

Scale as a result of crystallization and precipitation of minerals present in water have been one of the most common topics in flow assurance (according to the first technical report of the API[13]).This phenomena interferes with operational parameters (OPEX), resulting in additional costs on treatment, protection and removal, inhibition or reduction of the scale build up.These problems result in a loss of profitability that makes that unconventional wells (e.g. wells as the pre-salt layer, Canadian tar sands, ultra-heavy Orinoco oil in Venezuela and Angolan pre-salt basin) more challenging to exploited. Deposition can be minimized by chemical inhibitors or cleaning by acidification. Proper water sampling, handling, and analysis are very critical for flow assurance risk assessment[8].

In offshore production pipelines, there usually exists water together with oil and gas.Water is produced from the reservoir and, because water is an excellent solvent, it dissolve plenty of chemical compounds and gases inside the formation. Water also includes suspended solids and impurities. Inside the reservoir formation,

water and the chemical compounds are usually in equilibrium.When water, oil, and gas are flowing simultaneously inside the pipeline, there are quite a few potential problems that can occur: water and hydrocarbon fluids can form hydrate and block the pipeline; wax and asphalt can deposit on the wall and may eventually block the pipeline, corrosion may occur; with pressure and temperature changes along the pipeline and/or with incompatible water mixing, severe slugging may form inside the pipeline and cause operational problems to downstream processing facilities, and finally scales may form and deposit inside the pipeline and restrict the flow. Another aspect where operators found scale build up phenomena are during injection of water flooding operations.Precipitation of inorganic scale is a major issue in injecting brines with a high concentration of divalent ions(Mg^{2+}, Ca^{2+}).

Most scale deposits found in oil fields form by direct precipitation from the water present in a reservoir rock, or as a result of produced water becoming oversaturated with scale components when two incompatible waters meet down-hole[14].When water and gases flow together in the pipeline, at certain pressure and temperature conditions, they would form hydrate which can potentially block the pipeline.The challenge that engineers will face is, thus, how to design the pipeline and subsea system to assure to engineers that multi-phase fluids will be safely and economically transported from the bottom wells all the way to the processing plant.

Figure 1.1: Scale formation in actual pipe cross-section, Source: Subsea Technology Laboratory, COPPE / UFRJ.

Scale Removal

Once scales are formed in the production facilities, they can be removed either by mechanical means, such as pigging, or by dissolving using chemicals. When brush or scraper pigs are run through the pipeline, they can mechanically remove some of the scale deposits on the pipe wall. But if the deposits, which may contain scales, waxes, and/or asphaltene, are too hard, pigging may not be very effective. Acids can react with scales and dissolve scale deposits on the pipe wall. For calcium carbonate scales, either hydrochloric acid or chelating agents can be used. Calcium sulfate scale is not soluble to hydrochloric acid. Inorganic converters, like ammonium carbonate ($(NH_4)2CO_3$), can be used to convert it into calcium carbonate which can then be dissolved using hydrochloric acid. Since it is quite possible that hydrocarbons can deposit on the surface of the scales and hydrocarbons can interfere with the acid reaction with the scales, it is necessary to pre-wash the scales using hydrocarbon solvents. Furthermore, to keep the acid from dissolving the pipe wall, a corrosive inhibitor is also necessary to be added to the acid. Magnetic field treatment[15] have also been studied during the recent decades as a more cost-effective alternative and environmentally friendly technique. The use of coatings with materials that inhibit scale formation can also be a cost-effective and environmentally friendly alternative for fighting against scale[16].Another way to prevent scale depositions is using prediction models [17],[18],[19]. A hybrid combination of the previous described processes could be an improved solution.

Aim of this thesis

The complexity of multiphase flows in sub sea equipment and pipelines, along with the different nature and maturity of the fields, require a successful experimental methodology to pretest the possible candidates to control and inhibition of scale deposits in new production systems. In addition, it is important to generate models, measure, detect and study coatings that can reduce and prevent scale formation in critical sections.

To do the above, several and diverse tests must be performed. To this end, an experimental system must be constructed that can guarantee repeatability and versatility of each experiment performed.

This work aims to create and validate a mesoscale flow loop experimental facility to improve the understanding of scale deposition phenomena. To understood the acquired data, several techniques were used; from a classical semi intrusive approach using fouling resistance, pressure drop, and fluid characterization, passing through the non intrusive IR technique to detect and measure scale thickness to avoid semi intrusive tests. Finally, direct tests as weight measurement of a coupon section were

also performed to follow scale build-up inside the pipeline.

This work is separated in several sections:

- Chapter two presents the bibliography related to the scale problems, main precipitation problems in sub-sea systems, references in the area, and most important work within the experimental scale study.
- Chapter three presents the main analytical models, developed in Matlab, used to predict the scale build-up formation in the loop system.
- Chapter four presents the experimental loop, the main advances and drawbacks during the mesoscale system development.
- Chapter five presents a case study to evaluate the final loop configuration; the case-study was compared with the models developed in chapter four. Besides, a study of scale detection technique using an infrared camera is presented.
- Chapter six presents conclusions and future works.

The installation was designed and built in the Subsea Technology Laboratory in COPPE / UFRJ.

Other objectives include:

- Generate a deposition process using controllable values such as flow, pH, concentration and temperature.
- Test the IR technique to detect scale build-up in real-time during the experiment.
- Compare results with different analytical uni-dimensional models integrated into an iteration made in Matlab.

Chapter 2

Bibliography

2.1 Scale formation Process

Scale is as vast as the limitations that exist for its total understanding.The studies on the subject are usually linked to the type of equipment and fluid analyzed. Many of the water properties, like dissolved gases, suspended solids, and pH values would change with time and would change with pressure and temperature. Both lab and in-situ analysis are necessary to get accurate water characteristics. At oil platforms there are mainly problems with salt deposition, such as barium sulfate, calcium and magnesium carbonates. While sulfates are deposited due to mixture of sulfate-rich sea water, with water present inside reservoirs, rich in barium ions and strontium, carbonates are precipitate due to the change in saturation, which is very sensitive to variations in temperature, pressure and pH. Water based drilling fluid (mud) typically contain 65% wt. ,brine/water 30% wt. barite salts. The remaining 5% wt. are stabilizing additives.

The main ions in water that are of importance for flow assurance are listed below. The main negative charged ions (anions) in water are:

- Chloride
- Sulfide
- Sulfate
- Bromide
- Bicarbonate
- Carbonate

And the main positive charged ions (cations) in water are:

- Sodium
- Potassium
- Calcium
- Magnesium
- Strontium
- Barium
- Iron
- Aluminum

Cations and anions can combine and form different substances. When pressure and temperature change, the solubility of each ion will change.The excessive ions will precipitate from water and form solids, like scales.Bai[20] classifies the main types of mineral deposition origin in offshore facilities, as follows:

2.1.1 Calcium sulphate

Calcium sulphate precipitation is given by the following reaction:

$$Ca^{2+} + SO_4^{-2} \rightarrow CaSO_4 \tag{2.1}$$

This type of inlay can happen in different forms. Gypsum ($CaSO_4$, $2H_2O$) is the most common fouling in oil fields. It is associated with low temperature. $CaSO_4$ can be formed warm temperatures. Typically, it can precipitate about $37.7°C$ as opposed to gypsite due its low solubility. The gypsum can be found at a temperature above $100°C$. During the production life, Gipsy will tend to dehydrate and form anhydride. A recurring mechanism that induces the precipitation of gypsum in oil fields is the reduction of pressure (eg at the well head). The solubility increases with increasing pressure, because when the scale is diluted in water, the total volume of the system decreases.

2.1.2 Barium Sulphate

This type of scale is extremely insoluble and practically impossible to remove chemically. Barium sulfate is generated even at low sulfate and barium concentrations, it is formed through the following chemical formula:

$$Ba^{2+} + SO_4^{-2} \rightarrow BaSO_4 \tag{2.2}$$

Injection of seawater for secondary oil recovery is also a cause of scale formation. As the reservoir matures and sea water mixes with the oil reserve, these two incompatible waters mix together giving rise to the formation of barium.

Barium sulphate generally increases as temperature and salinity increase. Similar to gypsite, the solubility of $BaSO_4$ increases with pressure and is unaffected by pH change.

2.1.3 Strontium Sulphate

$$Sr^{2+} + CO_4^{2-} \rightarrow SrSO_4 \tag{2.3}$$

Strontium sulfate increases with water salinity (above 175,000 mg / L), temperature, and pressure. Again, pH influences the process. Deposits of strontium sulphate in large amounts are difficult to find with the exception of a few wells in the Middle East. Deposits of SrSO4 in production wells where reservoirs rich in strontium are mixed with injection water rich in sulphates.

2.1.4 Calcium carbonate:

Is the most common type of fouling in oil and gas fields. Calcite precipitation occurs when calcium ions are combined with carbonate or bicarbonate ions as the following formulas:

$$Ca^{2+} + CO_3^{2-} \rightarrow CaCO_3 \tag{2.4}$$

$$Ca^{2+} + 2HCO_3^{-} \rightarrow CaCO_3 + CO_2 + H_2O \tag{2.5}$$

The presence of CO_3 increases the solubility of $CaCO_3$ in the brine. Increasing CO2 also creates acidity in the water, decreasing the pH. Formation of calcium carbonate generally takes place with a drop in pressure, for example, in the well head. This reduces the partial pressure of CO2, increasing pH and decreasing the solubility of $CaCO_3$. Solubility of calcium carbonate decreases with the increase in temperature.
The chemical equilibrium constant in Eq.4.1 can be read using Chateliers cause and effect principle as:

$$K^{eq} = \frac{[CaCO_3][(CO_2)^{aq}]}{[Ca^{2+}][HCO_3^{-}]^2} \tag{2.6}$$

The principle explain that when CO_2 is liberated and removed by pressure reduction, the CO_2 concentration will reduced. To compensate for this effect, more $CaCO_3$ will be produced to maintain the constant K^{eq}.

Calcite formation is a typical problem in the presence of water in the range of 10% to 15% in the extracted petroleum composition, and is first observed by depositions into the wellhead duct. As the well pressure decreases through well life, the calcite-forming position moves progressively to the lower end of the production pipe until it forms inside the well.Gravel packs, perforations and screens may become clogged.Scale in extreme pressures can be found in the form of aragonite.

2.2 Scale problems in subsea and pipeline systems

Guan [1] presented the performance of subsea equipment in early and later field production life for a specific field, the work presented a historical analysis of the different equipment as the figure **??**, where saturation ratio(SR), precipitation and accumulation rate of $CaCO_3$ are presented.

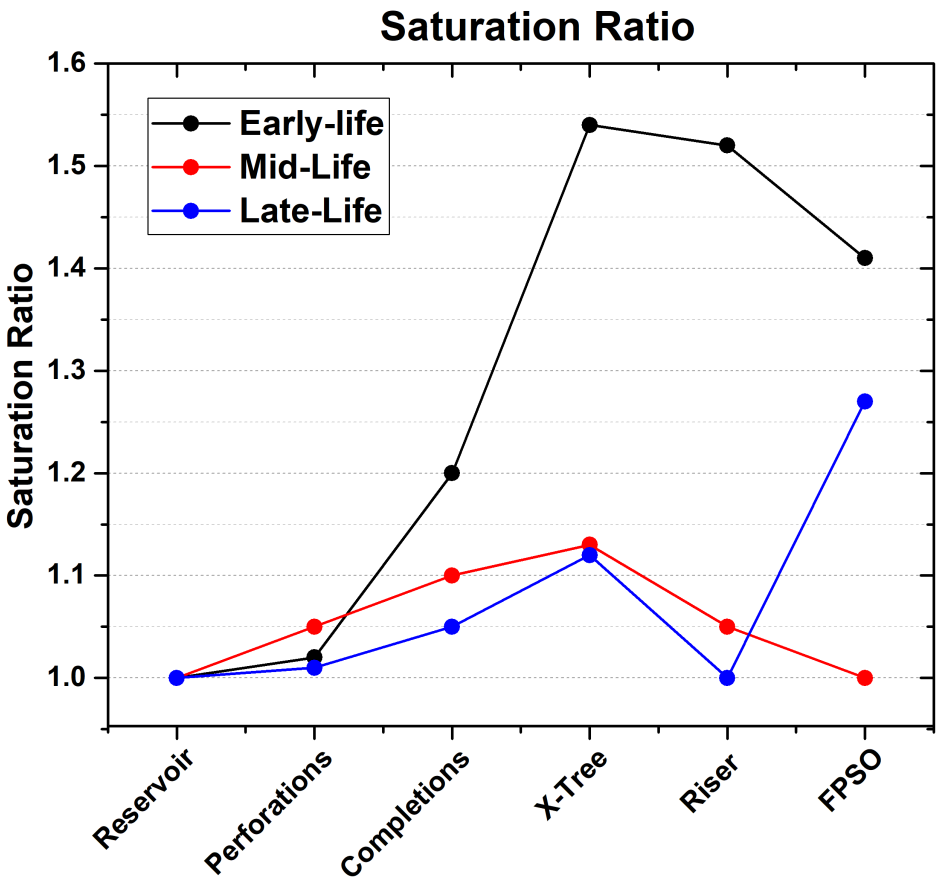

Figure 2.1: Saturation Ratio, [1].

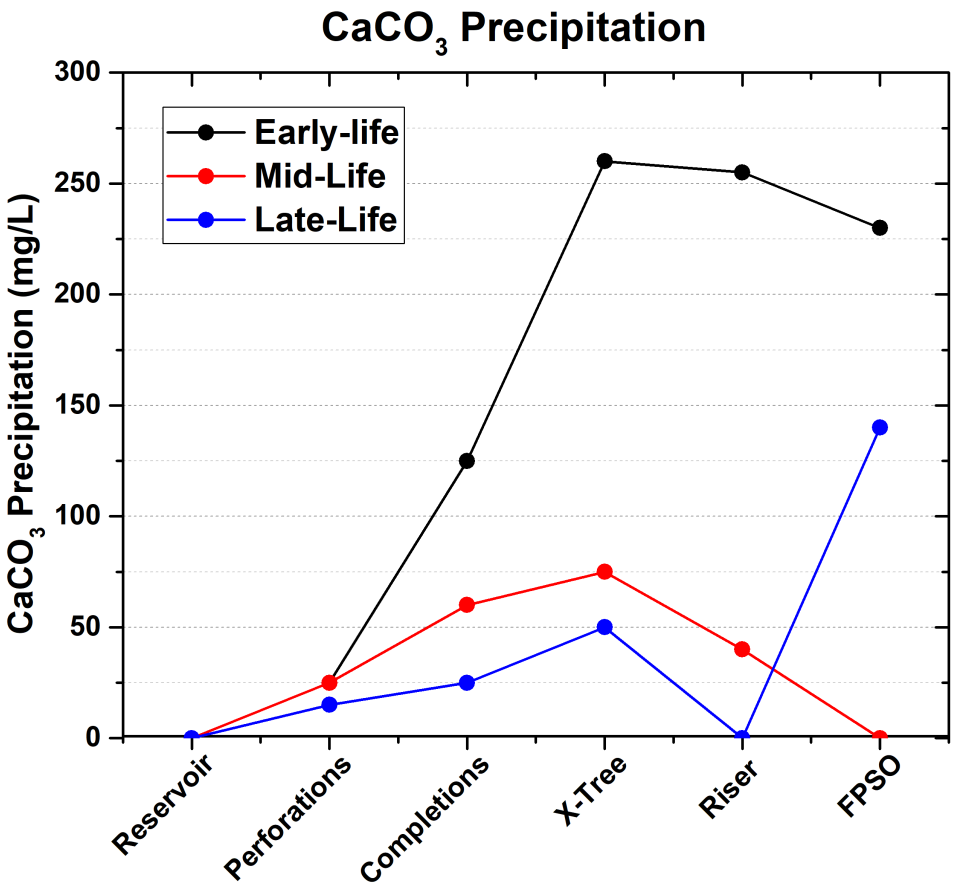

Figure 2.2: Precipitation of $CaCO_3$, [1].

Scale tendency

The likelihood of scaling is represented by the saturation ratio (SR) plot on the fig 2.1 SR increases from reservoir/perforation (equilibrium), Completion to X-tree, then decreases from Riser to FPSO (except late life case where an increase is seen from riser to FPSO). Greatest increases found in scaling risks at an early field cycle life which vary from 1.2 (Completion) to 1.5 (X-tree). This is mainly due to the higher temperatures experienced at an early life which generated greater calcium carbonate scaling tendency.

Saturation ratio is defined as the ratio of the ion product to the ion product at saturation conditions. For example, for calcium carbonate (CaCO3):

$$SR = (C_{Ca^{+2}} X C_{CO3^{-2}})/(C_{Ca^{+2}} X C_{CO3^{-2}})_{Saturation} \tag{2.7}$$

where $C_{Ca^{+2}}$ is the concentration of Ca^{+2} in the solution and $C_{CO3^{-+2}}$ is the concentration of $CO3^{-2}$ in solution.

For a given solution $SR = 1$, solution is saturated with CaCO3.

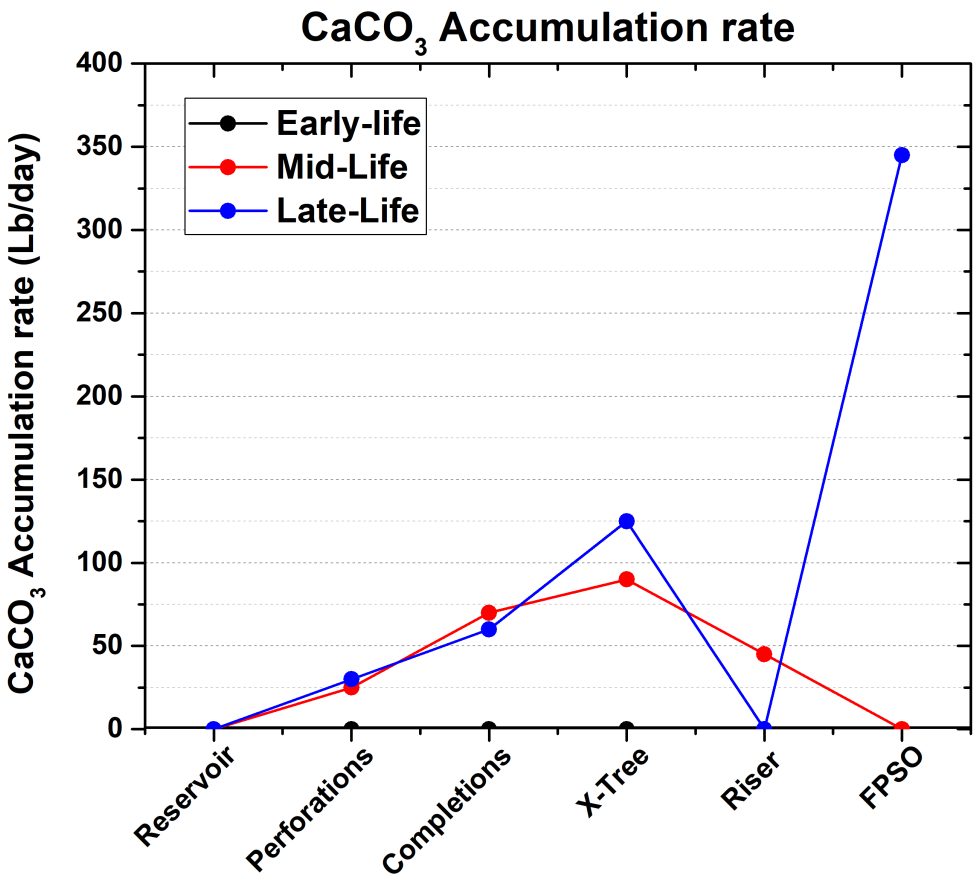

Figure 2.3: Accumulation rate[1]

If $SR < 1$, the solution is under saturated with CaCO3 and precipitation will not occur. If $SR > 1$, the solution is supersaturated with CaCO3 and precipitation can potentially occur.

A concept that is used more often than saturation ratio is called saturation index (SI) which is defined as:

$$SI = log_{10}(SR) \tag{2.8}$$

If $SI < 0$, the scaling ions are under saturated in the solution at the given condition and no scale precipitation is expected. $SI = 0$, the scaling ions are at equilibrium in the solution. $SI > 0$, the scaling ions are supersaturated in the solution at the given condition and scale precipitation is possible.
This index is very used at several scale precipitation prediction [21].

Scale amount

The maximum mass of scale when is fully deposited is represented by the max. precipitation plot in the fig. 2.2 . Similar trends were found – precipitation amount increases from reservoir/perforation (equilibrium), Completion to X-tree, then decreases from Riser to FPSO (again except late life case where an increase is seen from riser to FPSP). Again greatest increases found in scaling mass at an early field cycle life which vary from 100mg/l (Completion) to 250mg/l (X-tree).

Accumulation rate

This represents the daily maximum scaling rate when certain amount of water is flowing by2.3; it is therefore dependent on the amount of water production – the higher the water production rate, the greater the accumulation rate. It is therefore expected that very small accumulation rate due to the very small water production at early lifetime, higher accumulation rates at mid and late lifetime due to the much increased water production.

Solubility

Solubility is a parameter used to assess how much a substance can stay in a solution without precipitation and is defined as the maximum amount of a solute that can be dissolved in a solvent under given physical conditions (pressure, temperature, pH, etc.). The higher the solubility of a compound, larger will be the amount of the compound that can dissolved in a solution. The solubility of a compound can change when pressure, temperature, and/or compositions changes. Different compounds have different solubility. It is well known that the solubility in water of calcium carbonate, barium sulfate, strontium sulfate, or calcium sulfate is relatively small.That is why these compounds tend to precipitate from water to form scales. Water with dissolved salts is also an excellent electrolyte that is required for corrosion to occur. When free water is high enough to wet the inner pipe wall, corrosion may occur. The more salts or ions in the water, the more conductive the water is and the more severe the corrosion rate will be.

Water can significantly change the multiphase flow characteristics inside the pipeline and cause severe slugs to occur. For example, for the same total liquid flow-rate and the same gas oil ratio, the total amount of gas inside the pipeline will be much less with water cut of 90% than with water cut of 0%. With lower gas flow, the liquid amount inside the pipeline will be higher and it is harder for the gas to carry the liquid through the riser due to fewer gas energy. Thus, it is easier to form severe slugs.But based upon the above brief discussions, it is obvious that produced water has significant impacts on flow assurance risks.Also, in sub sea

systems, multiple wells are linked to the flow lines on the ocean floor where the produced brine from different wells commingle[22]. Such production system often increases the challenges of scale prevention and control.

The most effective way to mitigate flow assurance risks in production pipelines is to dispose the water sub sea and make sure no water will get into the pipeline. Unfortunately, the most effective way may not be the most economical way, nor the most practical way[8]. Currently, the most common strategy to mitigate flow assurance risks in offshore pipelines are thermal insulation and chemical inhibitions. But if the amount of water flowing inside the pipeline can be reduced (down hole separation and/or sea floor processing), the amount of chemicals needed for inhibition will also be less, resulting in less operation costs. The major factors affecting the scale precipitation from water are pressure, temperature, pH value, and dissolved solids in water.Boyun[8] summarized the impacts of these factors for the common scales in oil industries.

Table 2.1: Summary of Major Factors Impacting Scale Precipitations[8]

Scales	Temperature effects	Pressure effects	pH value effects	Dissolved solid effects
Calcium carbonate	Inversely soluble/Higher Temp. will form more scale	Less soluble with reduced pressure / If water goes to the bubble point CO_2 would evolve from solution and scale likely to form.	Less soluble with increased pH value	
Barium sulfate	For common temperature range, solubility increase with increased temperature.	Less soluble with reduced pressure.	Little impact.	More soluble with increased dissolved salt
Stronium Sulfate	Less soluble with increased temperature.	Less soluble in NaCl brines with reduced pressure.	Little impact.	More soluble with increased NaCl content.
Calcium Sulfate	Less soluble with increased temperature for the common reservoir temperature range	Less soluble with reduced pressure.	Little impact.	More soluble with increased water salinity

The main means of scale control is chemical inhibition, which includes both continuous chemical injection and periodic scale squeeze inside the formation.Scale inhibitors prevent scale deposition and they do not normally re-dissolve the deposits that have already formed.So the key function of a scale inhibitor is prevention, not remediation. Scale control strategies can be different at different stages of field life.At early life, only connate water or aquifer water breaks through. The most likely scales will be carbonate scales which will be the main focus for scale control strategy. Scale severity will increase with increased water cut. If seawater is injected at later field life, sulfate scales can be formed when the injected seawater breaks through and mixes with formation water. Strategies at this stage would include controlling both carbonate and sulfate scales. With production, the sea- water fraction in the produced water will increase with time, and the severity of sulfate scales will change accordingly.

Literature related to the inhibition of fouling in materials tends to work with one or more minerals dissolved in the fluid, Zhao [23], studied Ni- PTFE (Nickel-phosphorus-polytetrafluoroethylene) inhibitors of calcium sulfate to mitigate scale formation in membrane systems for seawater desalination.

When chemical inhibitors are used for scale control, inhibitors will work with one or more of the following three main mechanisms:

- Crystal nucleation inhibition
- Crystal Growth retardation
- Dispersion of small scale crystals in the flowing fluid

An inhibitor molecule works against crystal nucleation by interacting directly with the scaling ions in the brine, and thus prevents the ions from agglomerating into nuclei. Inhibitor molecules can also retard crystal growth by either adsorbing onto the crystal surface (the growth sites) or fitting into the crystal lattice to replace one of the scaling ions (usually the anion). By doing so, it distorts the crystal lattice or the growth steps thus preventing the crystal from growing rapidly in a regular morphology.

If small scale crystals have already formed in solution, an inhibitor may also prevent the crystals from adhering to each other and to other surfaces by dispersing them in the fluid. The small crystals are hence carried along with the fluid, and scale deposition is minimized. A particular inhibitor often inhibits scale formation with a primary inhibition mode. Some are better at exhibiting one particular inhibition mechanism than the other.Testing and selecting the right inhibitor for a given scale

problem are very critical for scale control([14],[24],[25]).The most important step for screening an inhibitor is water sampling. With representative samples available, water chemistry data which is the most important information needed to diagnose and analyze the scaling potential of produced waters can be obtained. Water chemistry data include concentrations of ions (anions and cations, like calcium, barium, strontium, bicarbonate, and sulfate) and pH. Accurate chemistry data of the produced water under system conditions (in-situ), along with system information such as production data, temperature, and pressure as well as gas composition are essential for assessing scale risks and for testing inhibitors. Obtaining representative water samples requires good practices. For a new oil/gas field, original formation water samples should be collected. Water samples must be preserved and stabilized at the time of sampling. Samples without preservation often go through changes including precipitation of scaling ions, evolution of carbon dioxide (CO2), and pH drift. If a sample is collected without using a pressurized container, pH and bicarbonate should be determined immediately on-site. This is because both will drift rapidly, resulting from CO2 evolution from the solution. It is also important to determine whether or not the samples have been contaminated by drilling muds and completion fluids before performing analysis. Finally, the water chemistry data should be examined by an expert to ensure the quality.Once water chemistry data is available, the scale prediction can be performed using simulation packages. There are a few commercial simulation packages available ([14], [22]). Based upon the simulations, the nature of scale and potential amount of scale that will precipitate can be assessed. And proper scale control technologies/strategies can be eventually developed. A very successful story on how to develop a new scale inhibitor for a specific field problem in the Gulf of Mexico was reported by Yuan et al. in 2003.

Boyun[8] enlisted the main characteristics that a successful scale inhibitor has to have :

- It must inhibit scale formation at threshold inhibitor levels under a range of brine, temperature, and pressure conditions.
- It should have good compatibility with the produced water to avoid the formation of solids and/or suspensions. Some scale inhibitors will react with calcium, magnesium, or barium ions to form insoluble compounds which can precipitate to form scales, thus, creating new problems.
- It should have good compatibility with valves, wellbore, and flowline materials, e.g., low corrosion on metals. Thus, a corrosivity test is necessary.
- It should be compatible with other chemicals, like corrosion inhibitors, wax

inhibitors, and hydrate inhibitors. The scale inhibitor should be physically compatible with other chemicals so no solids will form. The scale inhibitor should also be compatible with other chemicals so their individual performance will not be significantly interfered.

- It must be thermally stable under the application temperature and within the residence time. This can be challenging for some fields with high formation temperatures.
- The leftover residues in produced brine must be detectable for monitoring purposes.

For scale control in wellbore and pipelines, inhibitors are required to be injected continuously so it can avoid the growth of each scale crystal as it precipitates from the water. For maximum impact against further crystal growth, scale inhibitor must be present at the upstream of the point where scale precipitation occurs. That is why in a lot of cases scale inhibitor is injected at the bottom of the wellbore. If scale is a risk in formation, especially near the wellbore region, it is not practical to continuously inject inhibitor in the formation. Scale squeeze operations are required. The scale squeeze technique have been used extensively in North Sea fields for quite a long time [26].

2.3 Other approaches to scale formation (deposition) and inhibition

The surface composition of the material, absorption, electric charge, as well as the tendency to corrosion, can be properties that could affect scale formation. On the other hand, if this surface has micro-roughness, there is a minimal presence of contact points, which can reduce the possible formation of scale since the contact area between the body coating and an external body is reduced. The materials can have roughness in different length scales. Cheong [27] studied the effect of surface morphology based on biomimetics (the technique of copying functional forms in nature and using them in technological systems). The most famous biomimetic technique is Velcro. This concept in surface engineering is receiving attention as nature provides a broad spectrum of functional surfaces.

Eroini et al. [16], studied the capability of different materials to reduce or modify calcium carbonate ($CaCO_3$) deposition, in order to understand what constitutes a surface that minimizes the scale formation potential. Seven different surfaces (stainless steel, polyprophosphorocarboxylic acid or PTFE pre-treated stainless steel, PTFE, diamond-like carbon or DLC, ceramic coated stainless steel and polymer,

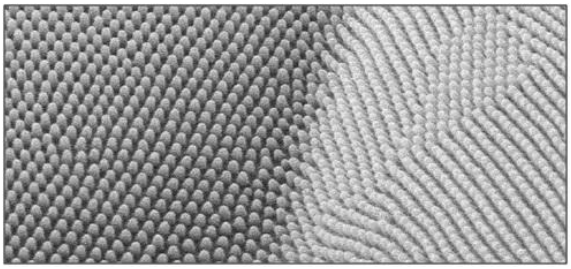

Figure 2.4: Morphology of the butterfly eye (courtesy "Biomimicry Institute", 2015).

and finally a super smoothened stainless steel surface) were tested in two Solutions of water with different Salt concentrations. Each surface was characterized by contact angle, roughness measurements and dispersion X-ray (EDX). The formation of calcium carbonate was evaluated by means of an electron microscopy (SEM) scanner. As a result, a ranking was generated indicating the scale inhibition capacity of each surfaces.Only a few isolated crystals were observed on these surfaces.

Ceylan et al.[28] studied the roughness effect on fully developed turbulent flow pipes, and generated some empirical formulas to correlate results related to heat transfer and fouling formation in heat exchangers.The correlation is limited to geometrical constraints.

Lalot et al. [29] generates a neural network to detect fouling formation in a cross flow heat exchanger, the model validation was based on more than one hundred experiments. The drawback in this case is that neural networks does not explain the physical phenomena and only have been limited to detect the fouling.

Albert et al.[30] studied the roughness and constraint effects on fouling formation in a double pipe heat exchangers using an experimental setup.Crystal formation and fouling built-up on the heat transfer surface give rise to two effects: an increased surface roughness followed by an additional constriction of the flow cross section as fouling progresses. These affect fluid dynamic as well as thermal performance of the heat exchanger.

Delrot et. al.[31] generated a neural network(NN) to detect fouling formation in heat exchangers, their used real data to test the network reliability.The NN is designed by exploiting the bilinear structure of a simplified model of the heat exchanger.

Yang et. al. [32] present a method based on the study of induction period in three applications; crude oil, crystallization fouling and protein fouling, these models detected the phenomena from induction time up to the steady fouling state.The model describes quantitatively the effect of material surface temperature on the fouling phenomena.Also describes in a quantitative way the influence of velocity over the induction time. The work recommends more research on the flow influencing

the phenomena, because it influenced in a more complex way the scale formation than the surface temperature. The roughness of the material its another effect hard to incorporate in the models.

Kumar et Al.[33] studied the phenomenon in critical components on underwater machines as safety valves for production wells (Sub-surface Safety Valves), which present fouling problems on the springs since formation of incrustation interferes with the free movement of the same and with the valve Flapper, for which they were coated with scale inhibition materials.

2.4 Empirical studies related to scale

Andristos[34] presents the results from a experimental system to study calcium carbonate deposits at isothermal temperature, the study observes a linear increment of scale deposition for small or moderate periods of time, and a asymptotic behavior in longer periods. The major observations were that higher velocities incremented the scale deposition on pipe walls, which is indicative of a mass transfer-controlled process.Calcite is the only $CaC0_3$ poly-morph found for temperatures less than $25°C$, whereas at higher temperatures aragonite dominates being stabilized kinetically.

Khan[35] works with three Reynolds numbers (in the laminar regime), three wall temperatures and three pipeline diameters, its uses the fouling resistance R_f as the main parameter to detect scale formation.It was observed that the influence of Reynolds number in the range investigated (Re =900-1700) was almost negligible.However, the influence of tube surface temperature and tube diameter on the fouling growth was found to be appreciable for the range investigated.In regard to the laminar Reynolds regime the reality can shows that the majority of the equipment in real systems works in the turbulent regime.

Charpentier et al.[36] studied scale formation under laminar and turbulent flow conditions for different materials in complex mineral scale environments where coatings and surface treatments were tested.The works presented final results of scale formation using a comparison between section weight measurements before and after the experiments, by using a coupon reactor system, the system can rotate at several Reynolds numbers.

Mavredakin and Neville[37]studied the $CaCo_3$ deposition phenomenon in a stainless steel tube in order to understand scale formation. First it was simulated deposition with the software "Multiscale". Scale formation was evaluated with scale measurement equipment such as the "Quartz Crystal Micro Balance" used to monitor the initial conditions of deposition on a surface. A bench was used to analyze the $CaCo_3$ formation at 80°C and in different water compositions with brine. The study allowed an interpretation of the areas where concentration of brine generated

a greater tendency to deposit on the tube surface.In this case the test bed uses a capillary tube system, where heated water circulates at 25 ml / min, which allows the formation of scale in a period of one hour due to the micrometer diameter. The experiment circulated was 400 $\mu l/min$.

Hamid[17] proposed a methodology using empirical models from the high-pressure experimental system; also, a CFD model was created to account for flow velocity. Then a Neural Network(NN) to predict scale formation was created, comparisons between the experimental data and NN model was made. The experimental system was limited because the higher cost derived from the use of higher pressures, also the experimental system does not allow to test higher flow velocity in the experimental setup.

Wang [38] studied the effect of flow velocity on the calcium carbonate fouling in smooth tube. A number of experiments were performed to determine the whole process of calcium carbonate deposition in a double pipe heat exchanger in a long term.The flow velocity mostly is studied ranges from 0.2 m/s to 1.6 m/ s, and flow state is turbulent flow.

Vazirian et al.[39] studied scale deposition at the end of multi oil-water separation facility during five months. Were tested different coatings and concluded that surface engineering techniques can mitigate the fouling phenomena and even improve the flow assurance on petroleum and gas facilities.

Paz,[40] *et al.*proposed a calcium carbonate scaling prediction method using Artificial Neural Networks(ANNs). The ANNs were fed with the initial concentration of NaH_CO_3 and $CaCl_2$ used for the experiments. These experiments were performed in a small temperature-controlled automatically stirred batch reactor, where acquiring real-time measures of temperature and pH was possible. The small size of the reactor allowed them to perform experiments under a variety of initial conditions of salts concentrations and temperatures. The quantity of gathered data was good enough for them to fed the ANN to improve the prediction method. This methodology, using a batch reactor, can be scaled up in order to develop a mesoscale loop which can be used to study different parameters as $CaCO_3$ accumulation within the pipes, this parameter would be difficult to study in a small diameter pipe as the accumulation of $CaCO_3$ would be minimal. Another characteristic that could be studied is the fouling resistance as it increases with the $CaCO_3$ accumulation.

Although there is an extensive bibliography on experimental tests, no laboratory tests were found that could describe the formation of scale in order to mimic phenomena that may occur in an oil well, most of the studies describes experiments of short duration and diameters excessively small that generate deposits in a short time (diameters in order of micrometers of the capillary type) or describe phenomena that occur in scale heat exchanger systems.

2.5 Models to predict scale deposition

Mathematical models to predict scale deposition have been developed over the years, specifically to predict fouling on heat exchangers, petroleum distillation facilities and well-bores, these models are known as deposition-release models. A large number of semi-empirical models are derived from these works, being developed and optimized to date, with variations in flow composition, loop geometry and configuration, fluid density, temperature and flow velocity, among others. In Chapter Three some remarkable models are described in more detail.

Early models such as Nelson [41], Kern and Seaton [42],Crittenden et. al.[43], Epstein [44] are based on the Arrhenius equation and are not able to predict the effect of fluid velocity and its ability to remove the deposit.

Takemoto et. al. [45], used data collected over a period of 3 years in an oil distillation unit, where it was possible to determine the correlation between the total fouling rate of the equipment and its wall temperature. This correlation was then successfully used to predict the thermal efficiency reduction of the preheating battery, operating with "light" oils. However, as the studies come from operational data, the range of results is limited. Consistent results of velocity and temperature were reported in this study, and it could be verified that the decrease in flow velocity and the increase in operating temperature led to increase the incrustation observed.

Ebert and Panchal [46] proposed a mathematical model to quantify the effects of flow velocity and the fouling by tube sides in oils at high temperature, from data collected from pilot plants studies, where the study of coking data by Scarborough et al.[47]was used. From the observations made, they adjusted the data obtained in a numerical model where the inlay rate is the result of a competition between the deposition process and the removal process. This model allowed users to estimate operating conditions where the fouling rate would approach zero. This information provides a quantitative basis for improving the unit in operational terms and new information for designing units and updating existing ones.

After the model presented by Ebert and Panchal (1995), many authors presented variants in subsequent years. Ebert and Panchal (1999) presented a review of the original model using pilot plant data and operating units, taking into account the Prandtl number raised to a power.

Polley et. Al.[48] presented a model based on the experimental results obtained by Knudsen et. al.[49] and similar to that proposed by Patterson and Fryer[50] with explicit dependence on the wall temperature, rather than the define temperature, and a removal term analogous to that proposed by Takemoto et. Al. [45]. Nasr and Givi (2006) proposed a new model for heat exchangers to preheat petroleum based on experimental results obtained in the Salehet study. Al.[51]. The model advantage

is a non-dependence of the Prandtl number, as well as an exponent determination of the Re number from the calibrated data of operational data. It was possible to calculate the operation parameters such as shear stress, film and wall temperature, thermal exchange coefficients, flow velocity and operational factors, where it was possible to obtain relations between the mentioned parameters and the evolution of scale resistance.

Al-Hadhrami[52], studied the inlaying of CaCO3 in a loop varying the flow velocity between 0.5 and 2 m / s, the test section was modified geometrically in the form of helical tube To assess whether the scale decreases in a tube having these characteristics, it has been observed that the scale decreases as the flow velocity increases inside the duct since geometry increases the turbulence effect inside the helix tube.

Foruatan et. al.[53] studied the parameters of precipitation in working conditions (temperature , pH, salt concentration). With the obtained data it was possible to generate an analysis program inspired by neural networks capable of predicting scale formation data for different cases and arrangements with a 5% error.

Harche et. Al. [54] studied the performance conditions of a crude oil preheating system. This paper aimed to extrapolate empirical models based on the Kern and Saton models (1959). The results show an exponential evolution of the scale deposition in this equipment, probably due to lack of maintenance. They also revealed the coexistence of four types of fouling; precipitation of mineral origin, presence of insoluble materials (eg. sand), incrustation due to chemical reactions, and incrustation due to corrosion.

Pakkonen [55] studied the accuracy of experimental results by uncertainty analysis, used SEM and XRD to determine the morphology and the composition of the deposited slats. The uncertainty analysis shows that the bias and precision uncertainties in the measured wall temperature are the largest source of uncertainty in the experiments.

The total uncertainty in the fouling resistance in the studied case was found to be $\pm$ 13.5% at the 95% confidence level, then Pakkonen [19] studied the formation of fouling from calcite ($CaCO_3$) in a flat surface heat exchanger. The scale deposition is evaluated from the inlay thermal resistance (R_f). The uncertainty of scale deposition is evaluated again. Thus the empirical model was evaluated through an experimental test. The work found a dependence on scale-up time with the fluid flow inside the exchanger. They concluded that the mass transfer term in the scale deposition process presents a large number of uncertainty parameters (including surface roughness of the exchanger).

The empirical models described above are structured for the analysis of heat exchangers, both in petroleum distillation systems used in refineries, as well as steam

boilers. The objective in a simplified way, is to describe the fouling process using models where scale rate is evaluated in terms of thermal resistance (R_f) or "fouling resistance". The model can be applied in pipes using input data based on physiochemical characteristics of the fluid such as viscosity, density, heat transfer coefficient (Cp). The major parts of the empirical models describe the phenomena through real-time measurements of the physical parameters (inlet and outlet temperature, flow rate, fluid density) and aims to predict at what time t will be reached a stabilization of the incrustation observed by the formation of an asymptotic curve described in these publications. Yang[18] combined the effect of fluid flow and heat transfer on scaling,then proposed a mathematical model for predicting CaCO3 formation, which is based on the model for calculation of deposition and removal mass rates. The model was used to predict the scaling in water injection well-bore of low permeability reservoir in the Shengli Oilfield. Prediction results were in good agreement with measurements. It was found that the scale layer thickness increases with the injection water time and scale-forming ions concentration, while it decreases with an increase on daily injection water rate. However, different geometry, composition and flows in the equipment causes that empirical prediction models present a certain degree of uncertainty, giving rise to repeat the tests and generate an adjustment curve to represent the inlay behavior. To study the inorganic scale in the loop, several sensors were used among them an IR Thermography camera, which can gives sensitive information related to temperature changes on external pipe wall. Currently there are few studies of experimental scaling and scale formation carried out using these IR in real time.More details on sensor systems are in chapter 2.

As described previously, there are several models to predict scale deposition phenomena. Most part of empirical models used thermo-physics properties of the fluid; viscosity, density, heat transfer and coefficients C_p [56].

Due to the complexity and variety of the studied compositions in literature, is necessary a simplification of the problem to controllable parameters in order to evaluate which physical magnitude will inhibit or accelerate a specific scale process, at this thesis Calcium Carbonate will be the main scale component, because it is the most common phenomena in scale precipitation and crystallization during oil production processes. The exposed empirical models only presents scale deposition in small diameter capillary systems(1/8 inch), [1], [57], [16], [58],[59], distillation batteries[60],[61] heat exchangers[52],[31] and rotating tanks, most of the works studied the phenomena during a short time, or low Reynolds number especially when are related to study the phenomena in pipes[62].

Prediction of fluid flow in offshore engineering is a task which still has an ongoing production of models and concepts to predict flow assurance in petroleum exploration and production, Shippen[2] enumerated the main focus of a design workflow

in the multi-phase area:

- The behaviour of the lower completion design (reservoir contact)
- The response of the upper completion design (tubing and artificial lift systems)
- The impact and proper design of surface equipment and connecting flowlines.

For systems in operation, multiphase flow studies provide insight into which parameters may be adjusted to maximize production, efficiency, and net revenue. Such operational parameters include gas lift injection rates, pump speeds, choke settings, and others. More-advanced analysis of multiphase systems further explores the impact of specific multiphase flow characteristics such as flow pattern, liquid holdup, and slug properties. This management are among others; prediction of erosion and corrosion, identification of unsteady flow (heading or liquid loading in wells and severe slugging in risers) and solids deposition.

Five models were studied and developed in Matlab software to predict mass deposition rate(Kg) ; three adapted asphalt particle deposition models [3], a deposition-release model[18], and an adapted paraffin wax deposition model [63], then they were compared with experimental results using direct mass deposition measurements as a way to correlate with the scale growth, those comparisons are on chapter 5. These models fall under the classification of empirical models of type "C" as stated by Shippen[2] where Slip between phases and the flow pattern is considered, with this, the models can be considered as multiphase models because those have the objective of model scale growth phenomena which encompasses two phases, a fluid one and a stable one corresponding to the transported Ca_CO_3 particles in the flow loop. A detailed chart showing the evolution of several models along the years is in 2.5. Correlations to predict liquid holdup and the friction factor[64] as well as methods to predict the flow pattern were developed.

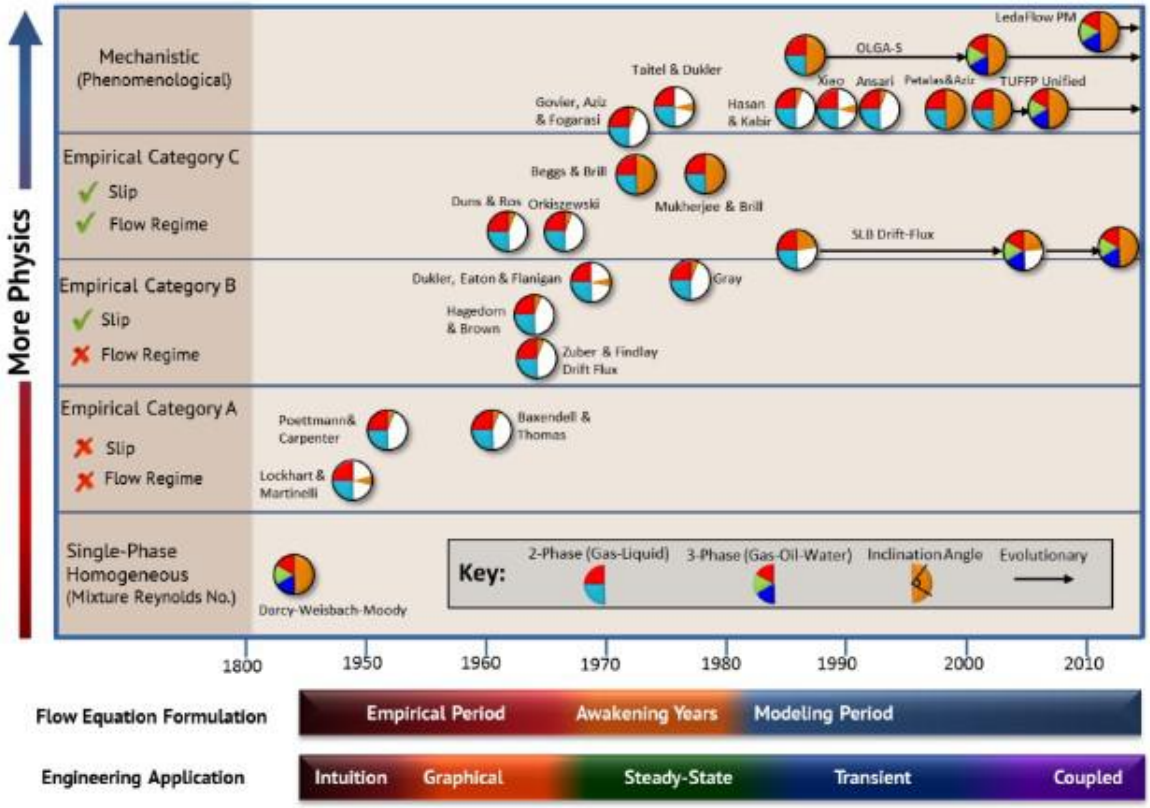

Figure 2.5: A chart describing the evolution of multiphase models according to [2]

Chapter 3

Scale prediction models

3.1 Deposition-release model

The models used the following entrance variables to predict the mass deposition rate; those variables were the main parameters which affects the scaling phenomenon, based on several authors:

The model has these assumptions for simplification:

- Fluid density is considered as water.
- Initial roughness of scale is as the stainless pipeline.
- The induction period of scaling layer was too short so is not taken into consideration
- Scale density is constant and stated as determined by Pakkonen [19]

Table 3.1: Main parameters affecting scale build-up in the models

Parameter	Obs.
Bulk concentration(C_f)	*Pipeline temperature affects the precipitation of inorganic scale and less directly asphaltenes and naphthenates; also several crystals may form in the experiment, those crystals also depends on this parameter; [65], [66],[67],[68]*
Bulk Temperture (T_{Bulk})	*Higher temperatures can precipitate more particles in the fluid; [18],[69], [70]*
Wall Temperature (T_{Wall})	*When the radial temperature drop is primarily outside the steel wall of a subsea pipeline, the inside wall temperature is very close to the bulk temperature. Rough calculations for typical pipeline conditions show that the inside pipe wall temperature in subsea pipelines are only 1–2C below the bulk temperature.[7]*
Flow velocity (Vel)	*Flowrate phenomena have only gradually emerged in software models to predict precipitation. The link between precipitation and deposition continues to be the weakness of software mod- elling. The deposition of solids is more complicated than the precipitation of solids. Laboratory flow-loop and field data are required to couple the phenomena of precipitation and deposition. Such data are expensive to gather and often difficult to interpret; [71], [72], [?], [38]*

3.2 Yang model

Yang[18] proposed an iterative solution to predict scale thickness based on the work of several authors,[42] [73] as the difference between deposition and removal rates more known as the deposition release model:

$$dm/dt = dm_d/dt - dm_r/dt \tag{3.1}$$

The crystal mass per surface area at a determined time $t + \triangle_t$ is calculated as a sum of the total mass per surface area on time t added to the calculated mass rate during the new computing time step $\triangle_t$:

$$m_{t+\triangle_t} = m_t + dm/dt * \triangle_t \tag{3.2}$$

The thickness layer is calculated as the deposit mass in each time step $\triangle t$ per surface area divided by the density ρ_f of the scaling layer:

$$X_f = m_{t+\triangle_t}/\rho_f \tag{3.3}$$

3.2.1 Deposition mass rate

The mass deposition rate is the sum of the crystallization deposition mass rate and the particle deposition mass rate:

$$\frac{dm_d}{dt} = \frac{dm_c}{dt} + \frac{dm_p}{dt} \tag{3.4}$$

Mass rate of crystallization

Yang proposed a formula for the rate of crystallization as:

$$\frac{dm_c}{dt} = \beta * \frac{1}{2} * \frac{\beta}{K_r} + \triangle_C - \left(\frac{1}{4} * \left(\frac{\beta}{K_r}\right)^2 + \frac{\beta}{K_r} * \triangle_C\right)^{1/4} \tag{3.5}$$

where $\triangle_C$ is the total concentration difference:

$$\triangle_C = C_F - C_s \tag{3.6}$$

C_F is the bulk concentration, C_s is defined as saturation concentration, calculated as in function of :

$$log(C_s) = \frac{\triangle H_o}{2.3 * R * T_f} + \frac{\triangle C_p}{R} log(T_f) + C \tag{3.7}$$

where $\triangle L_o$ is solution enthalpy stated as -81 3 , $\triangle c_p$is the difference of heat capacity of calcite as stated by Jacobs[74], R is molar gas constant, C is a parameter given by J. Lammer.

[75]stated Supersaturation of $CaCO_3$ crystals in function of Bulk temperature:
For Calcite:

$$\triangle C_p = -184.79+0.32322T_{Bulk}-3688200*{T_{Bulk}}^2-(1.2974exp-4)*(T_{Bulk})^2+3883*{T_{Bulk}}^{-2} \tag{3.8}$$

The T_f is the surface temperature of the scaling layer calculated as[76]:

$$T_f = T_{wall} - q * 1.4e{-}4 \tag{3.9}$$

The mass transfer coefficient is a function of the Sherwood number:

$$\beta = \frac{Sh * D}{d_o} \tag{3.10}$$

Sherwood number is according to Lammers:

$$Sh = 0.034 * Re^{0.875} * Sc^{0.333} \tag{3.11}$$

Where:

$$Re = \frac{Veld_o\rho}{\eta} \tag{3.12}$$

$$S_c = \frac{\eta}{\rho D_{coef}} \tag{3.13}$$

S_c correspond to Schmidt number, and D_{coef} correspond to the diffusion coefficient, this last therm is according to Stokes-Einstein equation[77]:

$$D_{coef} = \frac{k_B T_{Bulk}}{3\pi\mu d_P} \tag{3.14}$$

Where K_B correspond to the Boltzmann constant($K_B = 1.38 * 10^{-23} J/K$), d_p is the particle hydrodynamic diameter($CaCO_3$ m=36μm as stated by [18]), μ is solvent viscosity(in this case water) and T_{Bulk} is bulk temperature.

Deposition mass rate of particle

Following the Kern-Seaton model [42] the deposition mass rate of the particle as a function of the concentration of particle in the solution and particle deposition rate:

$$\frac{dm_p}{dt} = C_p V_d \tag{3.15}$$

The concentration of particles is a function of supersaturation as stated by Quan[78]:

$$C_p = -16.647 + 1.667Sb \tag{3.16}$$

The supersaturation degree is calculated as:

$$Sb = \frac{C(Ca^{2+})C(CO_3^{2-})}{logK_{spb}} \tag{3.17}$$

The K_{spb} is the solubility product of $CaCO_3$ crystals at the solution temperature(T_{Bulk}), is calculated as calcite, Vaterite and Aragonite by Busenberg[79]:

- For Calcite:

$$log(K_{spb}C) = -171.9065 - 0.077993(T_{bulk}) + 2839.319/T_{bulk} + 71.595log(T_{bulk}) \tag{3.18}$$

- For Vaterite:

$$log(K_{spb}V) = -171.9065 - 0.077993(T_{bulk}) + 3074688/T_{bulk} + 71.595log(T_{bulk}) \tag{3.19}$$

- And for Aragonite:

$$log(K_{spb}A) = -171.9065 - 0.077993(T_{bulk}) + 2903.293/T_{bulk} + 71.595log(T_{bulk}) \tag{3.20}$$

Figure 3.1: $CaCO_3$Calcite Crystals generated during the experiment

Following Quan et al.[78], the particle deposition rate is described as follow:

$$\frac{V_d}{u^*} = \tag{3.21}$$

$$\begin{cases} 0.07(Sc)^{-2/3} \longrightarrow \tau^+ <= 0.02(\text{diffusion regime}) \\ 3.5x10^{-4}(\tau^+)^2 \longrightarrow 0.02 < \tau^+ < 20(\text{diffusion Inertia}) \\ 0.18 \longrightarrow \tau^+ > 20(\text{Inertia}) \end{cases} \tag{3.22}$$

Details respect to those regimes are stated ahead.

Friction factor

Calculation of friction factor is not only necessary for determining pressure drop in pipelines and heat exchangers but also essential for the Nusselt number in turbulent tube flow. The parameter was calculated using the equation proposed by Azizi [64].

$$f = \left(1.805log(\frac{\frac{\epsilon}{D_i}^{1.108}}{4.267} + \frac{5.164}{Re^{0.966}})\right)^{-2} \tag{3.23}$$

Azizi proposed to estimate the friction factor of turbulent fluid flows in rough pipes over the ranges of $10^{-6} \leq \epsilon/D_i \leq 0.05$ and $2000 \leq$ Re $\leq 10^8$ for which this experimental loop satisfied the conditions.

The friction wall coefficient of the loop pipeline was analyzed (stainless steel 304L), measured by a profilometer model DEKTAK IIA, fifteen measurements were made on sample surface without surface treatment. The prove extracted for measurements and profilometer are in fig4.1. This parameter was incorporated into the models to calculate the friction factor.

Table 3.2: Specification of pipe wall roughness

Roughness Mean Value	Units
22606	Armstrong
2,2603	micrometers
Relative roughness e/D_i	0.000827949

Calculation of the removal mass rate

Removal mass rate is calculated as [80]:

$$\frac{dm_r}{dt} = \frac{K}{P}\rho_f(1 + \delta\triangle T)d_p(\rho^2\eta g)^{1/3}X_f Vel^2 \tag{3.24}$$

V_{avg} is the average flow velocity, above the scale growth, g describes the gravity force effect, P describes crystalline action force, K is a parameter equal to the number of

Figure 3.2: Profilometer and sections to roughness measurements

fault points in the fouling layer.$(1+\delta\triangle T)$ describes the temperature stresses, in the fouling layer. δ is the linear expansion coefficient and $\triangle T$ the temperature gradient in the fouling layer, d_p is the average $CaCO_3$ crystal diameter(36 μm).

An approach to K/P calculation is present by Krause:

$$P/K = 83.2V_{avg}^{0.54} \tag{3.25}$$

ρ_f is the average density of the fouling layer kg/m^3[] kg/m^3. Bulk velocity V comes as a function of flow rate Q, fluid density and tube diameter:

$$V_{avg} = \frac{4Q}{\pi\rho d_o^2} \tag{3.26}$$

Finally, the total scale thickness is the sum between the average total thickness from time t and the new growth within the time step $\triangle t$:

$$X_{fTot} = X_f + \frac{dm}{dt}\frac{\triangle t}{\rho_f} \tag{3.27}$$

3.3 Matzain Model

Matzain[63] developed a semi-empirical model, used as a wax deposition model, in this thesis was modified to attend scale deposition based on experimental analyses.

$$\frac{d\delta}{dt} = \frac{\Pi_1}{1+\Pi_2} D_{coef}[\frac{dC_w}{dT}\frac{dT}{dr}] \tag{3.28}$$

$d\delta$ is the thickness of deposited layer on the wall(meters), D_{coef} is calculated by equation 3.14, C_w is of particles, in this case, the particles were assumed to be composed entirely of $CaCO_3$ concentration in solution, r is pipe radial distance, dT/dr is the thermal gradient.

Π_1 corresponds as an empirical correlation accounting for the porosity effect

on the deposits build-up and enhancement mechanisms not considered by diffusion coefficients:

$$\Pi_1 = \frac{C_1}{1 - \frac{C_L}{100}} \tag{3.29}$$

Where C_1 correspond to 15 and C_L is defined as:

$$C_L = 100 * (1 - \frac{{N_{Re}}^{0.15}}{8}) \tag{3.30}$$

N_{Re} is defined as:

$$N_{Re} = \frac{\rho \nu 2 r_i}{\mu} \tag{3.31}$$

Π_2 corresponds to:

$$\Pi_2 = 1 + C_2 (N_{SR})^{C_3} \tag{3.32}$$

where $C_2 = 0.055$ and $C_3 = 1.4$.

In this model, for simplification, the flow regime value of N_{SR} is calculated as a single phase:

$$N_{SR} = \frac{\rho \nu \delta}{\mu} \tag{3.33}$$

Thermal gradient is given by:

$$\frac{dT}{dr} = \frac{T_{bulk} - T_f}{k} h \tag{3.34}$$

Where T_{Bulk} is inner flow temperature, T_f is deposit surface temperature, k is thermal conductivity, and h is the inner wall heat transfer coefficient, calculated as:

$$h = Nu * \lambda_f / d_i \tag{3.35}$$

Where λ_f is the heat conductivity of the test tube, d_i internal diameter and Nu is the Nusselt number. Wang [38] proposed a calculation of Nusslet number depending on flow regime as

Laminar flow:

$$Nu = 1.86 Re^{1/3} Pr^{1/3} \left(\frac{d_i}{L}\right)^{1/3} \left(\frac{\mu_i}{\mu_o}\right)^{0.14} \tag{3.36}$$

Transition flow:

$$Nu = 0.023Re^{0.8}Pr^{0.4}\left(1 - \frac{6x10^{-5}}{Re^{1.8}}\right) \tag{3.37}$$

And turbulence flow:

$$Nu = 0.023Re^{0.8}Pr^{0.4} \tag{3.38}$$

3.4 Models based on particle deposition

Shirdel, [3] presents several deposition models where the main factor is the transport coefficient K_t, which is analogous to particle velocity towards the wall, this factor can be calculated depending on the governing deposition mechanism, which are diffusion, inertia or impaction.

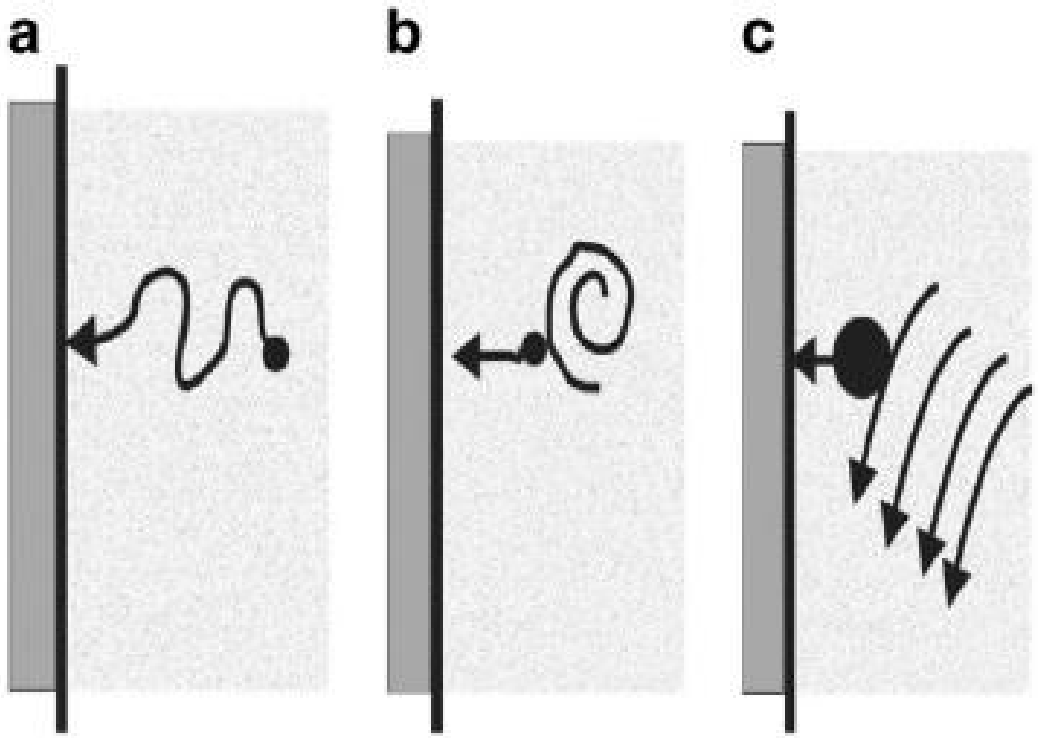

Figure 3.3: Deposition mechanism, (a) diffusion, (b) inertia, (c) impaction.[3]

Those values depend on the particle stopping distance equation:

$$S_p = V_p \frac{\rho_p {d_p}^2}{18\mu} \tag{3.39}$$

The particle stopping distance is defined as the distance a sphere (mass, m_p, diameter, dp, and density, ρ_p), with an initial velocity V_p, travels in free-flight through a

stagnant fluid before it stops because of the dragging force. Assuming that V_p is the particle velocity which depends on the particle position in the flow stream, stated by Friedlander and Jhonstone[81] as:

$$V_p = 0.9V_{avg}\sqrt{\frac{f}{2}} \tag{3.40}$$

Based on the S_p value, one of the three deposition mechanism becomes dominant, as stated below:

$0 < S_p^+ \leq 5$: Stopping distance is located in the sub-laminar layer.

$5 < S_p^+ \leq 30$: Stopping distance is located in the buffer zone.

$30 \leq S_p^+$: Stopping distance is located in the turbulent core.

The particle relaxation time, t_p, is the time for the speed of a free-flight particle to decay to 1/e (or 36.8%) of its initial value, defined as:

$$t_p = \frac{\rho_p d_p^2}{18\mu} \tag{3.41}$$

This is regarded as the particular time in which particles respond to changes in fluid velocity, being considered a measure of particle inertia. In general, particle motion is not affected by eddies with lifetimes shorter than tp. The equation can evaluate the lifetime of the near-wall eddies:

$$t_e = \frac{\mu}{(V_{avg})^2 * (f/2)} \tag{3.42}$$

The occurrence of slippage in the near-wall region can be evaluated by comparing t_p to t_e. The ratio tp/te is known as dimensionless relaxation time:

The dimensionless relaxed time of particle is defined as:

$$t_p^+ = \frac{\rho_p d_p^2 f/2.V_{avg}^2}{18\mu\upsilon} \tag{3.43}$$

Where V_{avg} is fluid velocity, μ dynamic viscosity, d_p particle diameter of the suspended solids and ν kinematic viscosity, f is the fanning friction factor determined by[64] and [82].This dimensionless parameter provides a quantitative measure of particle-fluid slippage and can be applied to classify experimental data in the three deposition regimes, diffusion ($t_p^+ < 0.1$), diffusion–impaction ($0.1 < t_p^+ < 10$), and inertia-moderated ($t_p^+ > 10$) the three regimes can be encountered at fig3.3.

The particle deposition rate, N_0, is defined as the number of particles depositing in a specific area of a pipe during a known period. It is equal to the radial particle flux, N, evaluated at the wall vicinity (y=0). It can be expressed as the product of a transport coefficient, K_d, by the average particle concentration in the flow C_f.

$$K_d^+ = \frac{K_d}{V_{avg}\sqrt{f/2}} \tag{3.44}$$

Particle deposition rates, frequently reported in the form of K_d^+ vs t_s^+. When those parameters are used to plot experimental data in a logarithmic graph, the result is a characteristic "s-shaped" curve like Fig. 3.4, The particle diameter was measured according to experimental results, where a $CaCO_3$ sample analyzed by digital microscopy gives d_p estimated according to the average size of $CaCO_3$ particles in the sample.

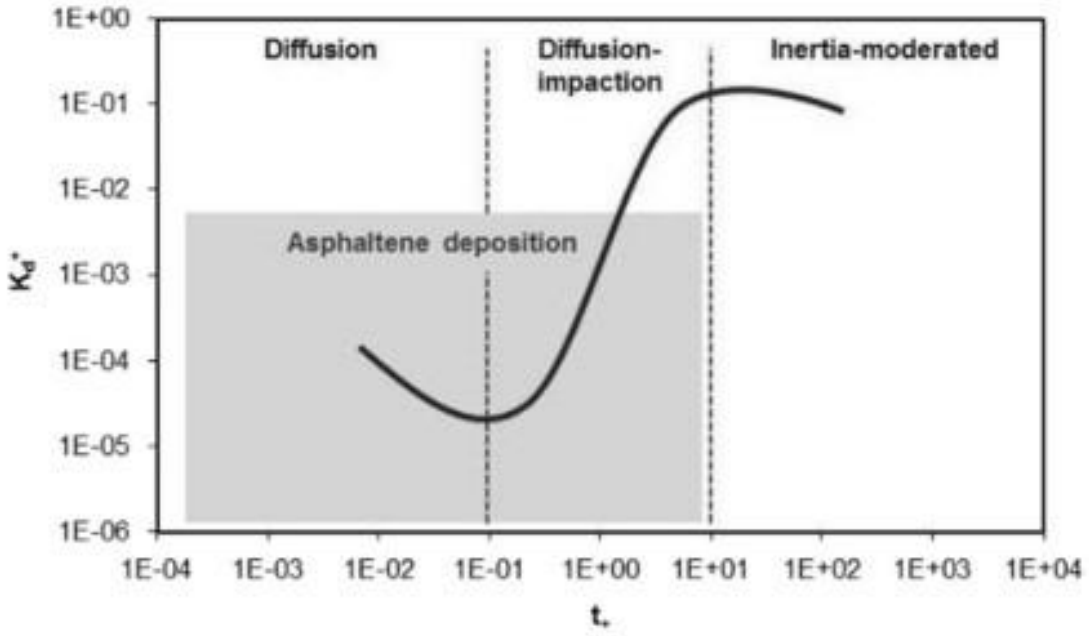

Figure 3.4: Deposition diagram of experimental data. Changes in dimensionless relaxation times, caused mainly by variations in particle size and flow velocity, can lead to different deposition regimes.[4]

3.5 Attachment process

A phenomenon that significantly affects the solid deposition is the attachment process. There are several active forces between particles and fluid, as well as the particles and the wall. The source of those forces can be electrostatic and polar attractions or the shear forces due to high velocity and viscosity of the moving fluids. In gas flow, since shear forces are weak, attachment of the particles is not pronounced. However, for liquids system, these forces are very significant.

One approach to include the attachment process is applying sticking probability(SP) function to the final transport coefficient, where the deposition coefficient is:

$$K_D = SPK_t \tag{3.45}$$

Watkinson and Epstein defined SP as:

$$SP \propto \frac{AdhesionForceBetweenParticlesandWall}{DragForceonParticlesontheSurface} \tag{3.46}$$

Using an Arrhenius type expression and drag coefficient to calculate adhesion force and drag force, respectively:

$$SP = K_d \frac{e^{-\frac{E_a}{RT_s}}}{V_{avg}^2} \tag{3.47}$$

Here K_D and E_a are provided by Yang [18]. The complete equation for particle deposition flux, considering the attachment becomes:

$$m_d = SPK_t(C_p - C_s) \tag{3.48}$$

Where C_p is the average particle bulk concentration in fluid as stated by Quan [78] and Kor [83], and C_s is the wall particle concentration.C_s is calculated as [18]:

$$log(Cs) = -\frac{-\triangle_L H_o}{2,3RT_f} + \frac{\triangle C_p}{R} * log(T_f) + C \tag{3.49}$$

T_f is defined as surface temperature of scale layer defined by[76]:

$$T_f = T_{wall} - q(1,4e^{-4}) \tag{3.50}$$

With m_d defined, the next models only changes the transport coefficient K_t depending on the three dominant regimes.Then, m_d is substituted for equation 3.5 and complemented in 3.4 for the new models approach.

3.5.1 Friedlander and Jhonstone Model

Friedlander and Johnstone considered large particles sizes $tp^+ < 0.1$ in their models to calculate the transport coefficient in the three conditions, depending on stopping distance value:

$0 < S_p^+ \leq 5$: Stopping distance is located in the sub-laminar layer.

$$K_t = \frac{V_{avg} f/2}{(1 + \sqrt{f/2}(\frac{1525}{Sp^+/5} - 50.6))} \tag{3.51}$$

$5 < S_p^+ \leq 30$: Stopping distance is located in the buffer zone.

$$K_t = \frac{V_{avg} f/2}{(1 + \sqrt{f/2}(5ln\frac{5.04}{Sp^+/5 - 0.959} - 13.7))} \tag{3.52}$$

$30 \leq S_p^+$: Stopping distance is located in the turbulent core.

$$K_t = V_{avg} f/2 \tag{3.53}$$

3.5.2 Beal model

Beal (1970) developed a model based on Brownian and eddy diffusion, using a similar approach as Friedlander and Johnstone (1957). Besides, Beal (1970) assumed a linear equation for mass and momentum flux.

The following equations present the transport coefficient for the different stopping distances obtained.

$0 < S_p^+ \leq 5$: Stopping distance is in the sublaminar layer.

$$K_t = \frac{V_{avg}\sqrt{f/2}}{(\frac{14.5}{3}Sc^{2/3}F(Sc, {S_p}^+) - \frac{14.5^2}{1.5{D_o}^+}Sc^{2/3}G(Sc, {S_p}^+) + (5 + \frac{50}{{D_{pipe}}^+\nu})(D_B - 0.959\nu)ln\frac{D_B + 5.04\nu}{D_B 0.04\nu} - \frac{250}{D_{pipe}^+}}$$

$5 \leq S_p^+ < 30$: stopping distance is in the buffer zone

$$K_t = \frac{V_{avg}\sqrt{f/2}}{5[1 + \frac{10}{[D^+]_{pipe} * (D_B - 0.959\nu)}]ln[\frac{D_B + 5.04\nu}{D_B + (\frac{S^+}{5} - 0.959)\nu}] - \frac{10}{[D^+]_{pipe}(6 - \frac{S^+{}_p}{5})} + \frac{1 - 13.71\sqrt{f/2}}{\sqrt{f/2}}} \tag{3.54}$$

$30 \leq S_p^+$: Stopping distance is in the turbulent core.

$$K_t = \frac{Vavg(f/2)}{1 - 13.73\sqrt{f/2}} \tag{3.55}$$

3.5.3 Cleaver and Yates model

Cleaver and Yates applied a stochastic approach to obtain the transport coefficient for small relaxation times ($t_p^+ \leq 0.2$). Where the diffusion mechanism is dominant:

$$K_t = \frac{0.084 V_{avg}\sqrt{f/2}}{Sc^{2/3}} \tag{3.56}$$

Later Epstein combined Cleaver and Yates model with Papavergos and Hedly model, which also is a stochastic approach, with this Kt was proposed for situations when the inertia and impaction are dominants:

$0.2 < t_p^+ \leq 10$

$$K_t^+ = 0.00035(t_p^+)^2 \tag{3.57}$$

$10 \leq t_p^+$

$$K_t = 0.18t_p^+ \tag{3.58}$$

3.6 Model algorithm

Based on the prediction models, a software was developed in Matlab described more in the flow chart on Fig.3.5:

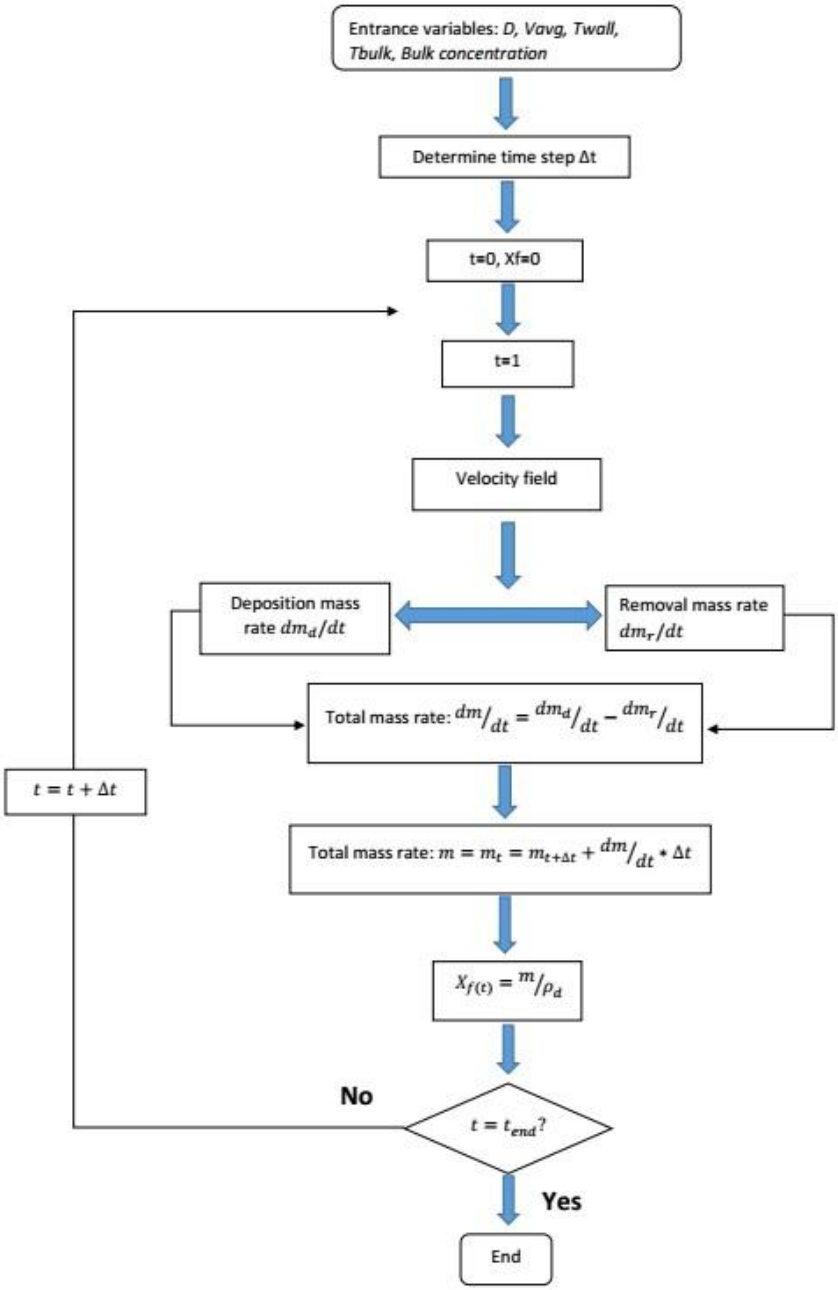

Figure 3.5: Scaling prediction chart

The models parameters are; Particle concentration(C_f), Bulk temperature(T_{bulk}), Flow velocity(lt/min) and Wall temperature(T_{wall}), these are the main factors which can affect the scale build-up process.

3.7 Heat Analogy

Describe the fouling process where the scaling rate is evaluated on therms of R_f (fouling resistance) with this value scale thickness is derived from having an approx-

imation of the tube scaling process and proceed with the mitigation strategies.

The scale formation model is derived from the work by Belmar and Beiny [5] on heat transfer exchangers:

$$R_{Tot} = R_o + R_f \tag{3.59}$$

Where R_{Tot} is the total heat resistance of the system m^2K/W, R_o is the heat resistance without fouling and Rf is the fouling resistance, rearranging the formula based on the work of Pakkonen [19] the fouling heat transfer can be determined by:

$$R_f = R_{Tot} - R_o = (((T_w - T_{bulk}))/q_t)_t - (((T_w - T_{bulk}))/q_t)_0 \tag{3.60}$$

Where q is the heat flux, t, and 0 denote time and initial time respectively. T_w and T_{bulk} denote the wall temperature at analyzed pipe section.Where T_{in} and T_{Out} are the inlet and outlet temperatures. T_{Bulk} is:

$$T_{Bulk} = (T_{IN} + T_{OUT})/2 \tag{3.61}$$

The heat transfer rate q from higher temperature to lower temperature comes by Fourier law:

$$q = -kA\frac{dT}{dr} \tag{3.62}$$

k is heat conductivity of pipe material(W/mk), A is surface area(m^2), T temperature in Kelvin and r radius in m. Where A is:

$$A = 2\pi rL \tag{3.63}$$

Replacing 3.29 in 3.28 gives:

$$\frac{1}{r}dr = \frac{-k2\pi L}{q}dT \tag{3.64}$$

Integrating form inside to outside pipe diameter gives us:

$$ln\frac{r_o}{r_i} = \frac{-k2\pi L}{q}(T_o - T_i) \tag{3.65}$$

Rearranging gives:

$$q = \frac{k2\pi L}{ln\frac{r_o}{r_i}}(T_i - T_o) \tag{3.66}$$

For flow assurance problems its more suitable to use the internal heat transfer area[**?**], the steady-state heat flow equation can be written as:

$$\frac{q}{A_i} = \frac{k2\pi L}{A_i ln\frac{r_o}{r_i}}(T_i - T_o) \tag{3.67}$$

The general heat transfer equation is:

$$q = UA(T_i - T_o) \tag{3.68}$$

Where U is the overall heat transfer coefficient(W/m^2K), the value of U in a circular pipe comes as:

$$\frac{1}{U_i} = \frac{1}{h_i} + R_{fi} + \frac{r_i}{k} ln\frac{r_o}{r_i} + (\frac{1}{h_o} + R_{fo})\frac{r_i}{r_o} \tag{3.69}$$

The overall heat transfer equation used the inner pipe radius. The individual heat transfer coefficients, h_i and h_o are referred to the inside and outside heat transfer areas, respectively. Hence the term r_i/r_o. The terms R_{fi} and R_{fo} are the inside and outside fouling resistances, respectively. The terms $_i$ and h_o comes in function of Nusselt number:

$$h_{i,o} = \frac{kNu}{d_{i,o}} \tag{3.70}$$

Where Nusselt is in the function of Reynolds and Prandtl number;

$$Nu = 0.023Re^{0.8}Pr^{0.3} \tag{3.71}$$

with Prandtl number:

$$Pr = \frac{C_p\mu}{k} \tag{3.72}$$

For a heating pipe, the Prandtl number changes to 0.4.

3.7.1 Fouling curves

The fouling process is indicated by fouling factor R_f described by heat transfer; this representation is the fouling curve $(R_f - t)$.Typical fouling curves are in figure 2.3.

The delaying time, t_d, indicates an initial time without fouling formation. t_d is not easily predicted, however, for some surfaces or heat exchangers systems, the fouling can be random, and a pattern can appear. After a cleaning process on affected surfaces, t_d tends to decrease. Most common fouling curves are:

- Linear curve, indicates a constant deposition rate (ϕ_d) associated to a remotion rate (ϕ_r) negligible in this case ($\phi_r \approx 0$) or a difference between ϕ_d or a constant ϕ_r. In this way the fouling deposition increases on-time generating a straight line ($R_f = a_t$) where"a" is inclination.

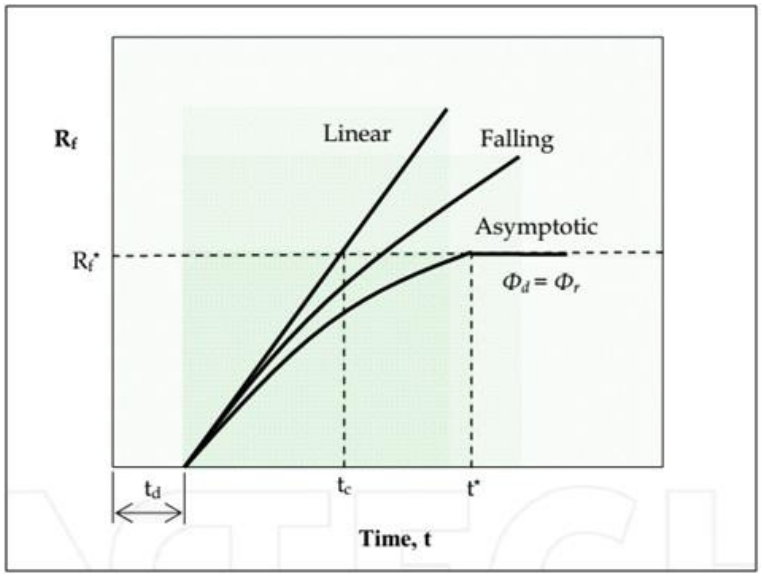

Figure 3.6: Fouling curves [5]

- Decay curve; Results in a decreasing deposition rate ϕ_d and constant removal rate ϕ_r. The deposition rate increases over time but not in a linear form.
- Asymptotic curve ϕ_d and ϕ_r are directly proportional until ϕ_d=ϕ_r.In this way, the deposition rate decays with time, then exist the chance of operating the equipment without an increase in the deposition.

On industrial operations, the asymptotic (R_f^*) curve can be reached in a matter of minutes, or otherwise can take as long as weeks or months, depending on operation conditions.

For this models the materials deposited for unit area (m_f) are related to fouling resistance(R_f), scale density(ρ_f), thermal conductivity(K_f) and deposit thickness(X_f) by the next formula:

$$m_f = \rho_f * X_f = \rho_f * K_f * R_f \tag{3.73}$$

where

$$R_f = \Delta R_f / K_f \tag{3.74}$$

Some values for K_f are in table 3.3

The curves on fig. 3.1 are assumed as ideals in as much as industrial situations these curves can't be observed explicitly. An approximated representation can is on fig.3.7.

The sinusoidal form may be due to fouling removal during short periods followed by a fast fouling increase. The segmented curve represents an ideal asymptotic characteristic.

Table 3.3: Thermal conductivity in some typical fouling composites[6]

Fouling Material	Thermal conductivity$(W/m*K)$
Alumina	0.42
Biofilm	0.6
Carbon	1.6
Calcium Sulphate	0.74
Calcium Carbonate	0.97[19]
Magnesium Carbonate	0.43
Titanium Oxide	8
Wax	0.24

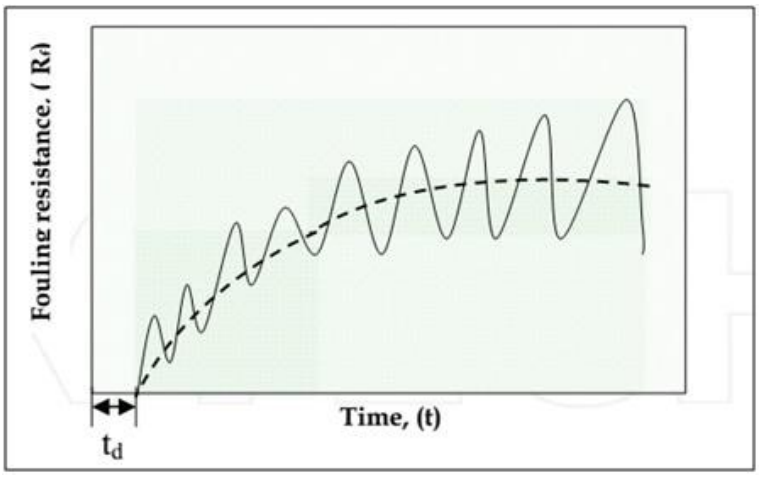

Figure 3.7: Simplified fouling curve and periodical fouling curve indicating the delay time [6].

Chapter 4

Experimental loop

The main factors to consider in a scale build-up experiments related to $CaCO_3$ are:

- Scale concentration: Higher concentrations should increase the amount of scale formed on pipe walls.The experimental systems works in a first moment with $CaCO_3$ and deionized water, to generate the scale, two solution of $CaCl$ and $NaHCO_3$ were combined in the tank:

  $$Ca^{2+} + CO_3^{2-} \rightarrow CaCO_3 \tag{4.1}$$

  Once the solution is combined $CaCO_3$ particles are formed and travel in the loop system, Shirdel[3] states that scale particles travel in the buffer zone of the pipeline system until reached a stopping distance depending on particle diameter and fluid conditions. Between the fluid conditions, the viscosity of the mixture can have an essential role because it could affect the flow regime, concerning this, a rheometer is used to test the different mixture viscosity used in the experimental system at different temperatures.Also, the concentration of particles(ppm) travelling in the loop system was monitored in three sections; tank, entrance and outlet of the loop system during all the experiments using a particle concentration turbidity equipment (DIGIMED DM-TU-EBC).

- Flow velocity: Flow velocity has a complicated role in fouling. The increase in velocity enhances mass transfer and promotes deposition, which is due to the increased turbulence and further ions transport. Increased shear at the interphase reduces the probability of the adhesion of the depositing material reaching the solution fouling layer inter-phase. Therefore, the increase in the flow velocity may either increase the fouling rate (mass transfer controls) or decrease it if the interfacial shear has a more significant effect (surface integration controls)[38]. Greater flow velocities lead to higher turbulence intensities, which increase transport rates in the hydrodynamic core by eddy diffusion. As

a consequence, large particles reach the boundary layer with higher velocities, and their deposition in free- flight due to particle inertia is enhanced. Submicron particles also tend to reach the boundary layer with higher velocities. However, they are so small that their momentum is still limited, and they keep following the turbulent vortex till reaching the tubing surface. The slight increase in deposition velocities observed for those particles is caused exclusively by the increase of eddy diffusion [4].

- Bulk Temperature: Chemical reactions in the fluid are affected by the temperatures since it determines the activation energy of certain chemical reactions.Also it determines the concentration of $CaCO_3$ particles, which varies in function of bulk temperatue as stated by [79].

- Thermal exchange surface: this parameter is used to control the rate of scale formation on the inner pipeline surface, the thermal exchange surface is enhanced at the loop system by the 4400 Watts resistances before the main studied section. The studied section consists of a bypass system performed to create the experimental condiction transduced in thermal equilibrium of the loop system, once the thermal equilibrium is reached the bypass position is changed and opens to the test section which is monitored in real-time by the IR camera at a distance of 0.4 m.

- pH: This factor determines the alkalinity or acidity suitable for certain minerals to form. During all the experiments with the turbidimeter measurements, pH measurements were performed.

- Surface Roughness: some surfaces are more likely to encourage the formation of biological fouling, and some improve mineral deposition. A rough surface provides a broader area that serves as a bond site that favours inorganic salts attachment. The wall roughness of the loop system was measured (stainless steel 304L) by a profilometer model DEKTAK II-A, fifteen measurements were performed on sample surface without treatment. The prove extracted for measurements and Profilometer are in fig4.1.

Table 4.1: Specification of pipe wall roughness

Roughness Mean Value	Units
22606	Armstrong
2,2603	micrometers
Relative roughness e/D_i	0.000827949

Figure 4.1: Profilometer and sections to roughness measurements

- Geometric Surface Configuration: is one of the major issues that could affect the fouling rate.Complex geometries can generate fluid phenomena which can encourage or diminish surface deposition, those effects can be expected in valves, manifolds, pumps, among others.

4.1 Loop configuration

The experimental loop, consists of a stainless steel mixing tank which concentrates $CaCO_3$ at fixed temperature, controlled by a C-704 process actuator, commanded from a main control system. From the tank, the fluid is conducted by a stainless steel gear pump, along the loop are several sensors ,described later, each sensor is connected to a real-time data acquisition system NIcompactDAQ(cDAQ-9174) and processed in a software developed in Labview.

After the pump comes an electrical resistance ,with maximum heating rate of 2200 Watts, it induces temperatures of 80 ° C on wall surface, temperature induction is controlled by a process controller C-704, connected to a temperature sensor in the loop, a especific section is monitored by the IR camera and three RTDs distributed on the wall.The test section is separated by flanges and a three way valve from the rest of the circuit, so it can be extracted and inspected during the experiment execution without stop the experimental process, a detailed description can be observed in figure 4.8 .At one section are inserted two cylindrical coupons which are measured after and before the experiment in order to have an quantitative measurement of the scale build up.Main components are described ahead.

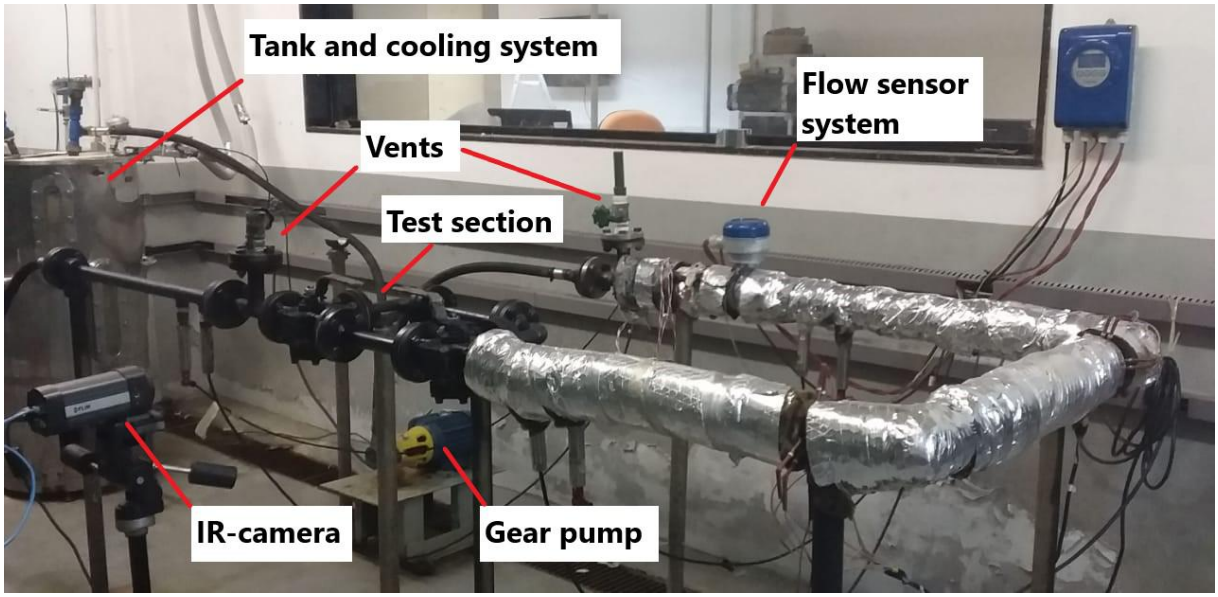

Figure 4.2: Experimental Facility constructed at Subsea Technology laboratory

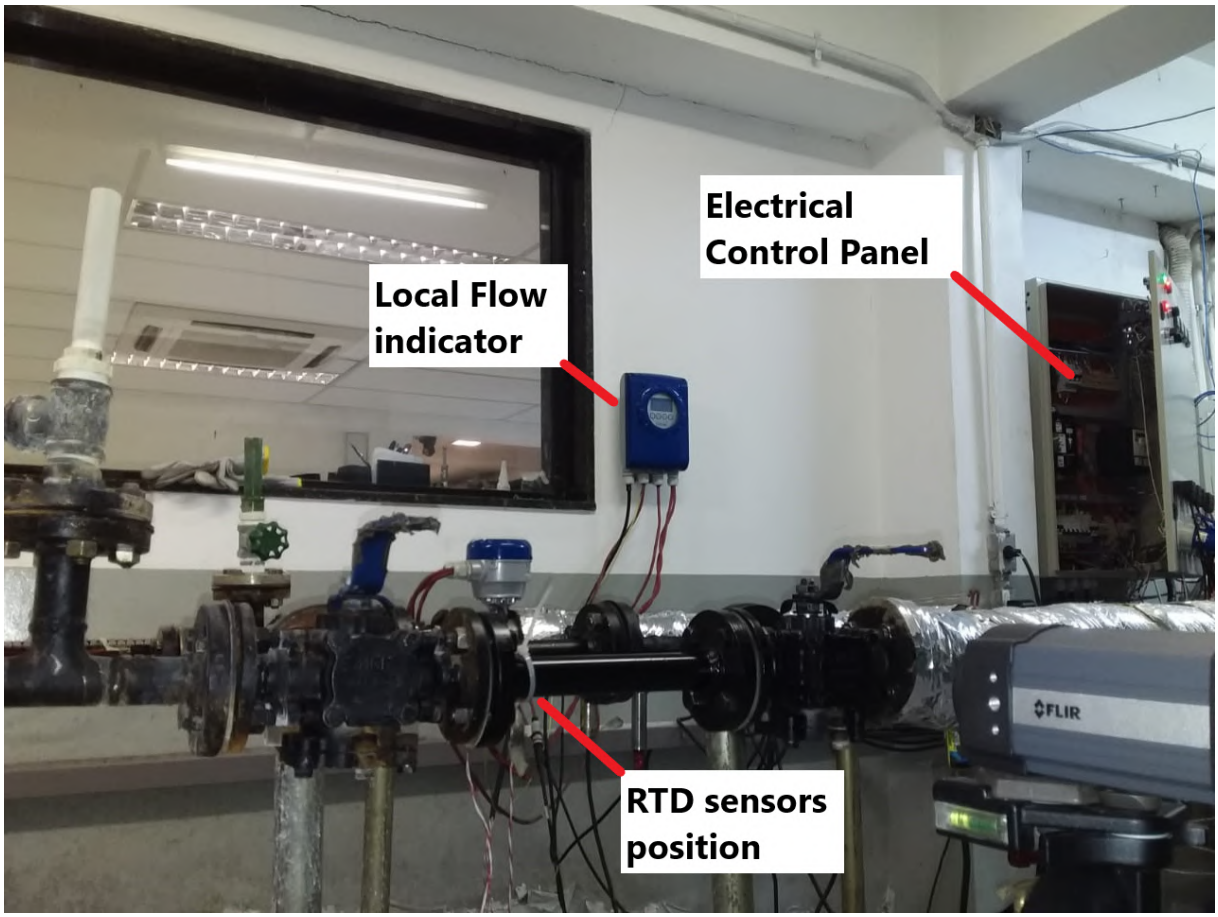

Figure 4.3: Experimental Facility constructed at Subsea Technology laboratory

[A]

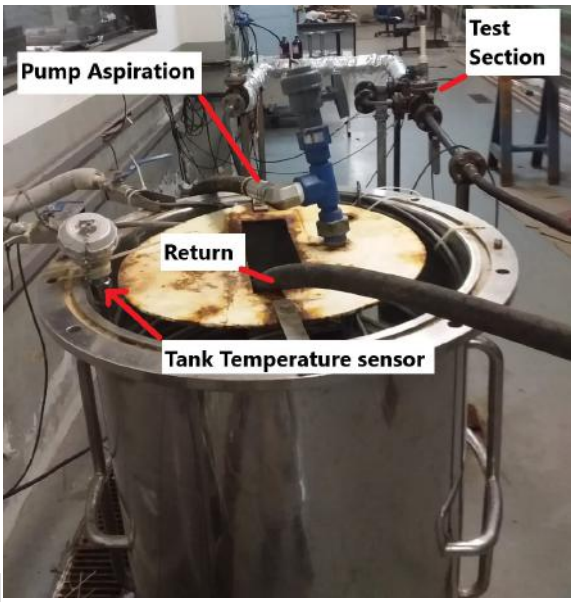

[B]

Figure 4.4: A)Tank System details, B)Tank system details

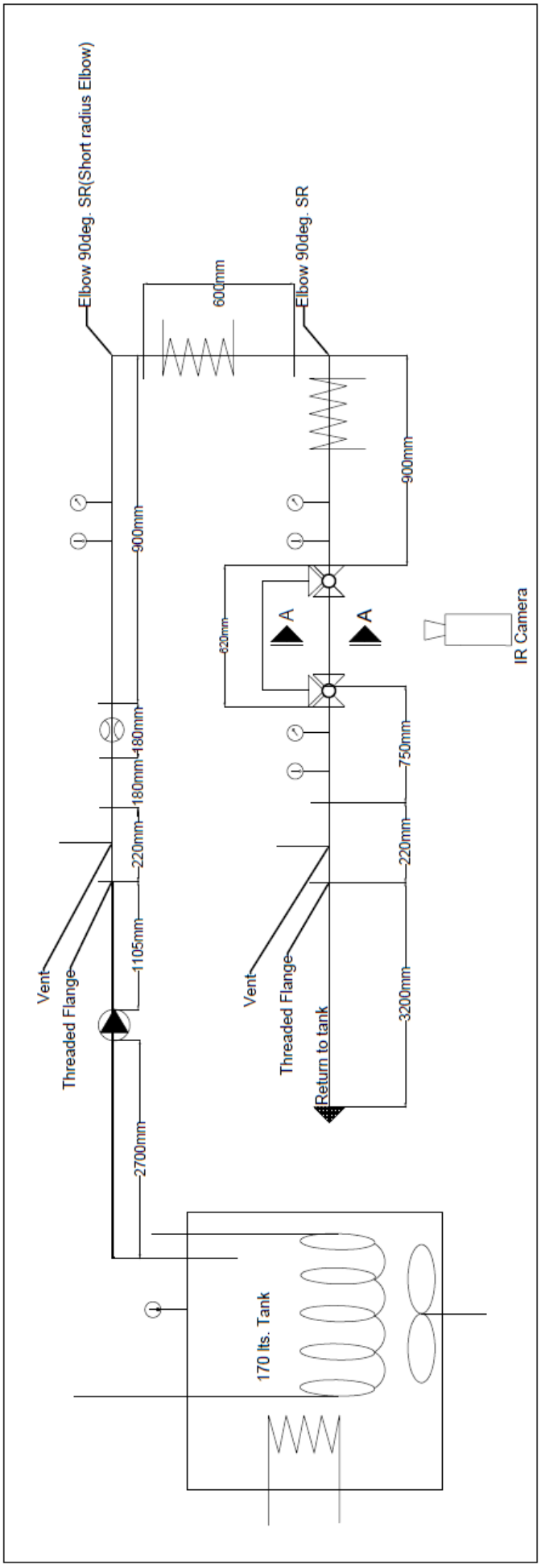

Figure 4.5: Experimental Facility ; Schematic diagram.

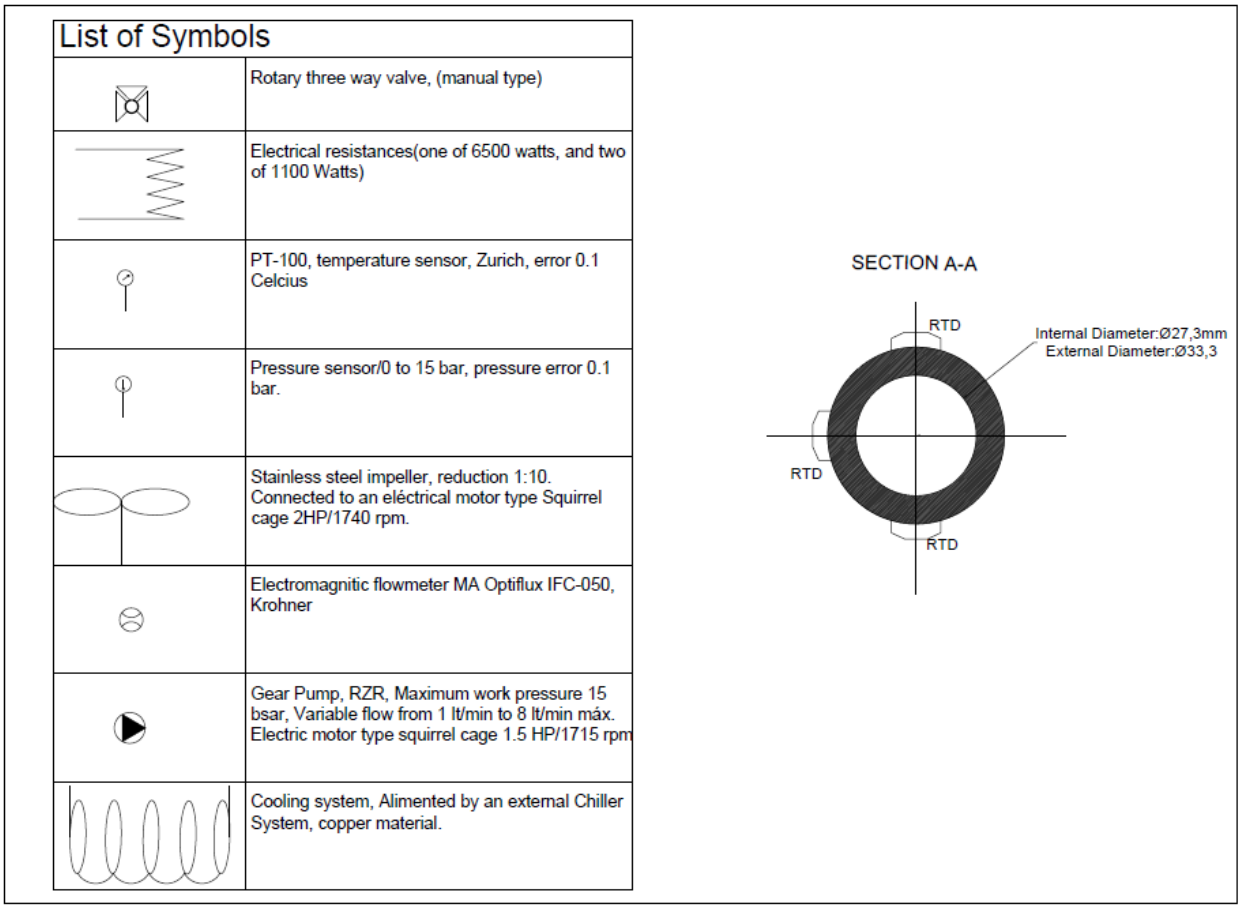

Figure 4.6: Symbols and pipeline test section details

De-ionization system

This sub-system consist on a filter for heavy particles and a pressurized chamber composed of a reverse osmosis(RO) membrane, this membranes are capable of generate 5000 liters during the service life, allowing to generate around twelve consecutive tests without changing the RO system.

Mixture tank

The mixture tank consists of a 170 lt stainless steel tank where its embedded an electrical resistance heater to mixture deionized water and salts at the specified temperature to generate the required fluid composition. It has a stirrer system composed of an 1870 RPMs electrical motor connected to a 1:10 gearbox, which is connected to the impeller to dilute salts and a temperature sensor, to control the heat resistance. As the mixture recirculates to the tank, the heat in the system increase as heated fluid returns from the loop system, to counteract this effect, a cooling system was projected which was also in the tank.

Pumping system

Consist of a frequency-controlled gear pump, maximum pressure of 15 bar, which can vary the capacity from 1 to 8 lt/min, can operate from -40 to 240 $\circ C$. The internal components in direct contact to the fluid can be exchanged as the particles, and Cl ion content can modify the material properties of the gears.

Heating system

The heating system consists of three resistances distributed in three points, one at the mixing tank to heat 170 liters, the resistance has a capacity of 6500 watts. Then there are two resistances before scale induction section, to induce the scale precipitation, these have a capacity of 2200 watts each one. Also, to avoid heat losses, the loop system is coated by mineral wool.

Cooling system

It consists of a section of copper tube inserted in the tank to prevent the fluid from reaching a temperature higher than that controlled by the electrical resistance, this problem was found in the first calibrations due to the fluid transporting the heat due to the presence of the electrical resistors placed in the experimental circuit. The system is powered by an existing cooling system in the laboratory which feeds other experiments through a manifold, the cooling fluid is composed of a mixture of water and glycol. Particular emphasis was placed on taking care of possible leaks of this mixture in the experimental system.

Mass Deposition Rate - Test Section

It was created a removable section to measure the mass deposition rate during each experiment. It was used as a by-pass to avoid stop the pump between mass deposition measurements. The bypass is shown in Figure4.8 and figure 4.9.

Data acquisition system

The required time to achieve the scale phenomena varies depending on scale concentration, induced heat and flow velocity. To detect when the process reaches an asymptotic curve. Measurements were made using three RTD(resistance temperature detector) in addition to the RTDs; an infrared camera was used to infer when the test section presented deposition, based on the theory that scale decreases the effective thermal conductivity of the pipe[84]. The acquired data is essential and gives information about scale stabilization depending on temperature, to know

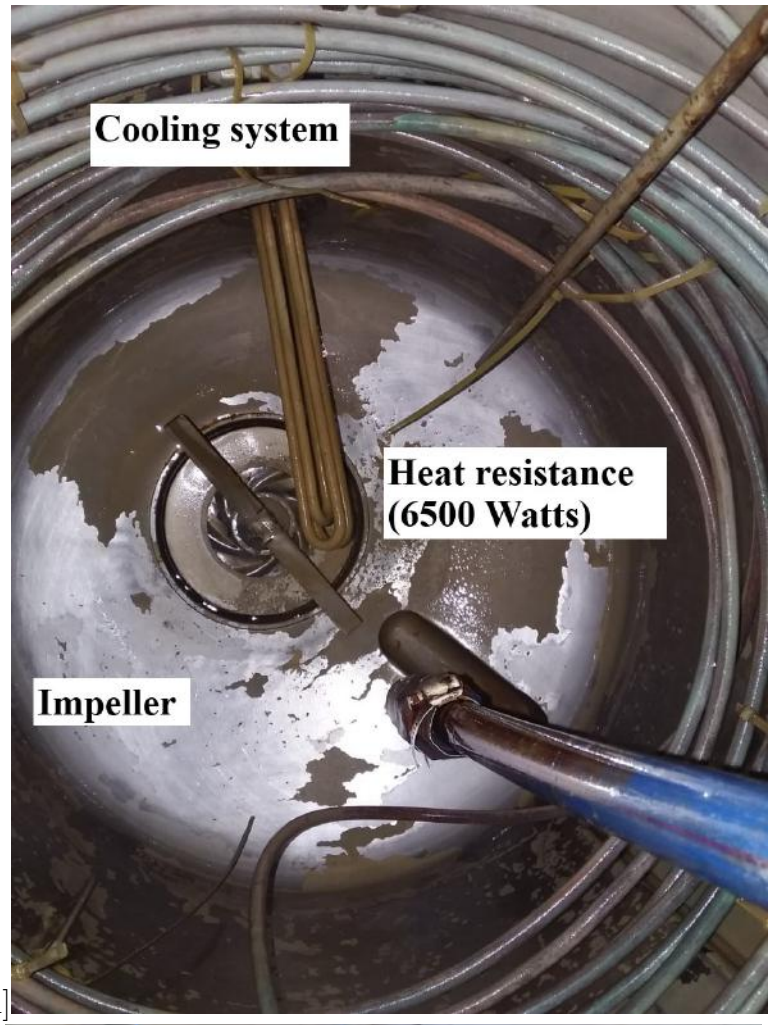

[A]

[B]

Figure 4.7: A)Tank resistance, B) Resistance on the loop system

which control parameter influences the scale build-up or to know when to stop the experiment and avoid major energy and waste disposal.

The data acquisition systems are composed of a NI-DAQ, and by an Infrared camera, the DAQ system logs the most of data, and the infrared camera determines the heat flow over the test section, principal acquired main parameters are:

- Bulk and wall temperatures are a critical parameter; these determine the accu-

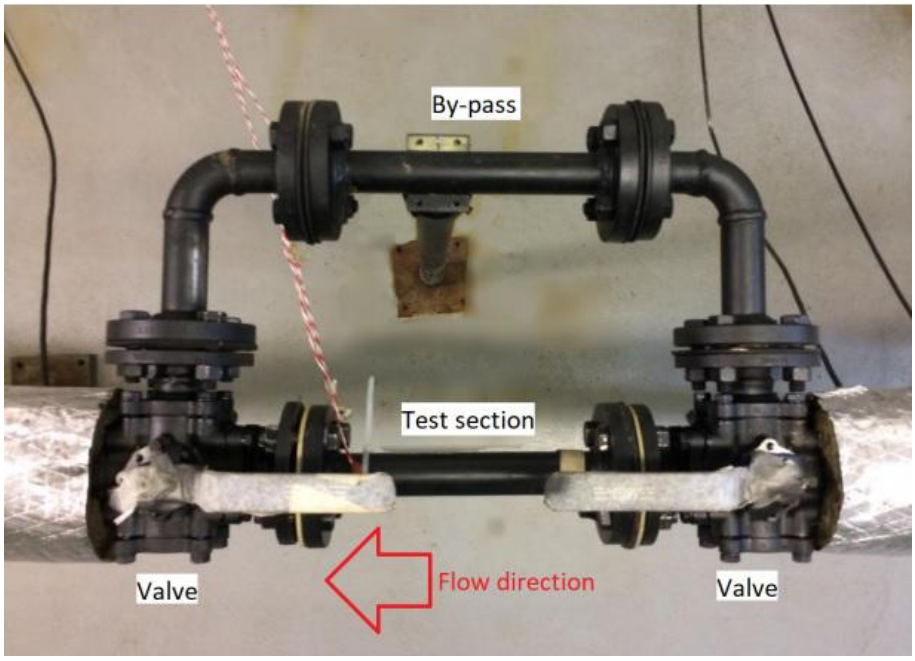

Figure 4.8: Scale build up measurement section with the Three-way valves in order to not stop the experiment.

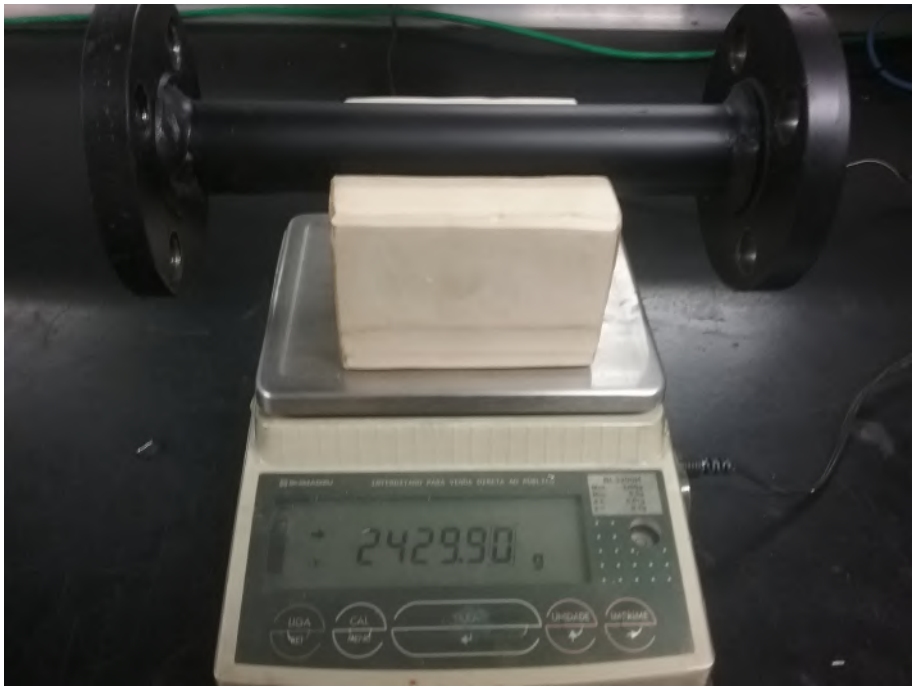

Figure 4.9: Scale build up measurement section

racy of Fouling resistance R_f.In the loop, three RTDs are on the test section, and one is used to measure room temperature. The mixing tank has another sensor connected to a PLC controller to control the heat resistance in the tank.

- Pressure: the relation of scale deposition and the pressure drop were studied,

Figure 4.10: DAQ system employed in the experiment

four pressure sensors distributed along with the loop system.

- The loop flow rate system has an external converter which permits a fluid flow visualization in the experiment zone and a transmission system to send fluid flow data to the DAQ system.

4.2 Scale detection techniques

Rostron [9]presents a comparison of different techniques to detect scale build-up in pipelines with different scope, table 2.3 compares the techniques concerning the studied in this work.

X-ray is a reliable way to detect deposition, but its use gets complicated and expensive for the amount of time and data which it is expected to generate the scale build-up through the pipe cant be determined in a short time also the image its on 2D which difficult the scale location. Da Silva[85] researched hammer impact (HI), it quantified the amount of scale depending on the pipe response, before any expected response an initial pipe response without fouling or failures must be generated, however the hammer impact over the pipe can modify scale deposition, finally noise produced by pumps and flow can affect the HI reliability.

Acoustic reflectometry [86] can be used to detect scale, but because of the size of the experimental loop, a rearrangement of the system would be necessary.

Tomography is getting attention lately because this technique can generate a 3D image of the pipe section, but has limitations related to its point to point measurement technique. To form an image, the equipment has to rotate over the pipe, consuming time and processing to generate one single image. Equipment cost is also one drawback.

One of the significant ways pipeline operators detect corrosion is with a

Table 4.2: Specification of main components and measurement instruments.

Component	Manufacturer	Description
NI cDAQ-9171	National Instruments	analog Imput module, four slots
PT-100 Temperature Sensors	Zurich	Temperature sensors, ranges between -20 and 100 degC
RTD Temperature Sensors	TCdirect	
Pressure Sensors	Zurich	pressure 0 to 15 bar
Flow meter	Optiflux IFC-050	Flow sensor current conversor
Gear Pump	RZR pump	Gear pump, maximum pressure 15 bar, variable flow from 1 lt/min to 8 lt/min, internal parts in direct contact with fluid can be changed,/electric motor type Squirrel cage 1.5 HP/1715 rpm
Mixer		Stainless steel mixer /174 rpm/ electri motor type squirrel cage/2 HP/ 1740 rpm
IR camera	FLIR systems	FLIR A325sc with 25º lens, 60 HZ, 320x240 pixels -20 to 350 deg C
Socket Weld Flanges	one inch internal diameter	Satinless steel ANSI B165/150 A182 F304
Stainless steel pipeline	one inch internal diameter	Satinless steel ANSI 304L

...

"pig"(pipe inspection gauge) a tool that travels down the inside of a pipeline looking for corrosion and other anomalies. Pigs are not new - the industry has long relied heavily on them—and the newest generation of pigs, known as "smart pigs," is considered an improvement over the pigs of yesterday. Intelligent pigs give a read on the state of the pipeline, such as cracks, corrosion, and metal loss. Operators receive this information in a control room and can then dispatch crews to fix the problem. As of 2012, 93 per cent of pipeline inspections were conducted using smart pigs.

Even though there is a high diversity of technologies for scale detection and measurement, the most used in industry and academy are heat transfer and pressure drop, the principal detection techniques used in these experiments were; IR camera,

Table 4.3: Specification of main scale detection techniques[9].

Detection Techniques	Types can be detected	Identify composition of scale	Identify location of scale	Identify scale thickness	In-situ or off line monitoring
Ultrasound	Inorganic and organic	X	Not applies	Not, needs more studies	in-situ
Infrared	Inorganic and Organic	Not	Yes	Need more research	in-situ
Radiation detector	Inorganic and Organic	Yes	Not applies	Not	In-situ
Acoustic emission	Inorganic and Organic	Not	Yes	Need more research	Off line and in-situ

Table 4.4: Specification of main components and measurement instruments.

Method	Description	Main factors affecting sensor during the experiments
Temperature sensors	Several sensors are embedded inside the pipe and on the pipe wall	analog Input module, five internal gaugues
Infrared camera	One section its monitored by the IR technique	Temperature sensors, ranges between -20 and 100 deg C
Pressure sensors	Tc direct	Ranges in PSI

Figure 4.11: IR camera installed to detect pipe scaling

temperature and pressure sensors, a more detailed description with their respective results are below.

Pressure drop

An operator of a pipeline suffering from deposition wants to know the amount and location of the deposits that form with time. Pressure drop, tracer testing and pressure pulse measurements, are among the tools that can be used to monitor deposition in pipelines. Monitoring of single-phase (liquid) flow pipelines is less complicated than the monitoring of two-phase (gas and liquid) pipelines. In the present context, stabilized (steady-state) flow of a water solution is considered a single-phase flow. The pressure drop between two points in the presence of deposits is acquired, the entrance and the exit of the main test section are equipped with to pressure gauges.

Heat transfer detection

As stated before, this methodology is based on fouling resistance, R_f calculation, a concept based on the principle that scale build-up inside pipes decreases the thermal conductivity of pipes, two main techniques are used; RTD sensors, Known as resistance temperature detectors, are the most commonly used in industry, based on 100 ohms of resistance at 0° Celsius.Most of the problems related to these sensors are the noise generated by electromagnetic systems, like electrical motors, converters and transformers embedded in the loop.

4.3 Experimental loop development

4.3.1 Attempts

Several experiments were carried out, the evolution of the system varied from changing the mixing tank completely, also as the main pump, as well as various equipment failures related to corrosion and scaling formation, the main experiments in beta phase are summarized in this section, as well as its modifications.

Experimental analyses were performed according to several attempts, two of them based on the work of Vazirian [39]the attempts describe two different processes dominating the scale formation:

Attempt 1-deposition process dominates:

corresponds to an experiment where crystals were formed at the same time that the fluid circulated inside the loop and gets an equilibrium state.

Attempt 2-adhesion process dominates:

Crystal formed inside the tank; then, when reached an equilibrium state(using ppm measurement as reference) mixture started to circulate through the loop, this corresponds to experiment two. This test measures how the presence of pre-formed crystals could change the scale deposition in the loop. It assumes that adhesion dominates and deposition is minimal.

These two scenarios take into consideration a recirculating system, with an initial mixture that reacts inside the system gets an equilibrium state represented by an asymptotic behaviour in the fouling resistance and hypothesis the mass deposition.

Attempt 3- adhesion process without re-circulation:

Crystals formed in the tank when the mixtures get stabilized, the pump starts to circulate the mixture in the pipeline system without returning to the mixture tank.

Attempt 4- adhesion process with re-irculation and maintaining mixture ions

Crystals formed in the tank and when the system gets stabilized the pump recirculates the mixture.The by-pass valve opens once the system gets a stable condition(stabilized temperatures and flow).

4.3.2 Attempt 1

The first experiment in this work followed the next procedure:

- The pump starts to recirculate deionized water
- Heaters were set at a maximum temperature
- Tank temperature was set at 50°C
- $CaCl$ was added to the mixture tank until diluted entirely in the loop system.
- $NaHCO_3$ was added to the tank
- As son as the second component was added, the reaction kinetics starts at the loop system.

The main control variables were:

- Flow velocity
- Initial $CaCO_3$ concentration

- Tank temperature
- Experimental length

The first experiment was conducted during 464 hours, mean acquired values are presented on the table 4.5.

Fouling Resistance

The fouling resistance curves detect the scale formation on time in three points using RTDs sensors and the IR camera, as the figures 4.13 to 4.15, these sensors presented a good correlation with scale fouling, the bottom RTD indicated that exists lesser scale formation in this zone.

The Rf curves on figures 4.13,4.14 and fig. 4.15 shows the phenomena described previously by Wang [38] indicating four distinct regions, a region where the thermal fouling resistance is positive (named the first region), a region where the thermal fouling resistance is negative (named the second region), a region where the fouling resistance increased steadily (named the third region) and a region where the thermal fouling resistance remains constant (named the fourth region). Each of these regions can be matched with different development phases in the crystallization fouling process: nucleation phase, growth phase and asymptotic/falling phase. Relatively small amounts of deposit can improve heat transfer, relative to clean surface, and give an appearance of "negative" fouling rate and negative total fouling amount. Negative fouling is often observed under nucleate-boiling heat-transfer conditions (deposit improves bubble nucleation [8],[87], [88]) or forced-convection (if the deposit increases the surface roughness and the surface is no longer "hydraulically smooth"[30]). After the initial period of "surface roughness control", the fouling rate usually becomes strongly positive.

Table 4.5: Variables used in the first scenario

Initial concentration NaHCO3 + CaCl2		gr each 170 lts	mol/L
Length	464 hours		
NaHCO3	2550	597 gr	mol/L
CaCl	7870	7313 gr	mol/L
Control variables	Mean Value	σ	Units
Flow velocity	1,63	±0,29	lt/min
Wall temperature RTD 1	71,91	±3,27	$°C$
Wall temperature RTD 2	62,58	±5,23	$°C$
Wall temperature RTD 3	73,27	±3,31	$°C$
Ambient Temperature	28,33	±0,68	$°C$
Bulk Temperature	66,51	±2,62	$°C$
Reynolds number	3200		

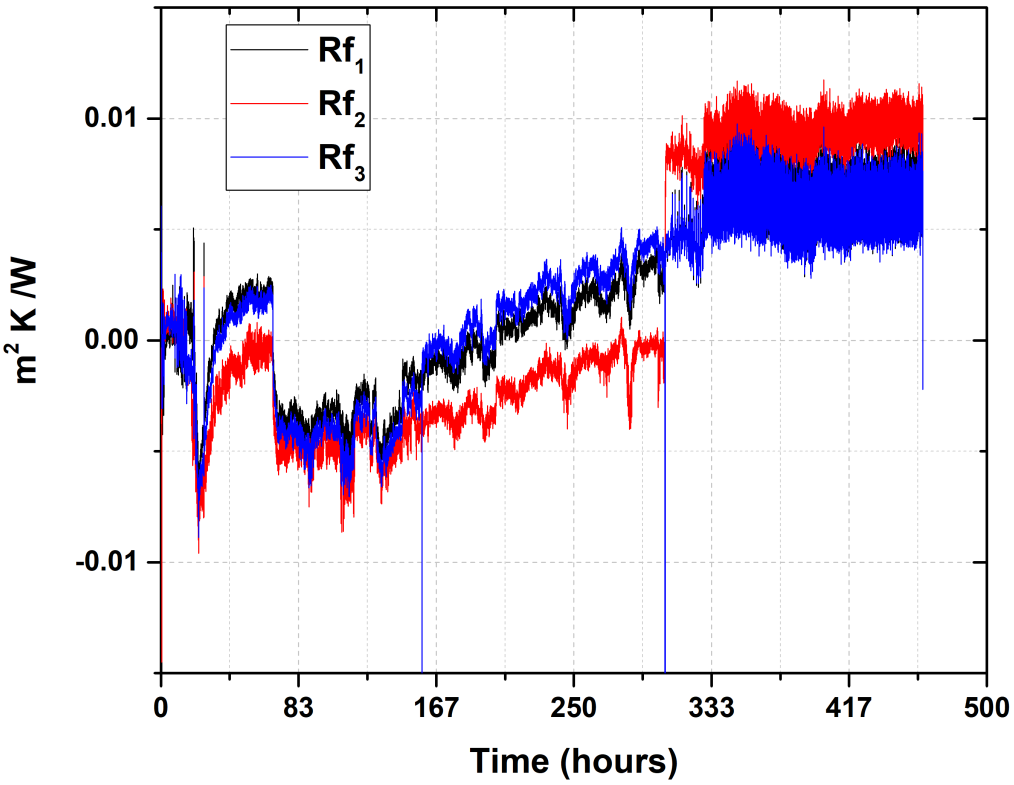

Figure 4.12: Fouling resistance using the three RTDs on the test section

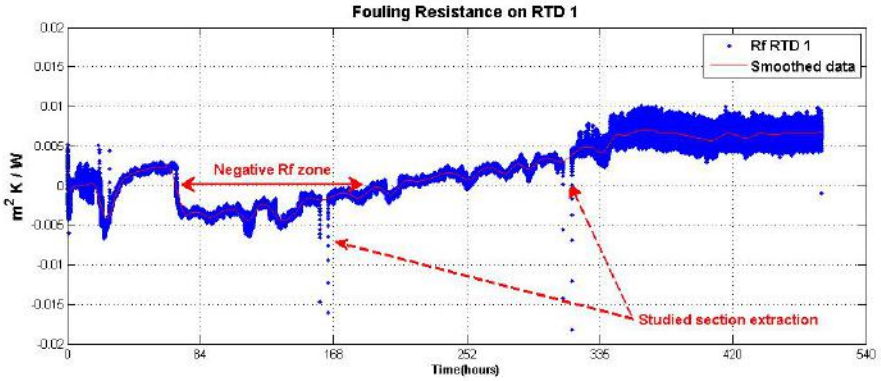

Figure 4.13: $CaCO_3$ growth on time based on Fouling resistance using RTD-1 on upper side of the test section

R_f was calculated using equation 3.44, results are ploted in figures 4.12, 4.13,4.14 and 4.15.

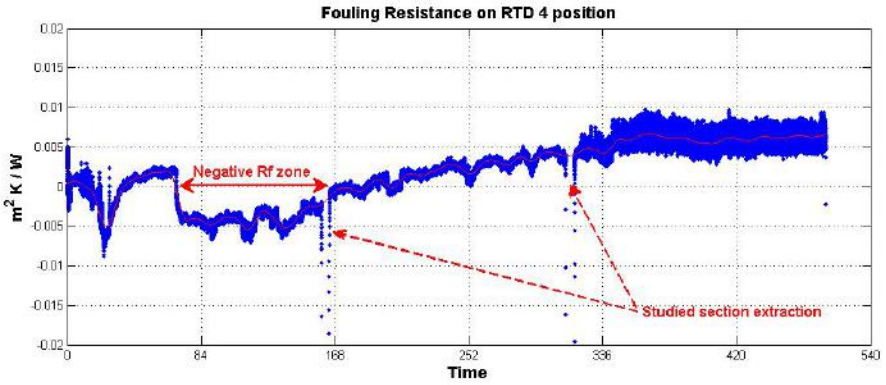

Figure 4.14: $CaCO_3$ growth on time based on Fouling resistance using RTD-4 on side of test section

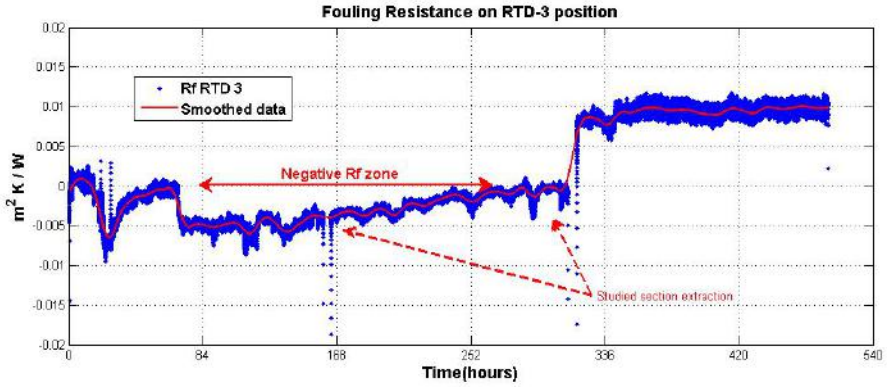

Figure 4.15: Fouling resistance using RTD-3 on bottom of test section

Pressure drop and flow rate

The pressure was studied using pressure difference between inner, and outlet sensors at the studied section, figure 4.16 shows pressure fluctuation during the experiment in PSI.

As stated by several authors, Gudmundsson [89], [90], and other authors [30], [91] studied pressure drop as a method to detect scale build-up during the experiment using the plot of the specific pressure drop(SPD) $\Delta p/\ Q$ the evolution of SPD because of scale growth in pipeline is represented in figure 4.17 .The gradient is known as Flow index FI.

Also figure 4.18 shows the probes inserted before the heating induction zone, this zone shows clearly a straight difference between the influence that presence of heat could have in a surface in comparison with another one without a direct heat induction, these zones shows that deposition is generated because gravity influences(The loop configuration is in a horizontal position), the main induction section presented gravity precipitation but this deposition could have been swept because of eddies

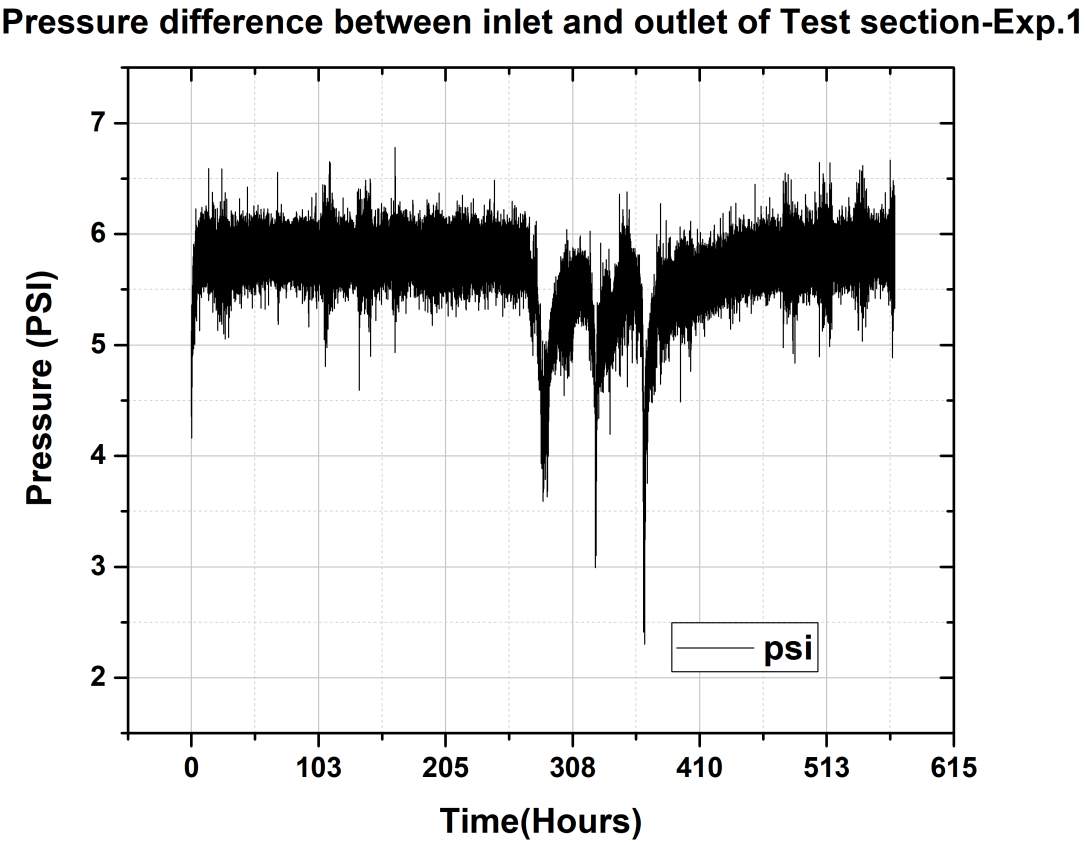

Figure 4.16: Pressure difference between inlet and outlet of studied section.

presented at the moment of change the flow direction at three-way valves to extract the main prove section to be weighted, those could explain the differences between the three fouling resistance curves at 4.13, 4.14 and 4.15, the last one on bottom generated by data logged on RTD sensor has the most significant difference because scale deposition generated the last week of the first experiment.

Mass measurement

Scale growth was achieved in less time than expected once the section test was open at the first week of the experiment and was detected at a simple view, can be observed at figure 4.19 that scale on the test section diminished in every extraction because the section was dried and then restored, when dried, crystals lose part of the ligations, once restored the three-way valve aperture generates eddies that can sweep away the weaker crystal bonds and deposited $CaCO_3$ particles at the bottom part. To compare figure 4.18 shows at different sections which remain inside the pipe for all the experiment and only extracted at the end compared with test section.

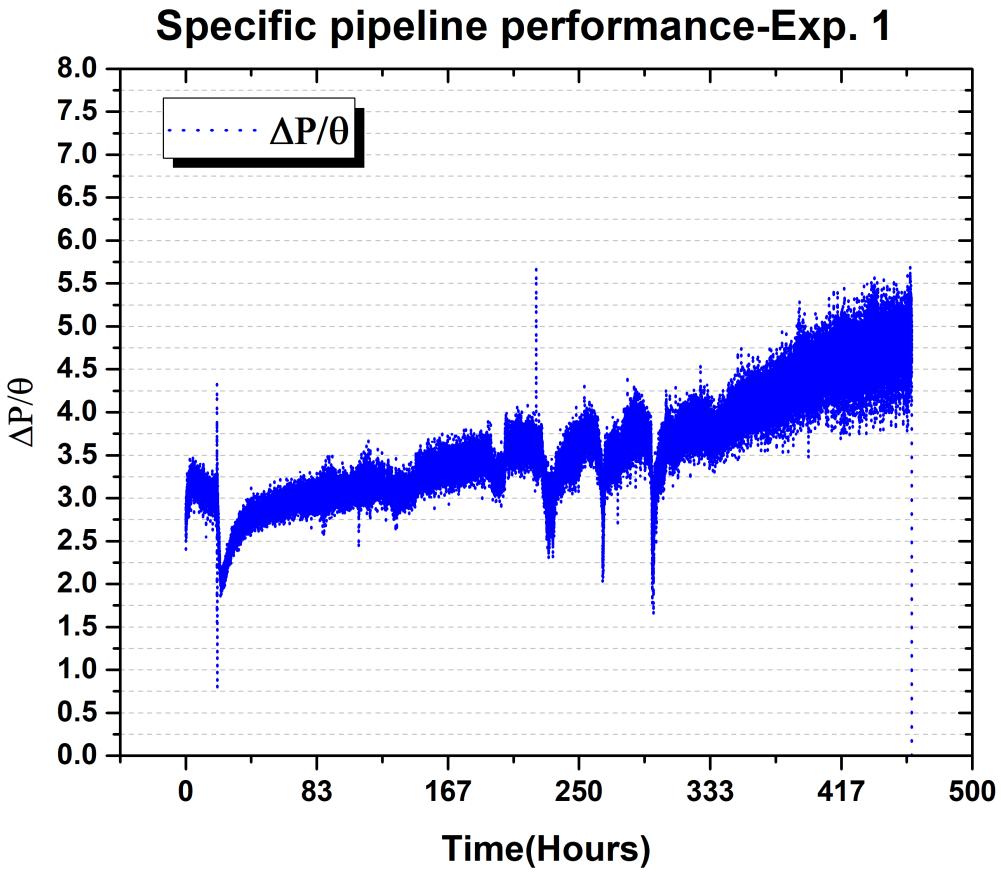

Figure 4.17: Specific pipeline performance during exp. 1.

Particle concentration and pH

A particle concentration turbidity equipment (DIGIMED DM-TU-EBC) was used to measure particle concentration for all the experiment, $CaCO_3$ concentration(PPM) was plotted to study concentration along with the experiment. Range varies between 0 to 4000 NTU(0 to 6000 ppm).samples of hard water to detect $CaCO_3$ concentration were measured every 30 minutes at the first day and twice in a day during the rest of the experiment; the concentration follows a decreasing curve. Also, pH and temperature are measured, ppm, pH and tank temperature were in figure 4.21. Turbidimeter and pH components are in figure4.20.

Samples analyses

Several samples were acquired to detect the different properties of scale depending on the loop section.

Using Chemical analysis by EDS (Energy dispersion X-ray spectroscopy) the samples of the deposited solids were taken inside the Loop system and analyzed, the

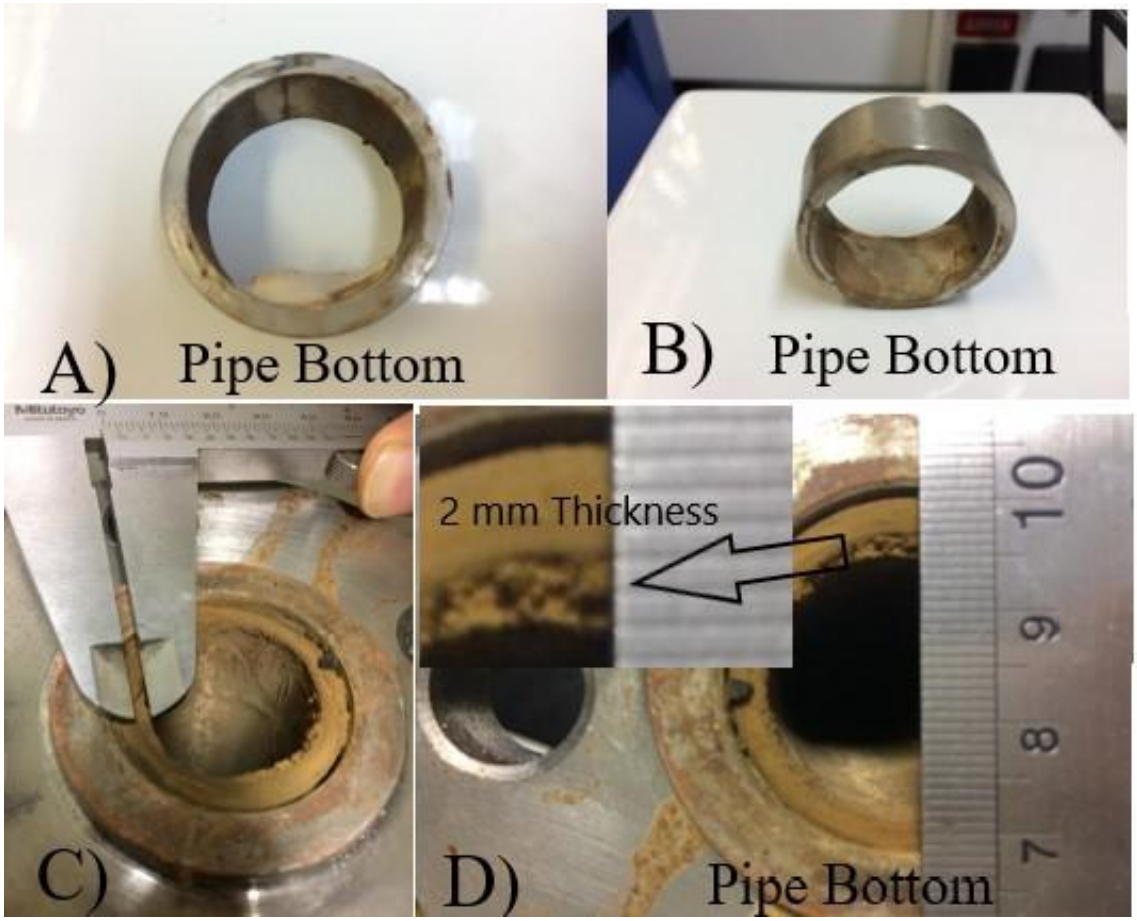

Figure 4.18: Scale growth on time-based section extraction; A)Pipe section without influence of induced heat on walls, with presence of deposition on the bottom of the pipe, the rest of the section remains almost clean, B) the Same section indicating presence of scale generated by deposition.C)Test section influenced by direct heating of pipe wall, scale thickness changes depending on pipe section, been most severe on top of the pipeline as shows figure D) Scale thickness on upper section of 2 mm.

EDS machine was a Thermos Phenon Prox. The EDS analysis can differentiate what kind of crystals are in a particular sample. By the identification of the elements that lie at different points in the system helps to identify the effects that temperature, flow and position can have on the deposition or encapsulation process of calcium carbonate. Some points analyzed were before and after the heating section, the test section and the three-way valve. The results are as follows:

It is possible to observe a difference in the crystals formations in the different points where the EDS analysis is done. The difference is influenced by the presence of other elements such as iron (Fe) as in image D, and also the change in temperature at samples A: before heating section and sample B: test section.

For sample D, EDS has the following results: Oxygen (35%), Iron (30%), Carbon (17%) and Calcium (13%). The results are approximate and do not reflect with the absolute certainty of the sample. Presence of iron is typical when a corrosion process

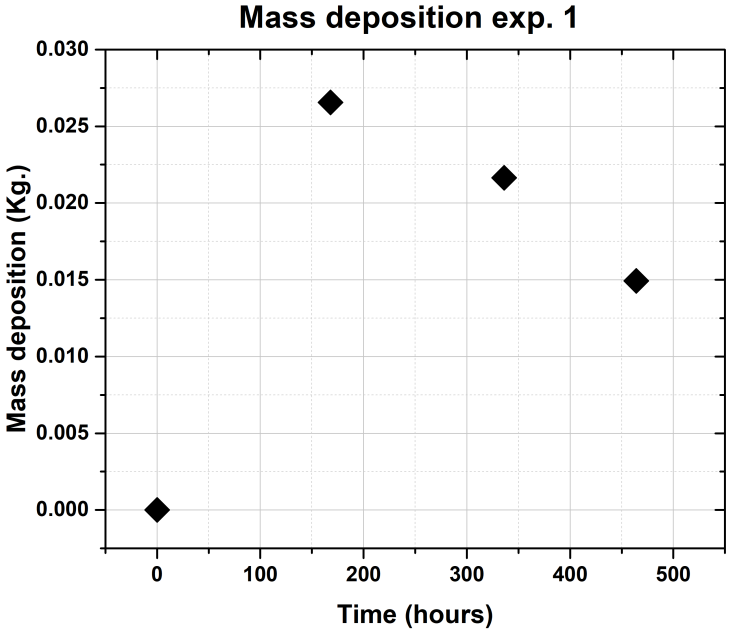

Figure 4.19: Mass deposition rate at first experiment, using dried weighting

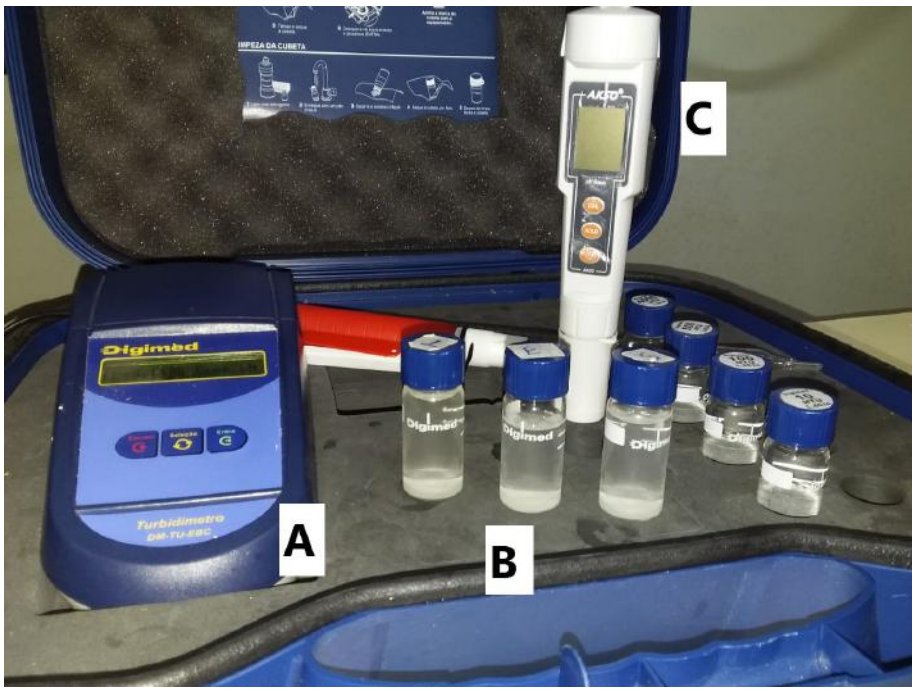

Figure 4.20: *A*)Turbidimeter *B*)Sample bekers for measurement of tank, entrance and outlet of the loop system, *C*)pH gauge

is occurring besides the incrustation. It is possible to see that the calcium carbonate crystals are surrounded by smaller crystals which are where the iron element is found by the EDS analysis. In sample B of the test section, it is possible to see two types

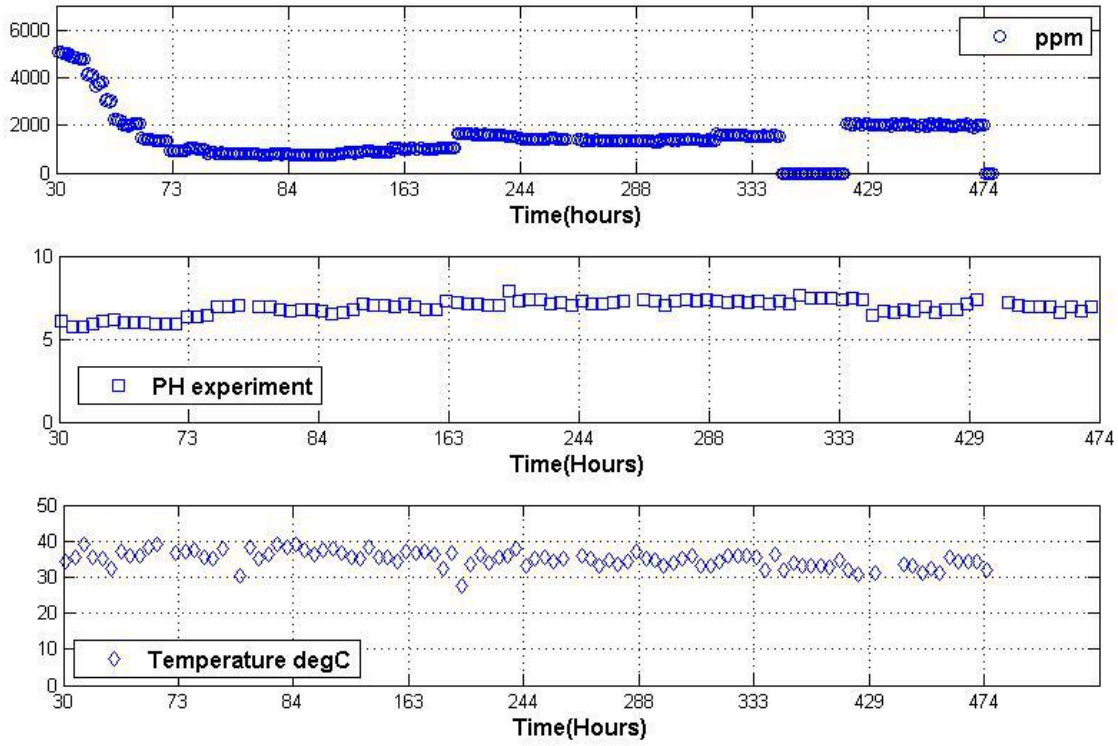

Figure 4.21: Particle concentration, pH, and tank temperature during experiment 1.

of crystals; the calcite crystals are the best formed. The EDS shows presence of O (47%), C (30%), Cu (19%), Cl (7%), Ca (5%). It is possible to see crystals of calcite of different size, influenced by the heating in the section. In sample A, the crystals are more significant than the crystals of sample C in the test section after heating. In sample C, it is also possible to see an accumulation of crystals where the EDS shows that there is the presence of copper (Cu). The presence of iron may be a consequence of small corrosion points inside the by-pass valves. The presence of copper is expected due to the cooling system.

4.4 Attempt 2

The experimental procedure was:

- A $CaCl$ brine is prepared in a tank at 50°C
- Another $NaHCO_3$ brine is prepared at 50°C
- The two solution was mixed until the PPM gets stabilized

[A]

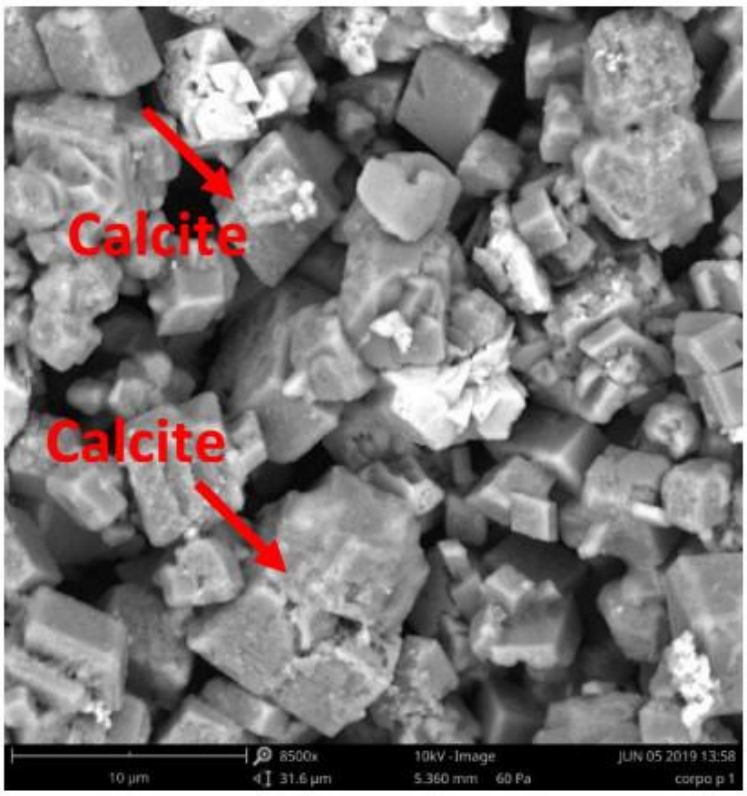

[B]

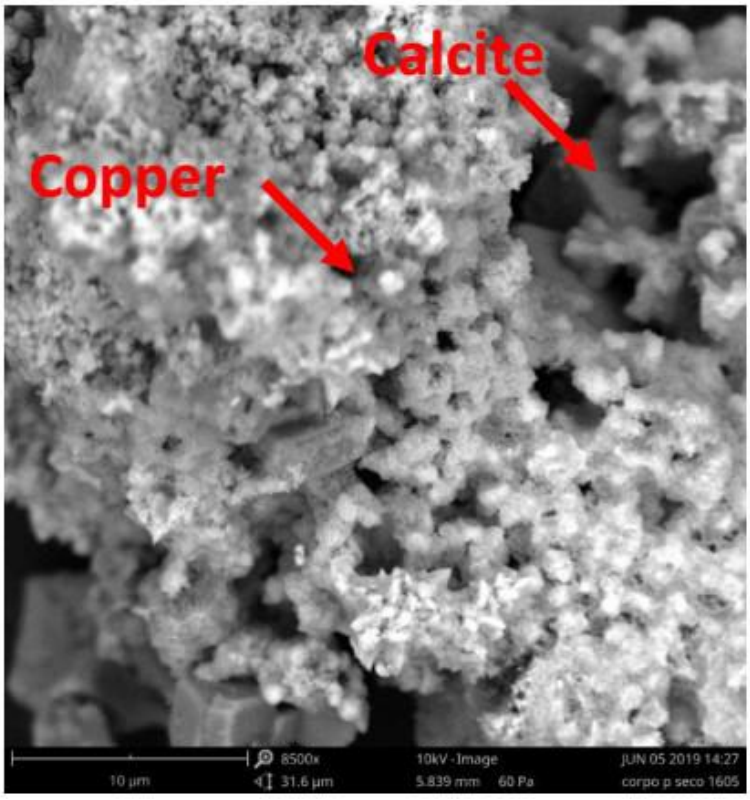

Figure 4.22: EDS: A)Before Heating section, B)Dried Test section

- The heaters were set at 2200 watts each one until reached an approximately 85°C at section test.

[C]

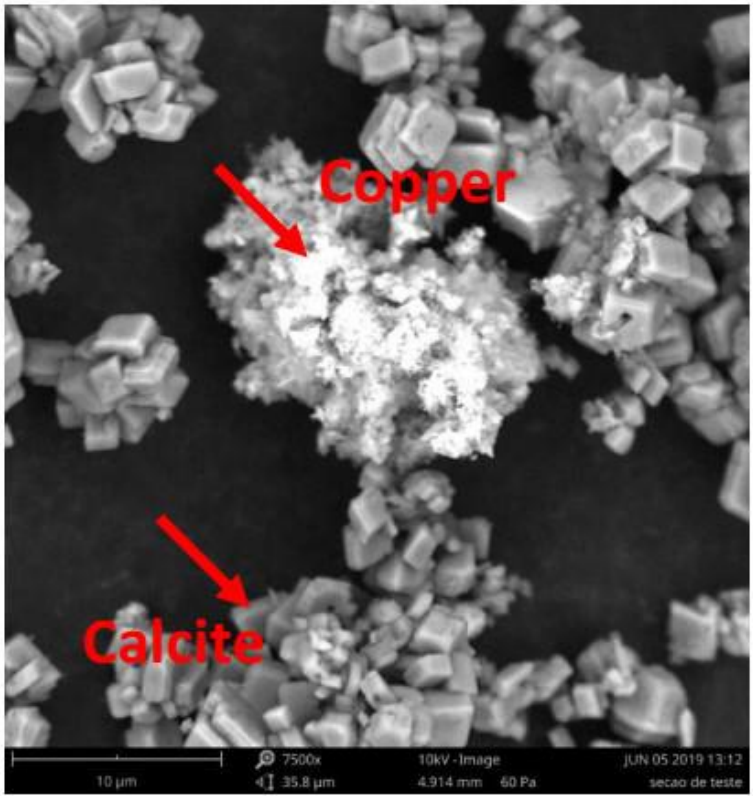

[D]

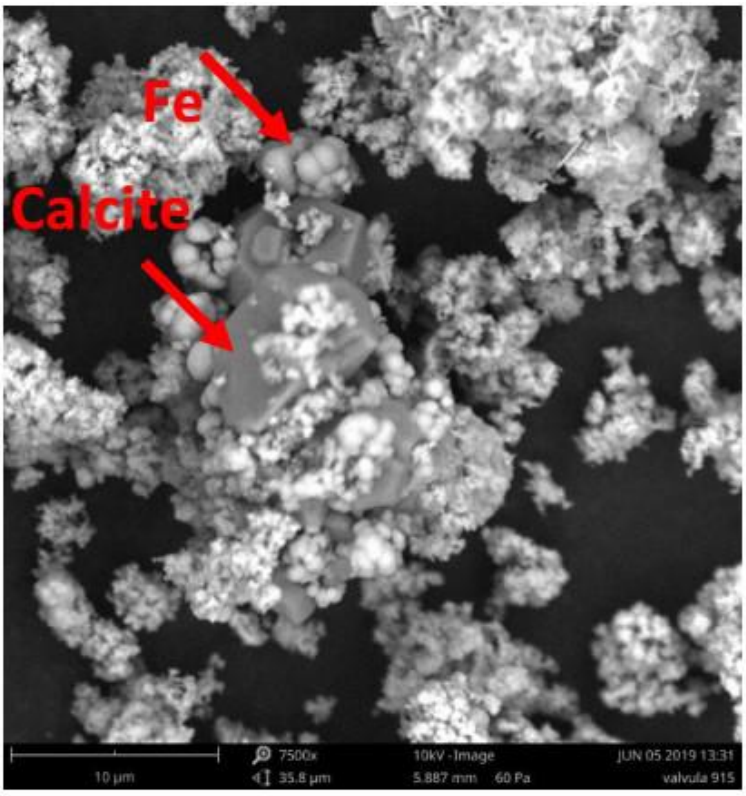

Figure 4.23: EDS: C)Test section, D)By-pass valve

- The pump started to recirculate the mixture in the loop.

Main variables are on table 4.6 The experiment length was 72 hours, the mass was weighted during the experiment, but without drying the measurement section as

Table 4.6: Variables used in the second scenario

Initial concentration NaHCO3 + CaCl2		gr each 170 lts	mol/L
Length	72 hours		
NaHCO3		1170 gr	mol/L
CaCl		7313 gr	mol/L
Control variables	Mean Value	σ	Units
Flow velocity	2,89	±0,54	lt/min
Wall temperature RTD 1	61,39	±8,37	$°C$
Wall temperature RTD 2	52,54	±6,32	$°C$
Wall temperature RTD 3	61,85	±7,97	$°C$
Ambient Temperature	25,14	±0,79	$°C$
Bulk Temperature	57,42	±5,3	$°C$
Reynolds number	4130		

the first case, this avoided the sweep of crystals and bonded scale on the section allowing a proper measurement during the experiment. Results of mass deposition are at figure 4.24

The scale weight against mass deposition of experiments two and three are at figure 4.24.

Those scenarios have demonstrated a significant prompt to scale deposition in lesser time; some images of scale build-up are present above.

As seen in figure 4.24, the scale build-up is in two forms, one as a deposition of particles, most of them because of the gravity effect and crystallization, at the upper walls. To determinate if heating the test section affects the scale build-up crystallization, another image from a section without the significant influence of heat is at figure4.26:

pH and PPM during the experiment are at figure 4.24. Respect to pressure, scenario two shows the same behaviour at the beginning of the experiment as figure 4.27.

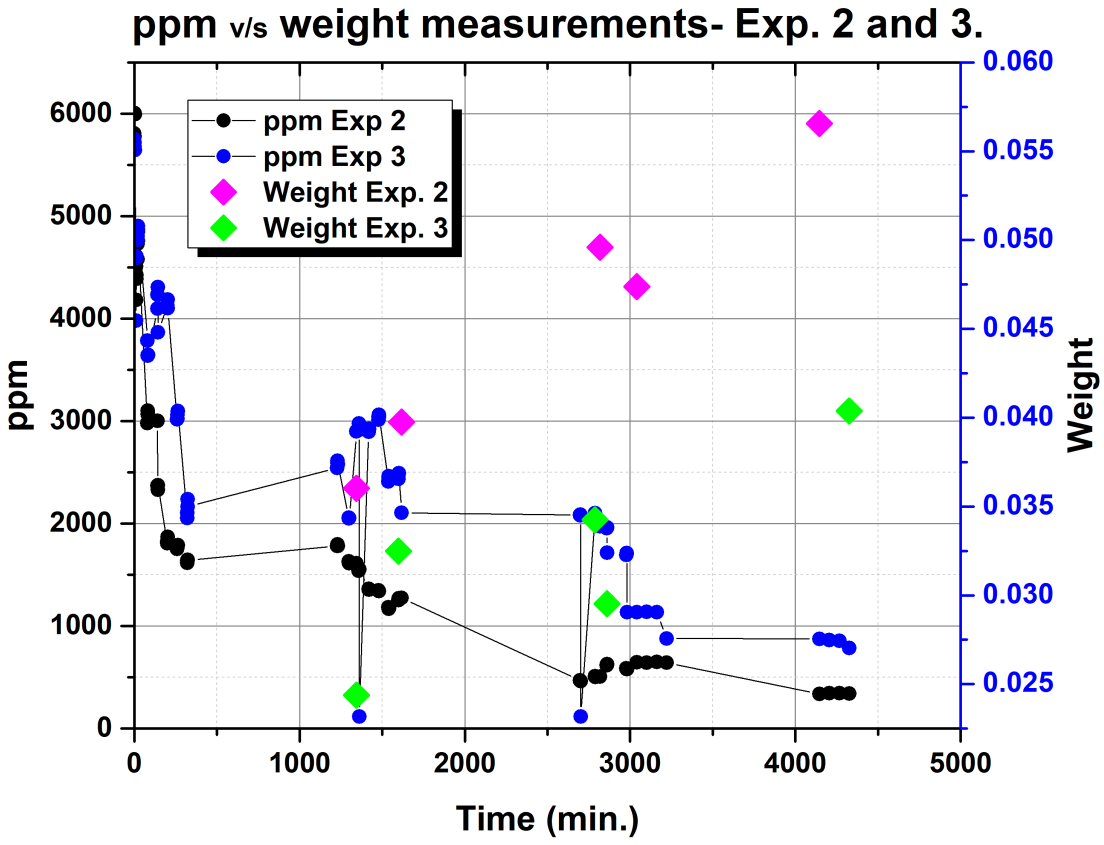

Figure 4.24: Particle concentration and weight on time for attempt two- exp. 2 and 3.

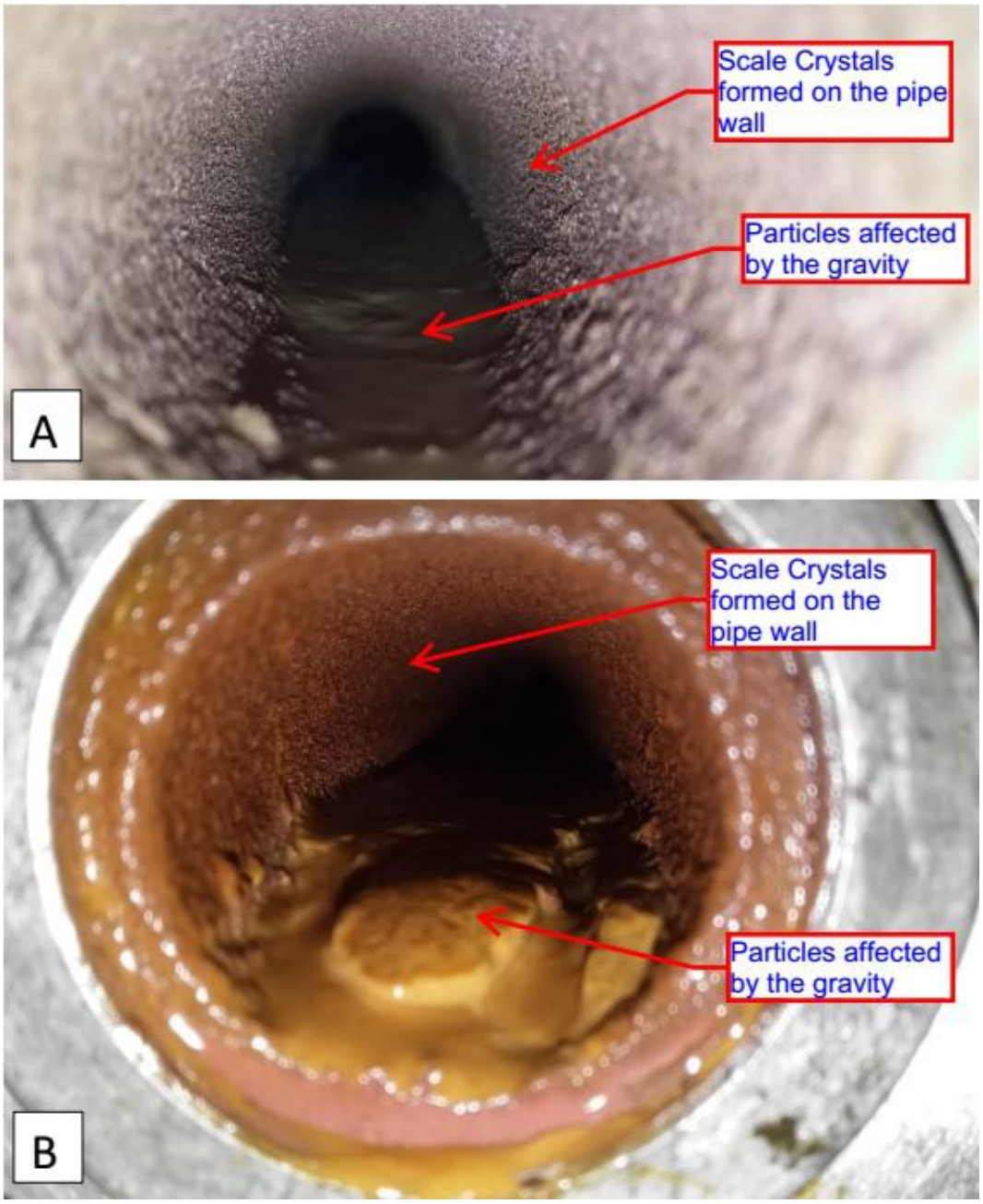

Figure 4.25: A)The entrance of studied section and B)Outlet of the studied section, Can be observed two kinds of deposition and high presence of corrosion particles because of Fe presence.

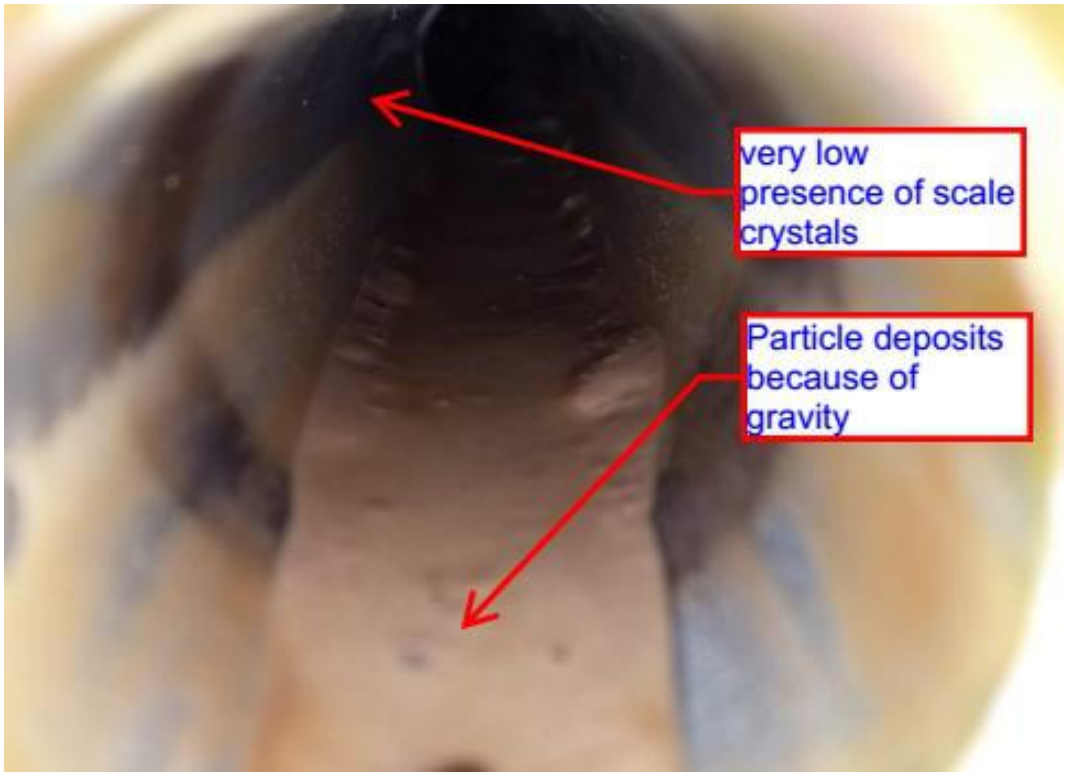

Figure 4.26: Section without the extensive presence of crystallization

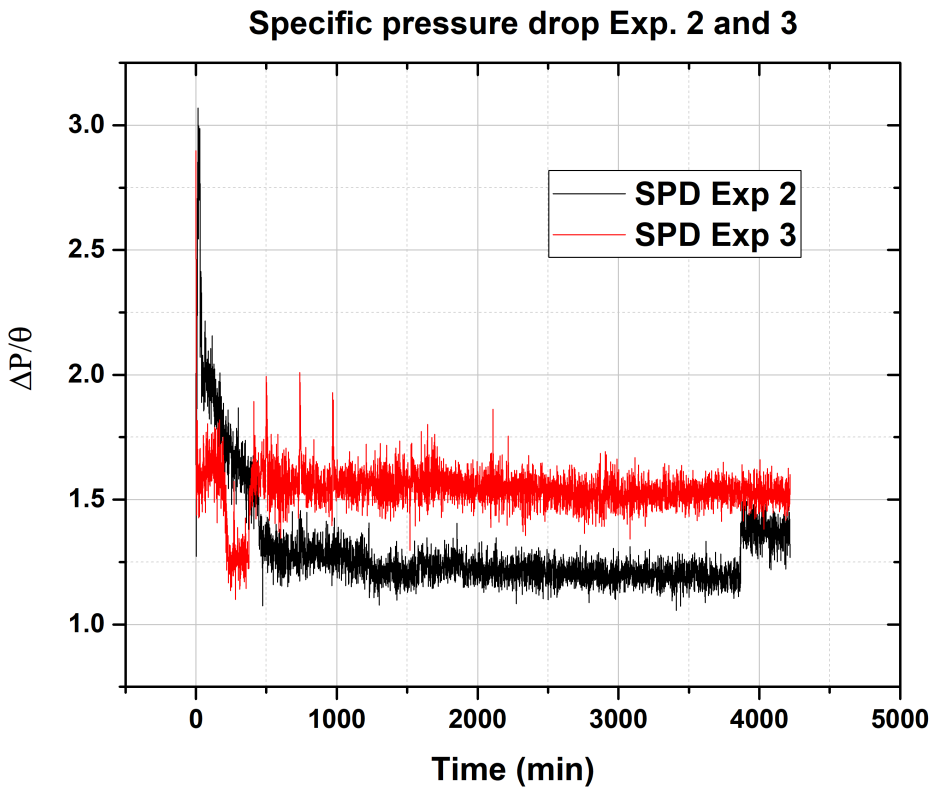

Figure 4.27: Specific pipeline performance during scale build-up the experiment at exp. 2 and 3.

Table 4.7: Observations from Test 1,2 and 3

Test 1	**Scenario 1, lenght 464 hours**
Main difficulties encountered	-Corrosion presence(Fe and Cu particles encountered at the analyzed deposits), because of other materials presents in the cooling system and by-pass valve system -Scale deposits diminished on time because of the drying technique -External factors affected data acquisition(power outages hindered the continuity of the test -Tank failure
Principal results	-$Foulingresistance$ curve was remarkable observed -Scale deposition during the first week could be used to compare with future model
Optimization	-Weight technique was changed to measure a wet prove, instead of dry in the oven for 6 hours
Test 2 and 3	**Scenario 2, lenght 72 hours**
Main difficulties encountered	-Corrosion accumulation augmented because of corrosion in the by-pass system -$CaCO_3$ concentration diminished during the experiment -Corrosion accumulation augmented because of corrosion in the by-pass system -$CaCO_3$ concentration diminished during the experiment -New power outages
Principal results	-Scale deposition using wet measurements gives acceptable growth results
Optimization	-A technique to avoid loss of $CaCO_3$ concentration was proposed. -Was proposed not to recirculate the fluid along the experiment; instead, a deposit tank was proposed. -The internal by-pass system is coated with stainless steel.

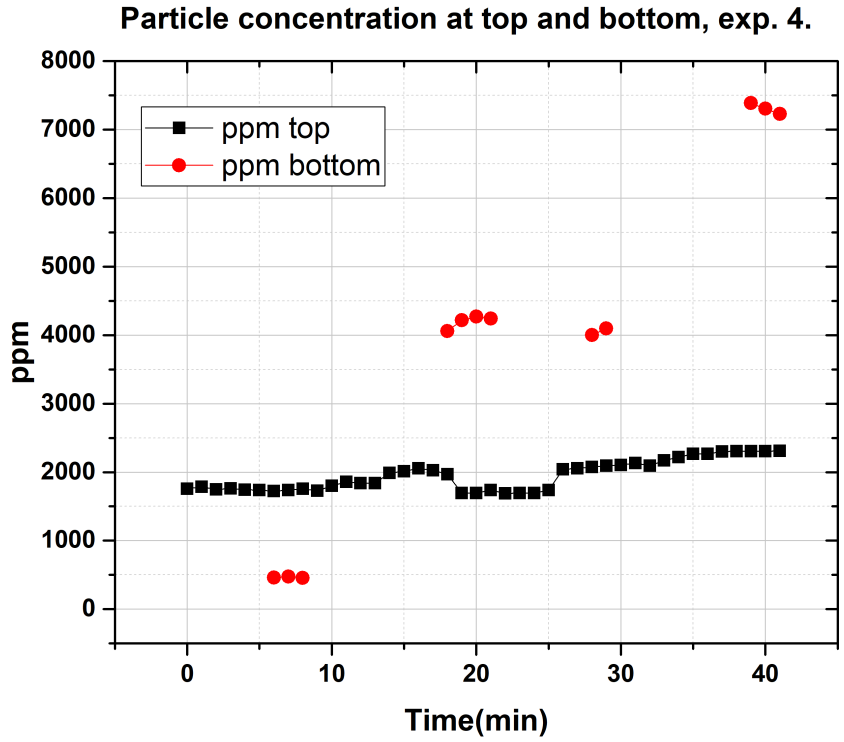

Figure 4.28: $CaCO_3$ concentration at the top and bottom of the tank during experiment 4.

4.4.1 Attempt 3

The main idea of simulate scale deposits in a pipeline wall based on a simulation of fluid flowing through the well-bore, as the particles of $CaCO_3$ during the field life are almost constant[92][93] the ppm during experiments should be constant, so the scenario 2 modification was modified based in this assumption:

- Solution of $CaCO_3$ was generated at 50°C
- Once the solution is stabilized with constant ppm the pump was turned on
- The solution travels along the loop and not returned to the tank

As the tank only has 170 liters the experiment was shorter than the predecessors, constant ppm are in fig4.28:

The concentration at the bottom tank gives a clue related to the salts consumption in every experiment, an extensive mass of $CaCO_3$generated in the last experiments were lost at the bottom of the tank because even with a stirrer system the particles tend to decant in the bottom, losing mass, and diminishing the performance of the experiment set-up. Also, this issue carried out another problem related to the

particles contact with the mixer shaft, which carried a failure of the stirrer system, as seen in figure 4.41.

Table 4.8: Observations from Test 4 and 5

Test 4 and 5	**Scenario 3, mean lenght 1 and 1,75 hours**
Main difficulties encountered	-The experiment length is limited because of the tank volume; this doesn't allow to perform experiments longer than 2 hours -Scale deposits are less in contrast to the concentration used in the tank
Principal results	-Measurements on tank bottom permits observe that part of the $CaCO_3$ decant on the bottom
Optimization	–The concentration of salts diminished to not waste material and avoid particles on the tank bottom -Was decided to measure the ppm at tank, entrance and outlet of the loop system in order to get more data related to scale process

4.4.2 Attempt 4

The scenario four its the final experimental procedure achieved to control the scale build-up, Table 4.9shows that solution used at the first experiments a supersaturated mixture, which generated a problem related to particle concentration because the most of $CaCO_3$ particles were deposited on the bottom tank, with this was decided to diminish the concentration at the experiments. This problem carried an issue related to control of concentration on the tank and in consequence, in the loop system. The above caused a wrong lecture of the concentration of the particles on the tank, as a consequence during the most extended experiments to control the tank concentration, deionized water was excessively added causing a general swept of the scale deposits in the loop system.

Table 4.9: Scenario 4; main experimental results

Brine composition	***Length, hours***	T_{Bulk} $\circ C$	**Q, lt/min**	***Solution concentration*** C_F	***Average particles in the bulk fluid*** C_p	***Average Trapped particles*** K_d	***pH***	***Final weight , gr***
	1,125	56,9		2419	1269	103	5.8	7,85
CaCl solution, 7313	2	59,77		2111	2054	278	6	14,87
	2	54,68	5	1611	1563	122.8	5.8	10,19
NaHCO3 solution, 1170	4	56,87		1701	1801	87	6.3	14,15
	8	53,4		2214	2306	348	6.1	2,42

Table 4.10: Scenario 4; main results and events

Test 6 to 11	**Scenario 4, main results at table4.9**
Main difficulties encountered	-Particles deposited in bottom part of the mixture tank; this doesn't allow to control the concentration during the experiment
Principal results	-Measurements on tank bottom permits observe that part of the $CaCO_3$ decant on the bottom
Optimization	–The concentration of salts diminished to; have more control over the system, to not waste material and avoid particles on the tank bottom -Was decided to measure the ppm at tank, entrance and outlet of the loop system in order to get more data related to scale process

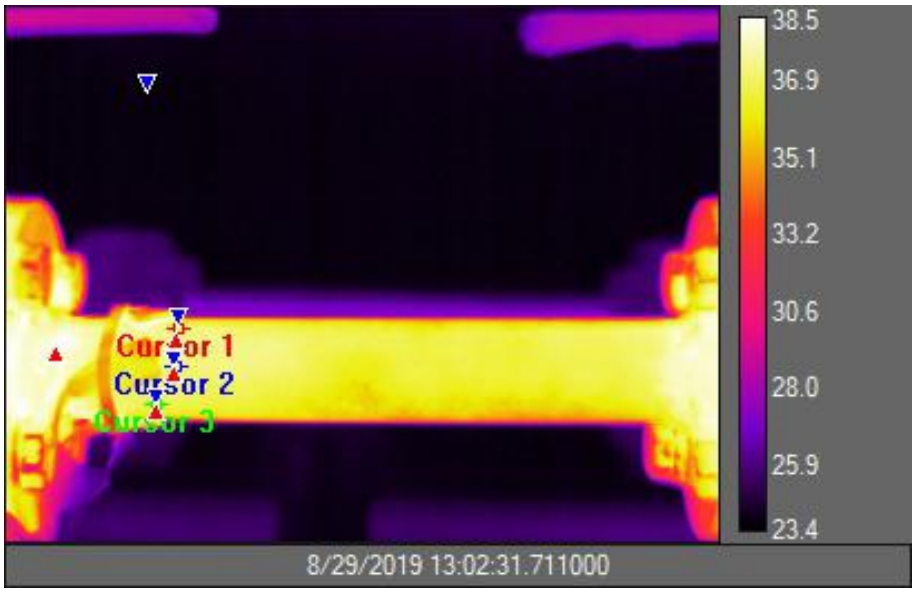

Figure 4.29: Cursor indicating RTDs position on main studied section

4.5 IR analyses

The work of Dulce [84], Saifi [94], and Endo [95] used IR Thermography to investigate pipeline temperature emission to detect the presence of corrosion and scale formation, this technology enabled the detection of different thermal conductivities on external pipe walls depending on the amount of scale deposited or corrosion inside them. Although neither of these works could estimate with accuracy the thickness of fouling, IR Thermography can indicate if the studied section of the loop presents more or less scale build-up, delivering qualitative information regard to scale deposition and severity during the experiment. Special consideration must be made regarding the surface of the studied body, a better-finished surface, can guarantees acceptable emissivity ϵ to the camera. For large ϵ values, reflection contributions of opaque objects are small. However, objects like metals with very low emissivities pose problems since emitted radiance is low and reflected radiance is high. Because of this, an opaque paint was used at the prove surface, this kind of paint generate low light reflexivity and with this, the IR image acquires less external noise, and the studied object (ϵ) tends to 1, near the ideal black body radiation. Also, was performed a calibration between the RTDs and IR, the three RTDs were calibrated using three cursors over sensors position as figure4.29 on the main studied section, the plotted results on 4.5, 4.31 and 4.32, showing a good correlation between sensors and IR camera. Therefore, in IR Thermography noise can be understood as the emissivity of adjacent bodies such as people, electrical sources such as cables, resistances and luminaries.

IR image can be beneficial to detect several images in real-time; the attempt to

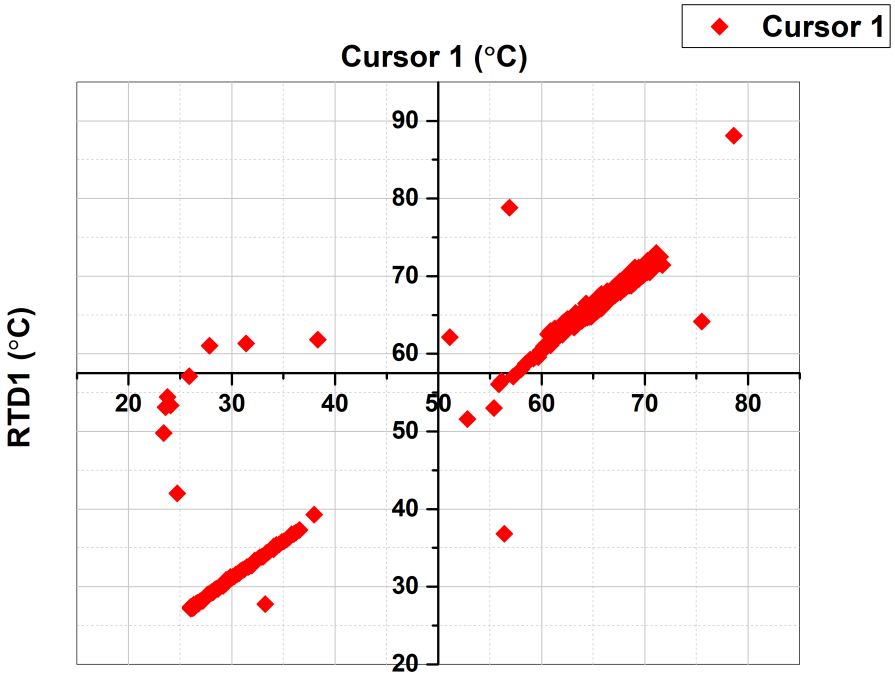

Figure 4.30: Calibration curve between cursor and RTD-1

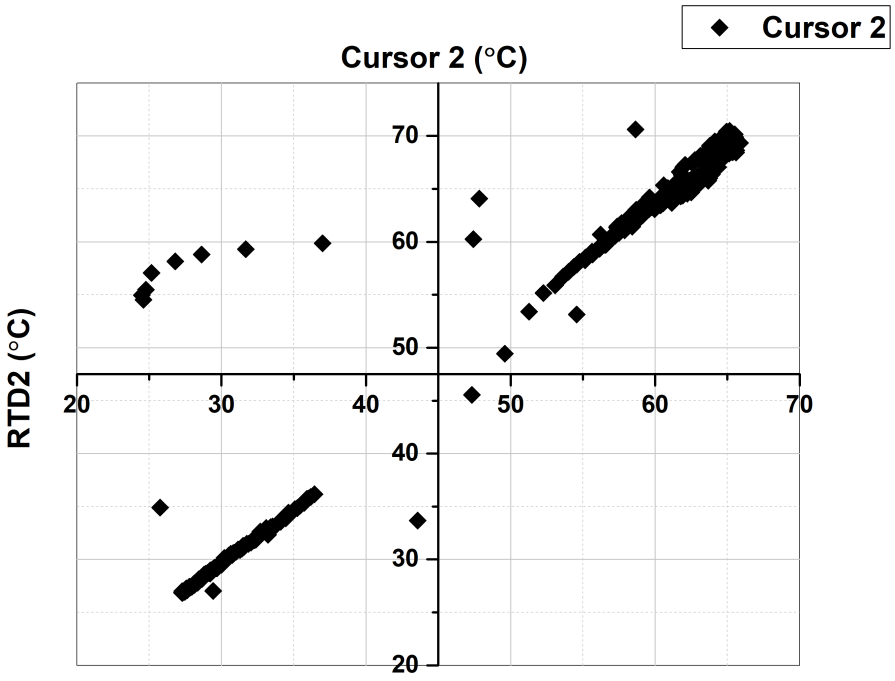

Figure 4.31: Calibration curve between cursor and RTD-2

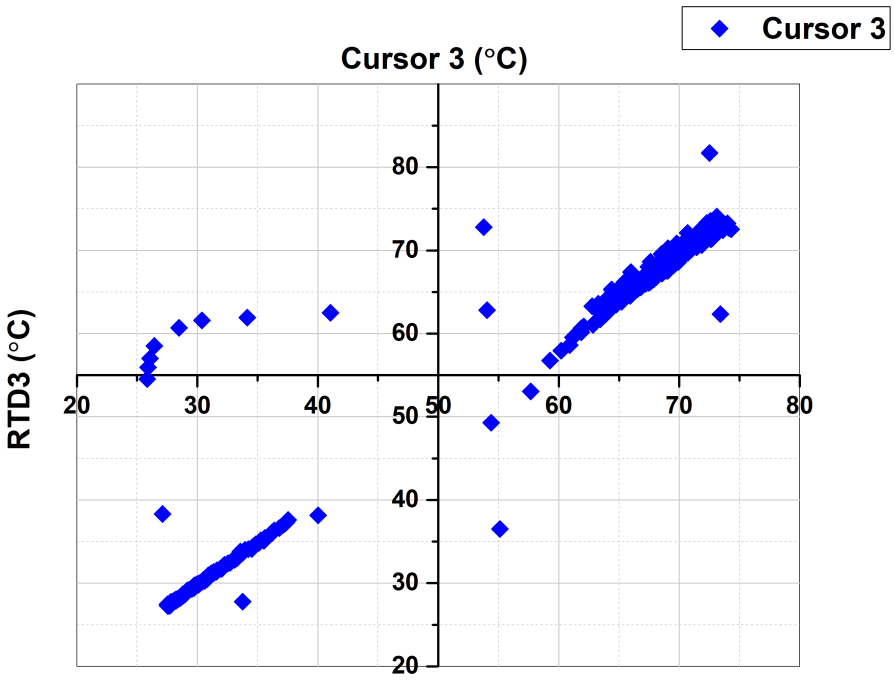

Figure 4.32: Calibration curve between cursor and RTD-3

detect scale formation was very iterative by the use of different filters.

Filters

The use of spectral bandpass (BP) or narrow bandpass (NBP) filters is the easiest way to perform spectrally resolved IR thermal imaging. A large variety of these BP and NBP filters covering the whole spectral region of IR are available.

One of the filters was APE(Advanced Plateau Equalization) as shows Fig.4.34.

Another methodology was using Matlab algorithm to enhance scale formation as 4.36.

Another filter mechanism was the Gaussian filter, filters evaluation to get the optimal scale build-up image can be found at 4.33.

Some filters do not comply the primary purpose of detecting scale build-up, as the case of B, C, D and F(in this case an extra noise was observed) A suitable case was E by using Gauss filter and APE, a detailed image can be observed at figure4.35.

Figures 4.34 and 4.36 shows that IR camera was able to detect the scale growth qualitatively on time. IR images were compared with the inner test section once the test was stopped. Figure 4.35 shows another phenomenon detected at the end

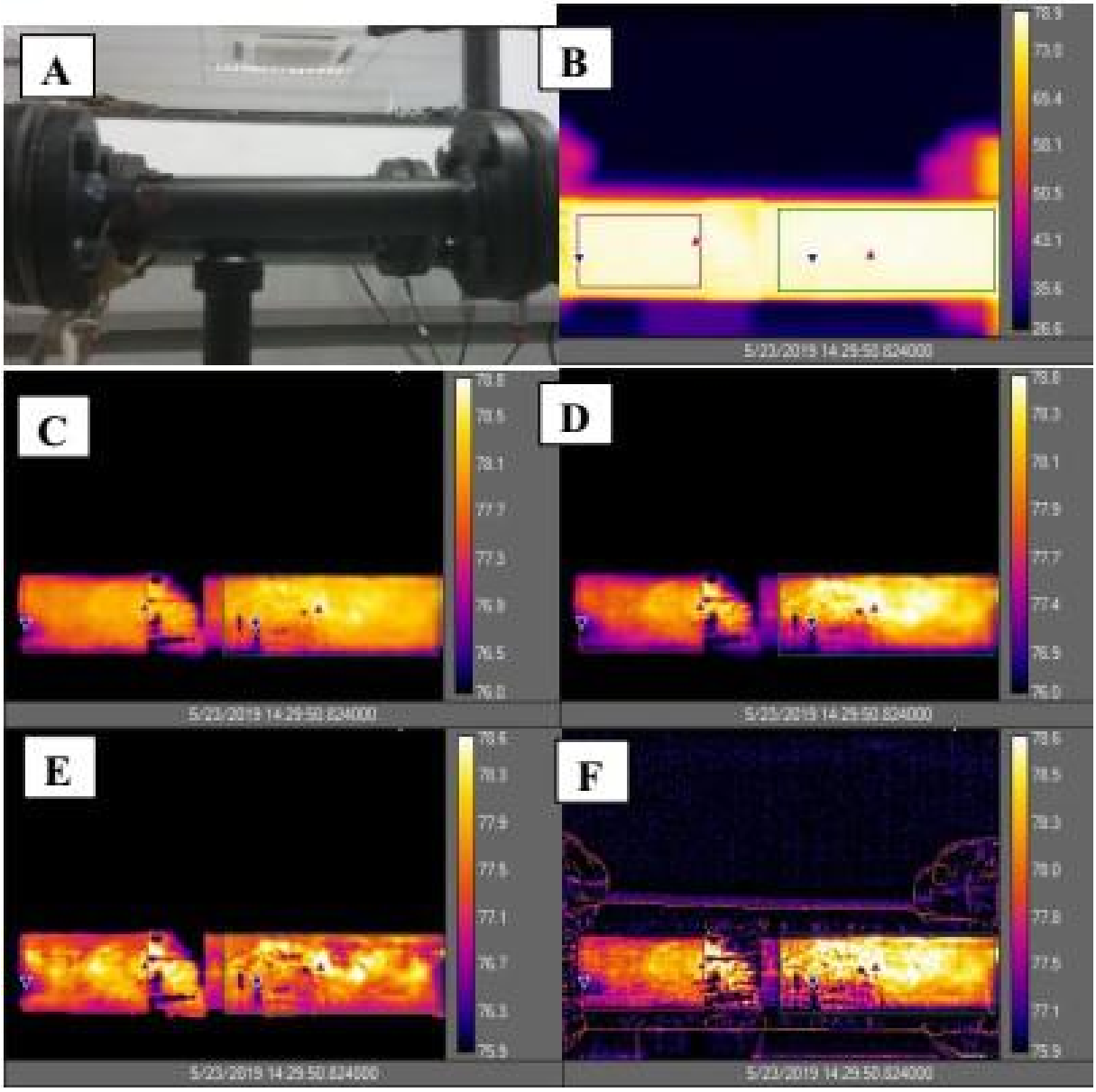

Figure 4.33: Scale growth based on A.-Test section visible spectrum.B.-IR linear spectrum using 2 ROIs.C.-Gauss filter and linear mapping.D.-Gauss filter plus Plateau equalization.E.-Gaussian filter plus APE(Advanced plateau algorithm).F.- Enhancement using Gauss plus DDE(Digital Detail Enhancement)algorithm.

of the first experimental test; scale growth is more intense at the top of the test section than on the bottom, where is almost a null presence of scale. This was because two possible facts; Particles swept away at the moment when valve changes of position or the effect that gases formed by the air bubbles trapped inside the loop have, these affect the removal of scale because they can remain on the walls affecting the flow and transport of particles, were observed several cases during the first experiments, this problem can lead to errors of embedding measurement in the experiments, because they can generate a sweep once the air bubble moves violently

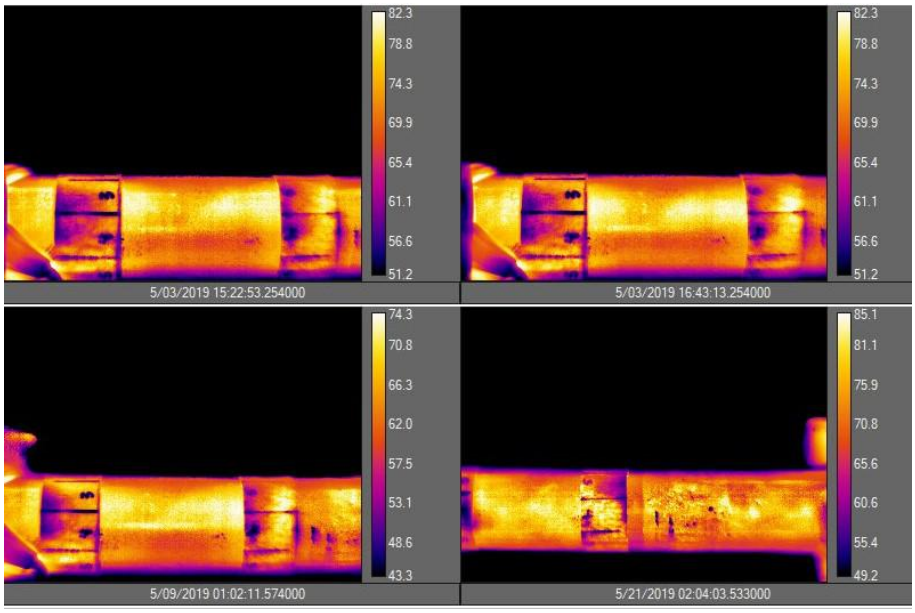

Figure 4.34: Scale growth on time observed at IR images using APE filtering during different periods of the experiment.

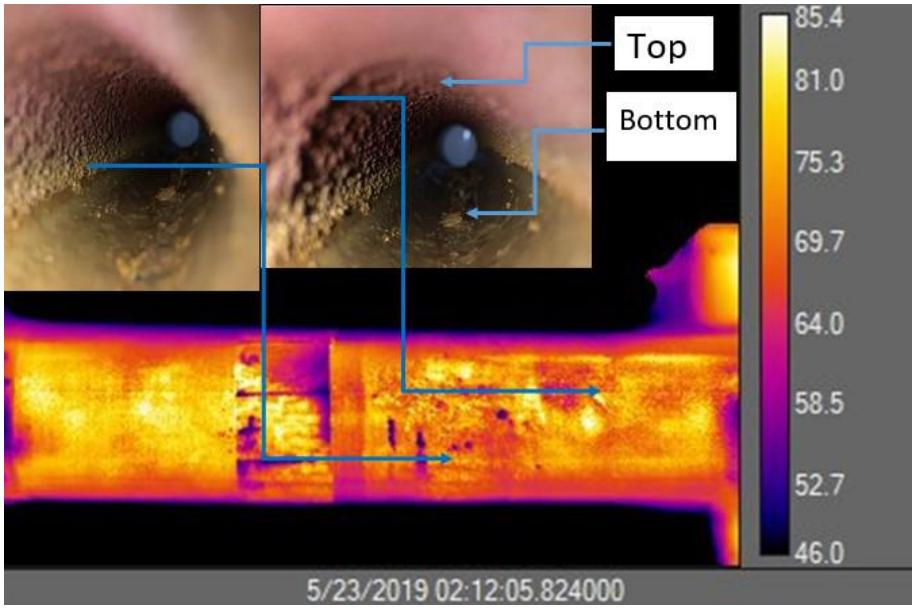

Figure 4.35: Scale growth on time observed on IR images using APE filtering, compared with the inside section of the test can be observed a correlation between the IR images and scale growth inside the pipe.

or compresses the particles trapped in the loop by accumulating them in individual sections and sweeping them in others, several examples can be observed on images presented at 4.37 and 4.38.In response to this phenomena, two vents were installed at the entrance and exit of the loop so that the bubbles can exit and reduce the risk of generating essential changes in the control parameters of the loop.

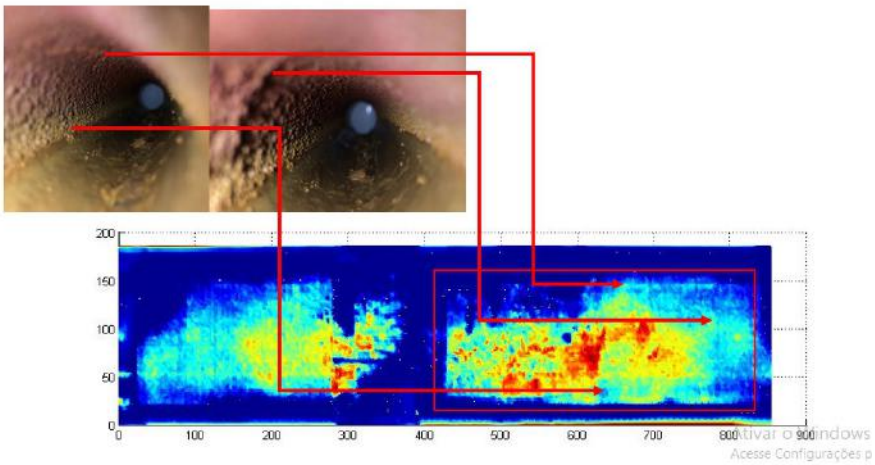

Figure 4.36: Scale growth at experiment 1 observed on IR images using Matlab enhancement at the final stage of the experiment this allows detecting scale formation irregularities.

As seen in figures4.37 and 4.38 the scale deposition is most prominent at the bottom section:

4.5.1 Other issues related to experiment optimization

During the experimental calibration, several problems are registered, most part because of the erosive and corrosive nature of the mixture as can be seen on fig.4.40, affecting several sections and main spare parts as the equipment employed in the loop configuration some are in figs.4.41, 4.42.

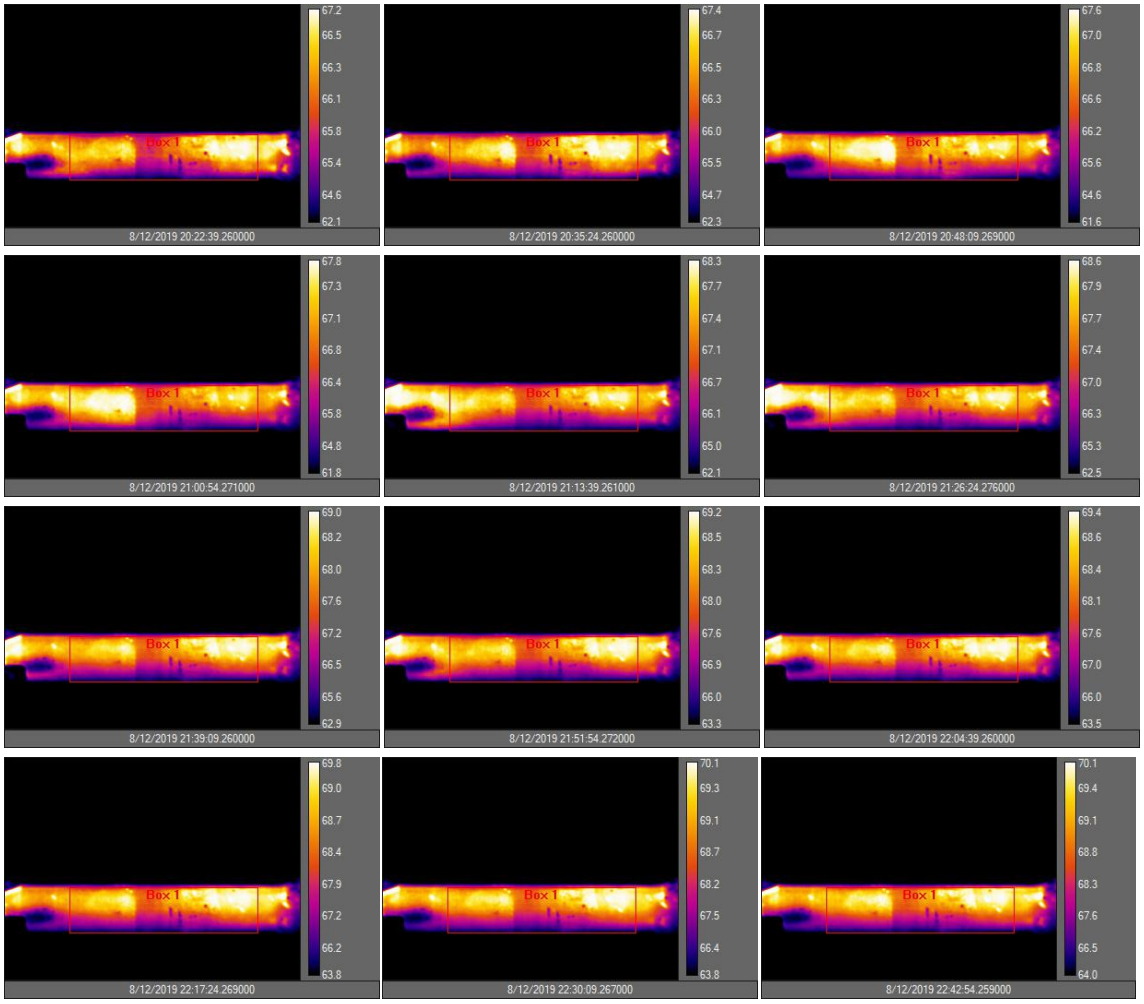

Figure 4.37: Scale evolution on time using Gaussian filter, exp. 2.

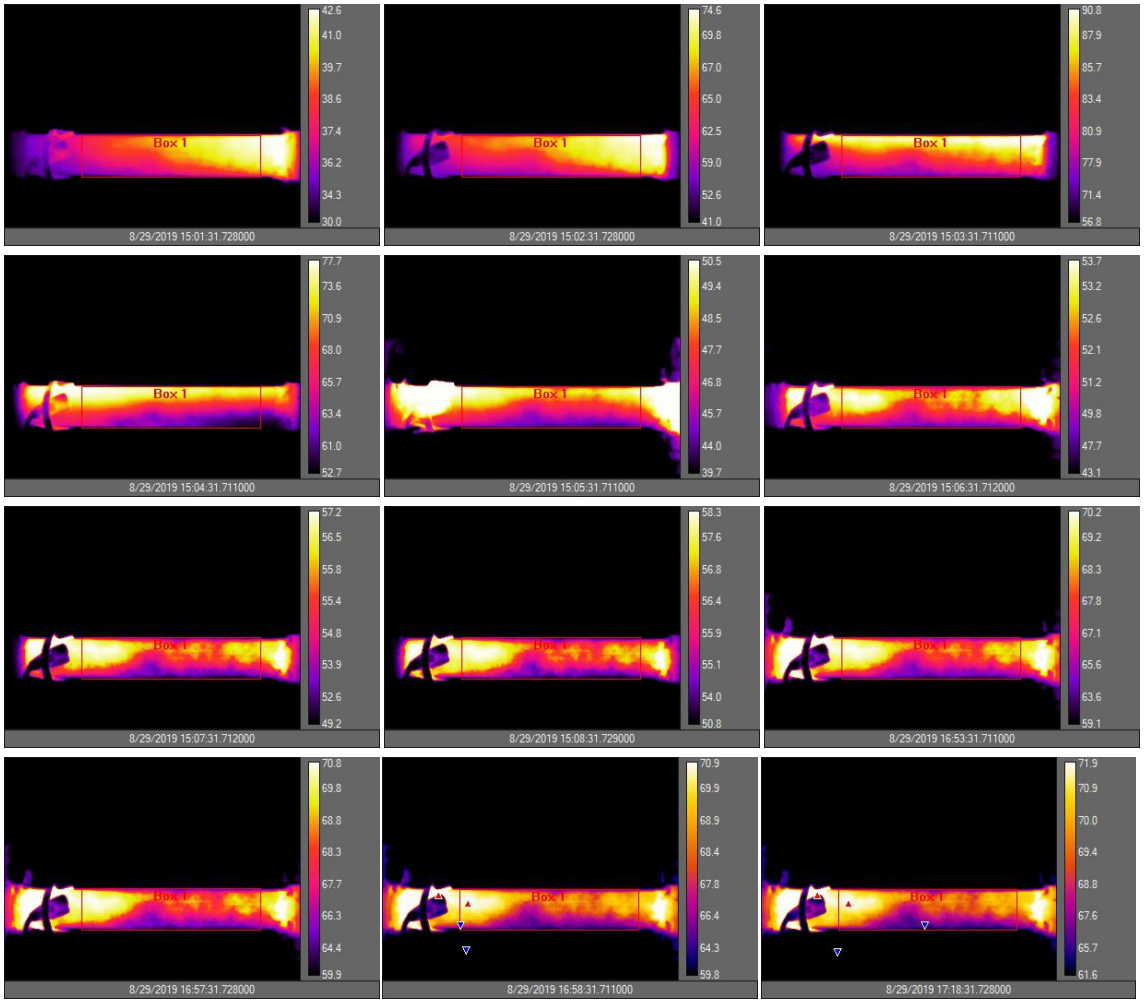

Figure 4.38: Scale evolution on time using Gaussian filter, exp. 3.

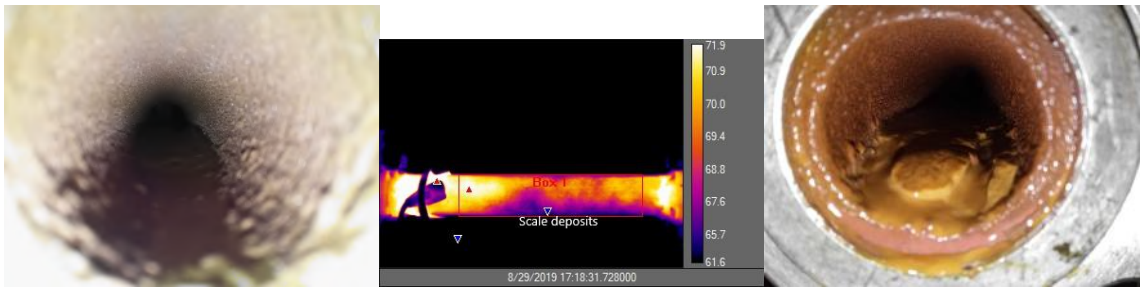

Figure 4.39: Scale deposits at pipeline bottom, indicated by lower temperature, the brown color indicated presence of Fe corrosion

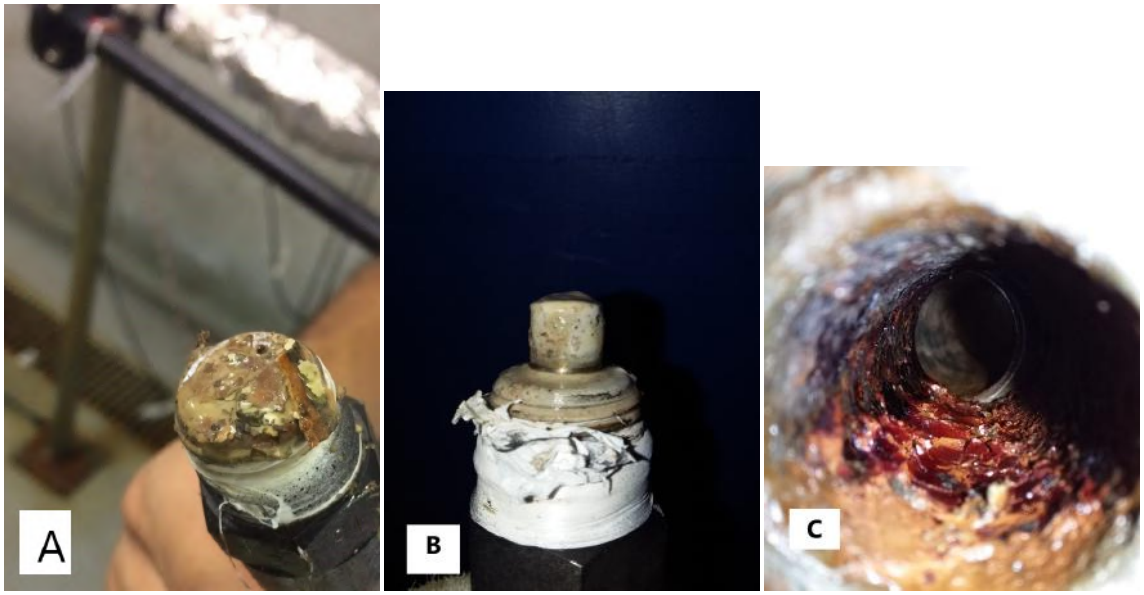

Figure 4.40: Scale encountered on several sections; *A*) In-line temperature sensor, *B*)in-line pressure sensor, *C*)By-pass valve inner section

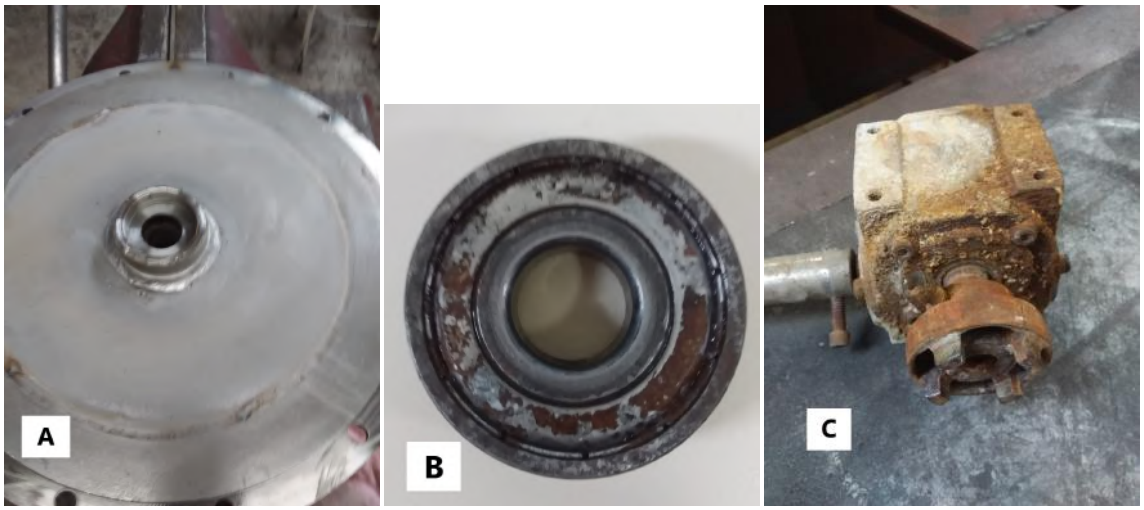

Figure 4.41: [A]Particles accumulated at the bottom of the tank system, causing erosion and damaging the bearing system [B] of the impeller in the tank, causing mixture leakage and in consequence damage over the reduction box system[C]

Figure 4.42: Erosion and misalignment presented in the first pump

Chapter 5

Case study-Experimental results

The main problem encountered during the calibration of the experimental system in chapter three was related to withdrawing the sample for weight measurement. Due to the vortex generation, once the valve was open/close, the flow swept part of the deposited particles. The method proved to be inadequate to generate an incrustation growth curve over time, especially for short periods.Because of this, a case study was performed in another approach, by controlling temperature, flow, ppm and pH. After each experiment, the body is extracted, dried in an oven and weighed, then cleaned. Once it is clean, the body is re-inserted into the system, and a new experiment started. The length of the experiment were 1, 2, 4, and 8 hours; this approach was used to have a scale build-up curve to be compared to the developed models.

5.1 Methodology

- The deionized water was heated at the $60°C$.
- Then,828 grs. of $CaCl$ was added in the tank.
- Once the water dissolved all the $CaCl$, 800 grs. of $NaHCO_3$ is aggregated, in this reaction, CO_2 is liberated.
- Once the reaction is completed and stops to release CO_2, ppm in the fluid was measured in the tank. Once the PPM gets a stable NTU measurement to control the tank concentration, the pump started, and the mixture recirculates into the system through the by-pass system.Once the loop temperatures are reached the by-pass changes the position to the main test section, this section was weighted previously.
- During the experiment, ppm measurements were carried out at the tank, entrance and outlet in the loop approximately every 15 minutes.Special care was

taken to measure at the middle section of the entrance and outlet of the loop system as can be seen in fig. 5.1.Before and after each measurement, the pipette was cleaned to ensure correct measurements.

- Before the experiment ends, the pump is stopped and the valve before and after the test section are open to the by-pass. The test section is then removed and weighted wet, then dried in an oven and weighed again.

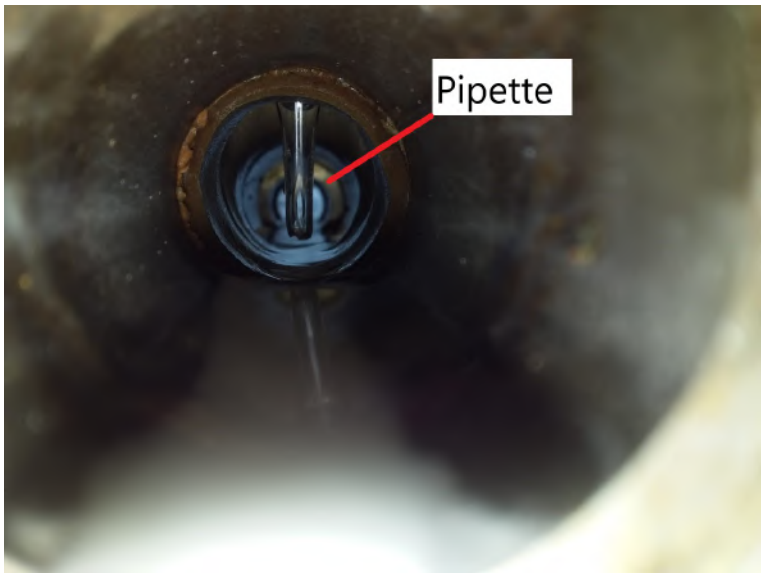

Figure 5.1: Measurement position to take fluid samples at the inlet and outlet of the loop system.

Cleaning procedure

After every test, the hard water tank was cleaned thoroughly. After the previously used artificial hard water was completely drained, a tap water jet using a hose was then flushed onto the inside wall of the tank together with a cleaning brush to remove any scales formed inside the tank. Traces of $CaCO_3$ agglomerated deposits were drained out of the tank. Then, tap water is introduced into the tank and circulated in the loop system for at least four hours. When most visible traces of the hard water previously used were gone, the tap water was completely drained out, and new distilled water up to 0.170 m3 (170 l) was supplied to the tank. Later de-ionized water was recirculated with 1 lt of Acetic acid to remove and dissolve the rest of $CaCO_3$ in the loop.

5.2 Experimental results

The main parameters are enlisted for the experiments 13,14,15 and 16.Concentration was measured along all the experiments, in three main parts; tank, entrance, and

outlet.Concentration in all the experiments are in tables 5.1,5.2,5.3,5.4, 5.5 :

Table 5.1: Exp. 13, 60 minutes

Test-13, 60 min.	**Parameter**
T_{Bulk}	60,56± 1,9
T_{Wall}	71,6± 1,1
T_{Tank}	60,69± 3,8
Flow	2,7± 0,9
ppm Tank	1892 ± 111
ppm In	2044 ± 157
ppm OUT	1286 ± 152
$\triangle$ ($ppm(ppm_{IN}$- ppm_{Out})	769 ± 193
pH	6.1
Wet mass	16,26
Dry mass	4,556

Table 5.2: Exp. 14, 70 minutes

Test-14, 70 min.	**Parameter**
T_{Bulk}	60,3± 2,34
T_{Wall}	73,7± 1,2
T_{Tank}	60,05± 1,45
Flow	2,4± 0,29
ppm Tank	1615 ± 273
ppm In	2337± 84
ppm OUT	1286 ± 152
$\triangle$ ($ppm(ppm_{IN}$- ppm_{Out})	713 ± 214
pH	6.08
Wet mass	20,47
Dry mass	5,7354

The concentration measurements during experiments can give a piece of useful information about the particle concentration at the loop entrance, assumed as the C_F value. Finally, another parameter is the average trapped particles in the loop system which can indicate a particle deposition rate No, useful to determine the deposition regime of the experiment. Those values were added to the models to compare with mass measurements. However, the concentration measurements during the experiment still present difficulties related to the bubble formation during experiments, as explained at the end of chapter two. The main parameters and mass deposition results of the case-study are presented at case study tables.

Table 5.3: Exp. 15, 120 minutes

Test-15, 120 min.	**Parameter**
T_{Bulk}	59,3± 1,5
T_{Wall}	69,2± 1,2
T_{Tank}C °	60,26± 2,67
Flow(lt/min)	2,5± 0,23
ppm Tank	2546 ± 207
ppm In	2913± 221
ppm Out	2196±317
$\triangle$ ($ppm(ppm_{IN}$- ppm_{Out})	755 ± 490
pH	6.4
Wet mass (gr)	28,12
Dry mass(gr)	7,88

Table 5.4: Exp. 16, 240 minutes

Test-16, 240 min.	**Parameter**
T_{Bulk}	57,4± 1,7
T_{Wall}	66± 1
T_{Tank}C °	60,39± 0,97
Flow(lt/min)	2,34± 0,26
ppm Tank	2682 ± 118
ppm In	2758± 403
ppm Out	2056±218
$\triangle$ ($ppm(ppm_{IN}$- ppm_{Out})	702± 576
pH	6,9
Wet mass (gr)	49
Dry mass(gr)	13,88

Table 5.5: Exp. 17, 480 minutes

Test 17-480 min	**Parameter**
T_{Bulk}	59,58±1,31
T_{Wall}	68,2±2,7
T_{Tank}	60,63±1,62
Flow	2,32±0,08
ppm Tank	2199±205
ppm In	2591±427
ppm OUT	1894±239
$\triangle$ ($ppm(ppm_{IN}$- ppm_{Out})	696±561
pH	6.3
Wet mass	49 grs.
Dry mass	16,14 grs.

5.2.1 pH

Average pH at tables5.1 to 5.5 indicates that exists a direct correlation between the pH, mass gain, and the time that mixture requires to reach an equilibrium state. pH indicates that as the experiment progresses over time, the mixture releases CO2 and leaves the fluid less acidic; consequently, in some moment, it reaches a chemical equilibrium in the solution.

5.2.2 Approach using heat analogy

As stated in chapter one and two, a useful parameter to analyze the scale formation inside the pipeline is the heat analogy, using the fouling resistance R_f, this parameter can give relevant information related to the heat transfer comportment during the experiments.The works of [59][17][38], [78],[76] and models [96],[18],[97] cited different fouling density values depending on experimental control variables, a good estimation of $CaCO_3$ fouling density was proposed by Pakkonen [19], this data was used to calculate the mass deposition rate as:

$$m_d = \frac{\rho_f R_f \lambda_f}{t} \tag{5.1}$$

Here λ_f is the Calcium carbonate thermal conductivity (W/ m K),R_f which corresponds to the fouling resistance calculated as equation 3.60 in chapter 3, t is the time step in each iteration as stated in chapter 3. For the sake of simplicity, the fouling density and thermal conductivity are based on the work of Pakkonen [19], 1100$[kg/m^2]$ and 0,97 W/mK respectively.

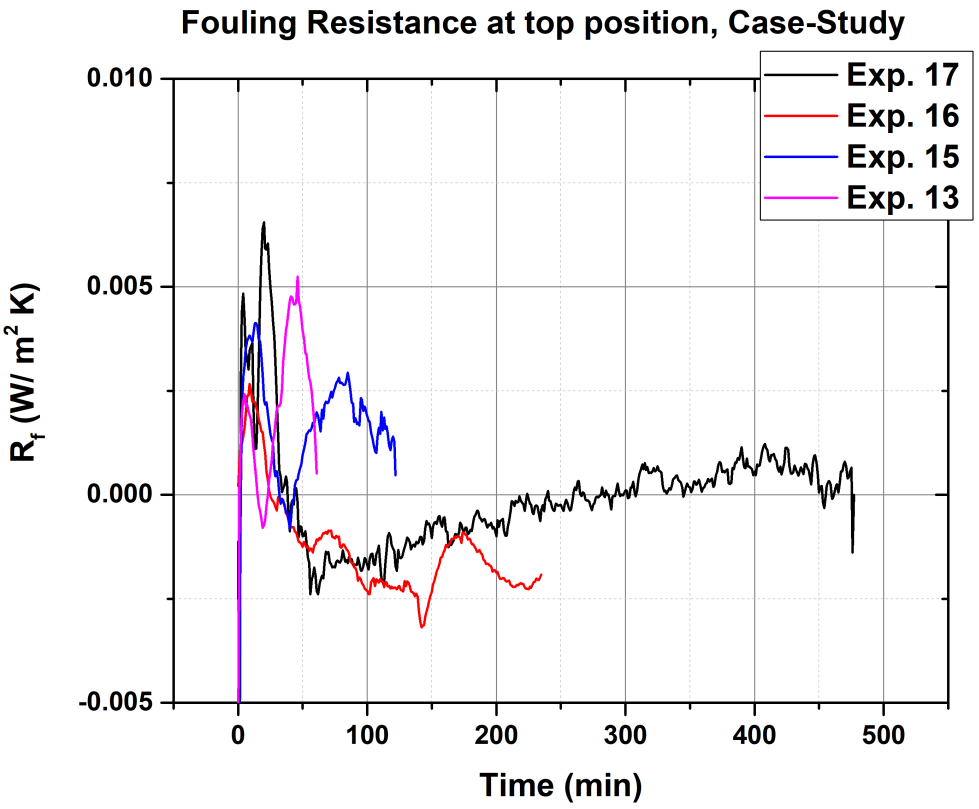

Figure 5.2: Fouling resistance at top section.

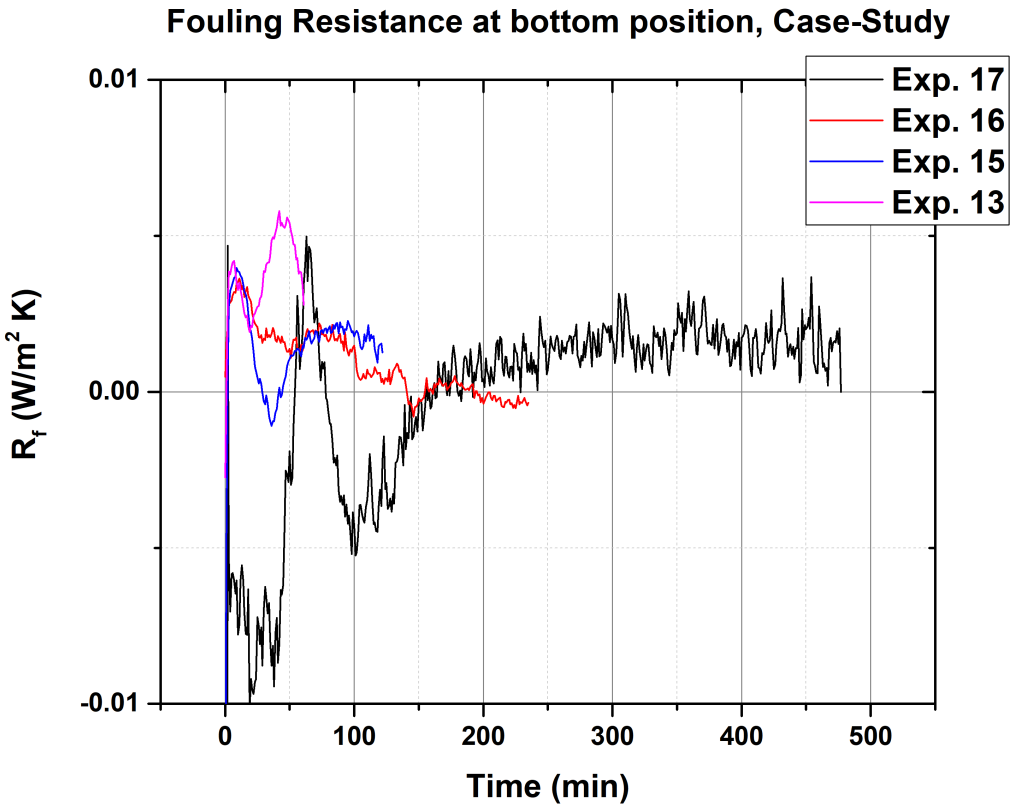

Figure 5.3: Fouling resistance at bottom section.

As can be observed the heat analogy in this study didn't give conclusive results as an indicator of scale build-up in the line, because of the mass rate changes in the function of fouling resistance which shows even negative values. Several authors justify the negative value of R_f [98],[30], [38], the principal reason is that at the beginning of the experiment there is a nucleation period when crystal formed on the wall, this leads to an increase of the pipeline roughness, augmenting the heat transfer surface, in consequence, the wall temperature diminished and generates a negative fouling resistance. These parameters are corroborated by the average temperature from the IR cameras. As the scale deposits formed the increase of Crystals and deposits in the pipeline diminished the average wall temperature.

XRD analyses

One of the major indicators of the improvement of the loop system during the different phases of experimentation at chapter four was de composition of the deposited crystals at the test section, those crystals were analyzed to observe the deposits composition, the images from the experiments shows that the loop systems generates two main $CaCO_3$ crystals, Calcite and aragonite as the figure 5.4.

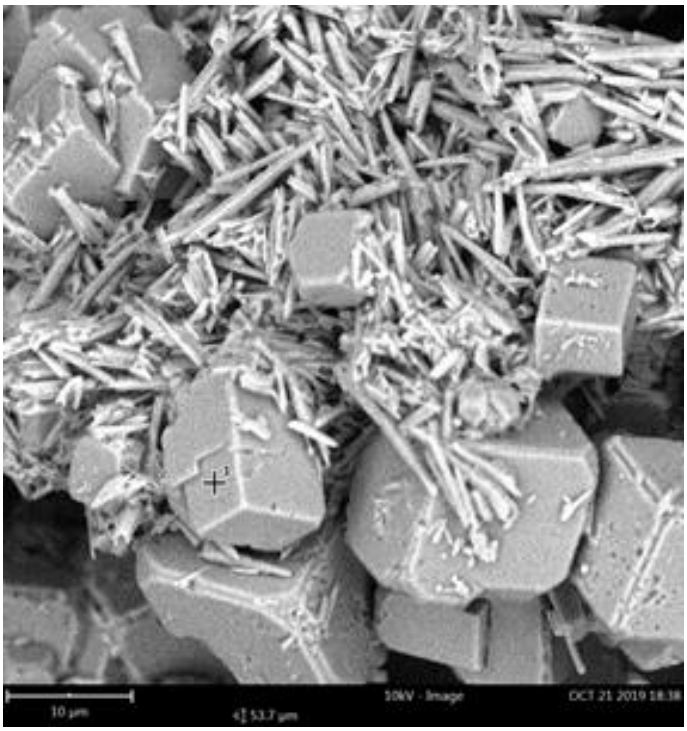

[A]

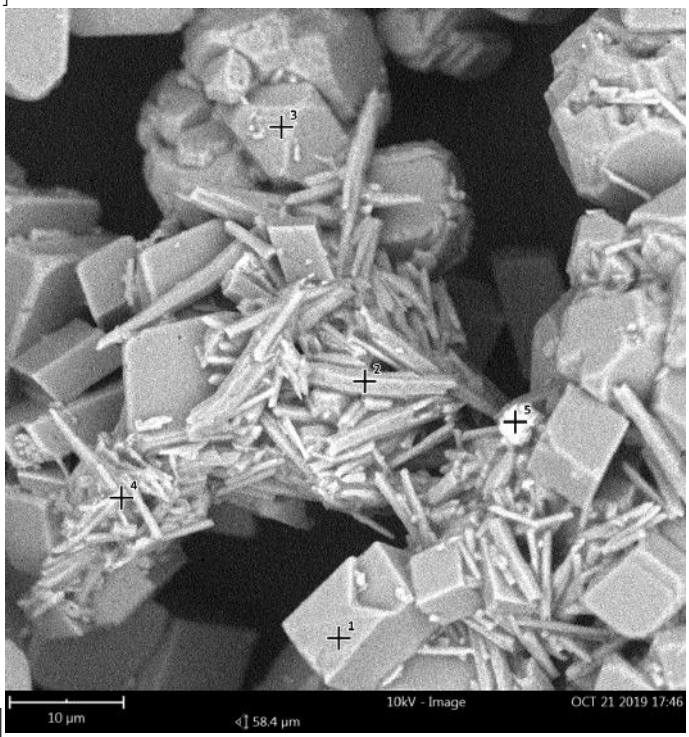

[B]

Figure 5.4: A)Crystal deposits at case-study, B)A close up, Aragonite and Calcite can be observed.

IR analyses

The IR images acquired during the case study were able to detect the scale deposits on time as described in chapter two, some remarkable scale deposits were founded at the 2,4 and 8 hours experiments, IR can show the scale build-up on time:

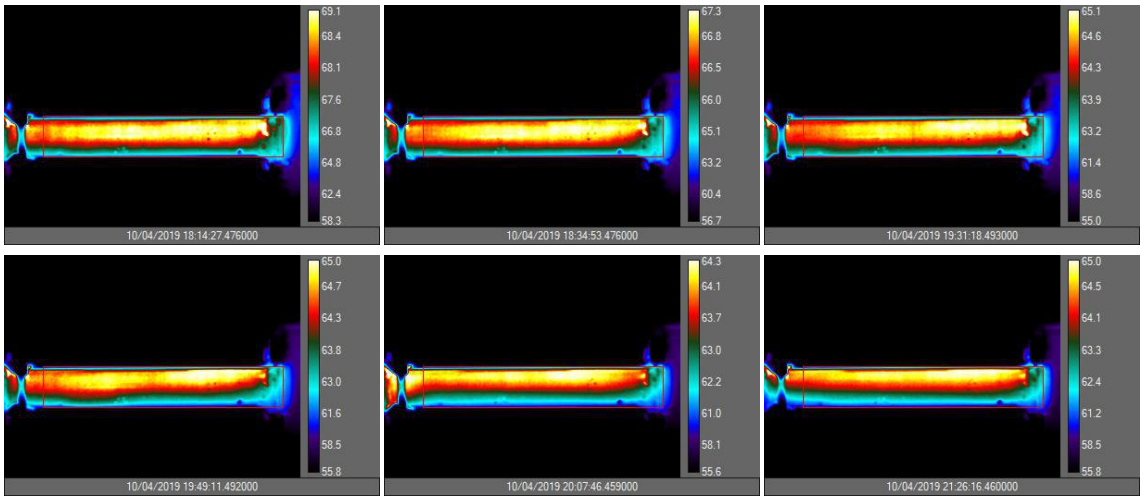

Figure 5.5: Scale evolution on time using Gaussian filter, exp. 16.

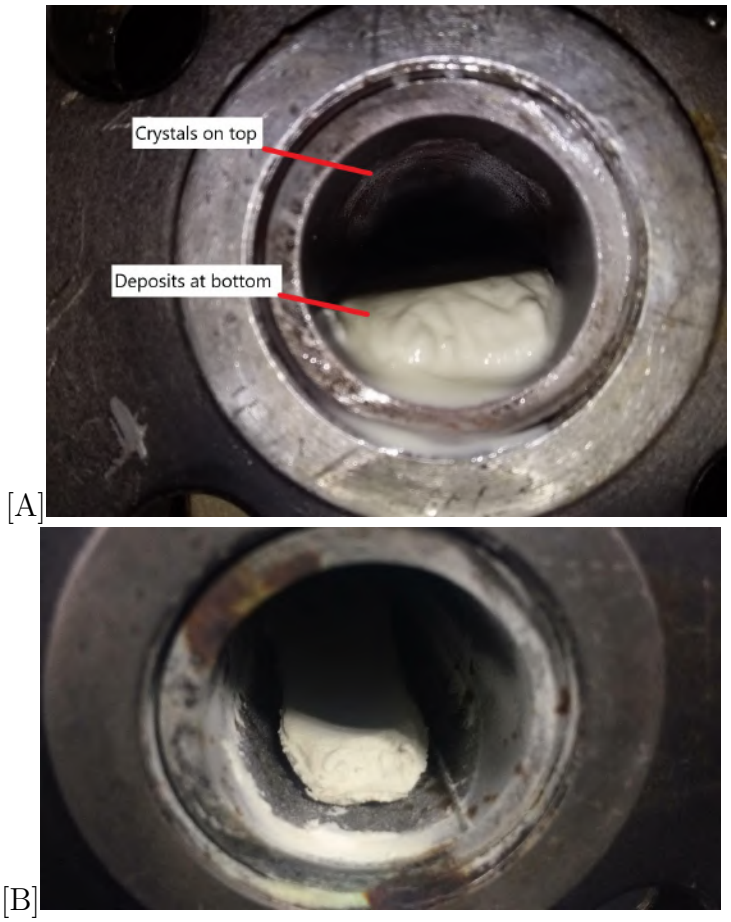

[A]

[B]

Figure 5.6: A)Deposited scale at bottom and some crystals forming at the upper section of the pipeline, B)Dried deposits after the oven at $70 \circ C$ for 4 hours

[C]

[D]

Figure 5.7: C)Measurements of deposited scale, D)Measurement of the deposited scale

[E]

[F]

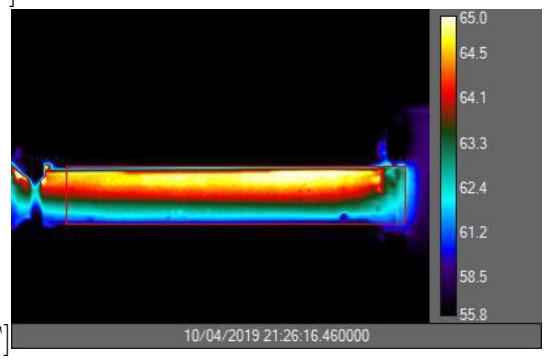

Figure 5.8: E)Deposited scale at the bottom of the test section, F)IR image from the same section showing the scale deposits represented by the lower temperature at pipeline bottom

Pressure drop analyses

In practice Gudmundson [89], [90], and other authors [30], [91] proposed that pressure drop is a method to detect scale build-up, the method could use a formula which comes as the specific pressure drop:

$$SPD = \frac{\Delta P}{Q} \tag{5.2}$$

This value gives information about the pump performance changes depending on scale formation inside the pipeline.

The specific pressure drop could indicate a scale build-up in the pipeline experiment using the equation 5.2 proposed by Gudmunson[7]; SPD value is in figure 5.9, for each experiment in the case-study, as can be observed as scale build-up increases, the SPD value should increases slightly as the deposited scale starts to change the fluid flow and friction in the line. The chaotic value indicates that the pressure in the experiment is not a sensitive value to describe the experimental system in this case, in comparison with other parameters as temperatures. Also, the SPD value is generated by a post-processing data which does not give an inline indication as the experiment is in course.

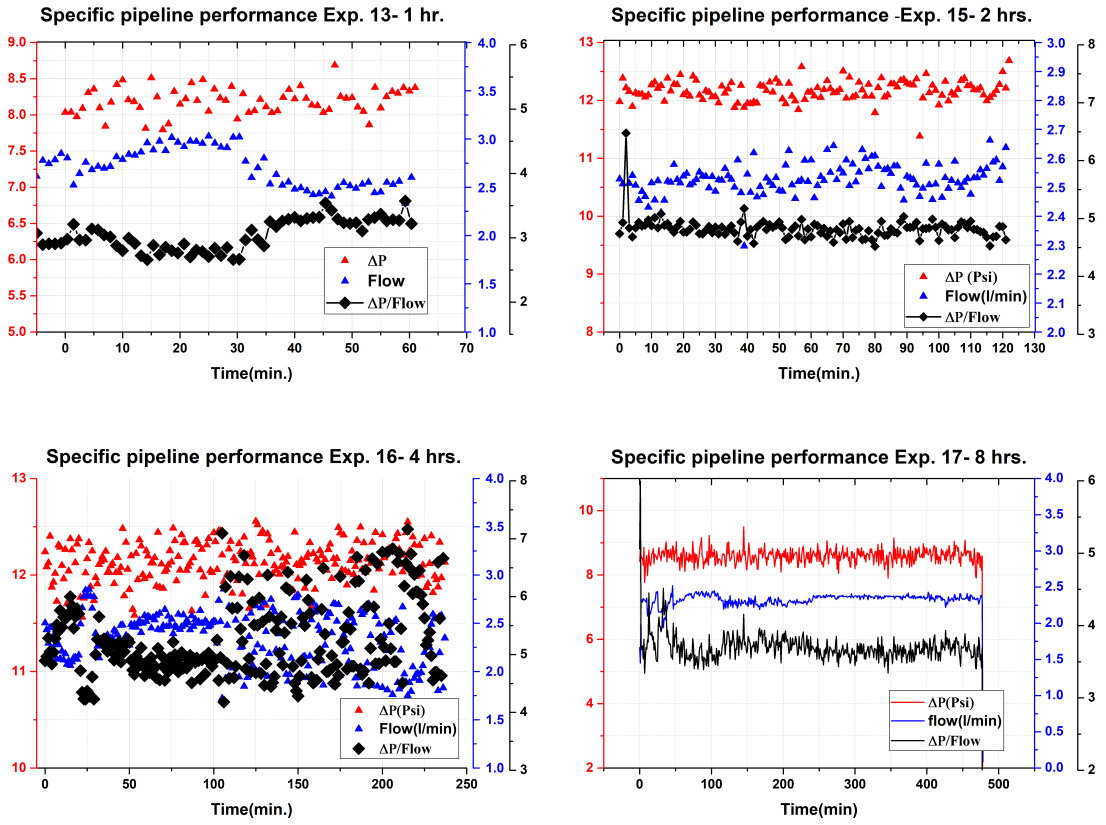

Figure 5.9: Scale evolution on time using Specific pipeline performance(SPD) at case study experiments.

5.3 Models approach using weight measurement

Several works weight probes at experimental tests [16], [39], [78], [99] the works measured weight at the end of each experiment, this generates a straight line of the final weight generated by scale, in this case, using control parameters, the scale measurement at the end of each experiment allowed to generate a curve of the scale deposition evolution in time, by the by-pass, described at chapter 3 . Scale curve was compared against the five mass deposition models described in chapter 4. In the first comparison, the models used the mean values which of all the experiments in the case-study:

$$m_d = m_f * 2\pi r_i L \tag{5.3}$$

were L corresponds to the section length(0,24 m) and r_i is the inner radius(0,01365 m).

5.3.1 Model comparison and Sensitivity analyses

The mass deposition models are compared against the deposition curve generated in the case study experiments; the weight is compared using dry weight (Test section was weighted after dried in an oven during 2 hours at $70°C$).

The results in 5.10 used the parameter from mean values of the experiments of case-study, indicated that Yang[18] model can be more suitable to describe the scale build-up in comparison with the other models,[3],[63].

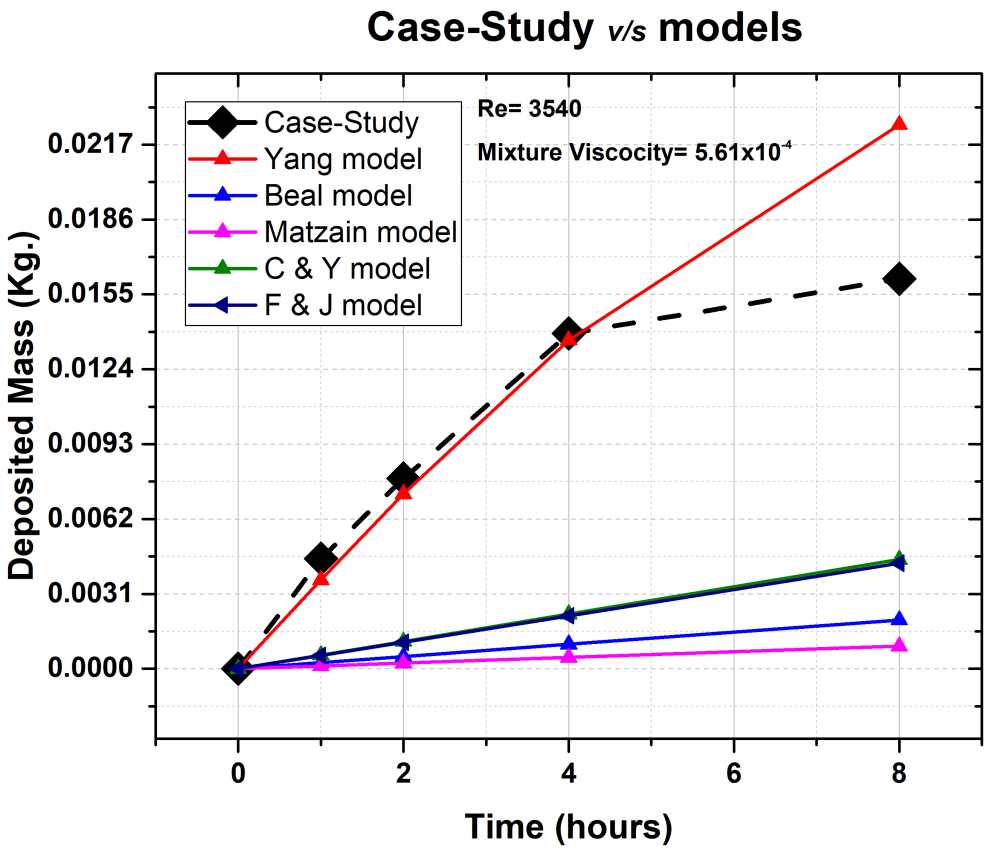

Figure 5.10: Models compared with Case-study.

As can be observed the Yang model shows a better prediction in comparison with the others, respect to this a sensitivity analyze was performed using Yang model, based on test 16, where the four-parameter values were analyzed giving the results at figure;

The Yang model presents sensitivity in all the four variables, respect to Bulk and wall temperature; those parameters can influence the bulk concentration parameter directly because the calcium carbonate nature to been inversely soluble with temperature.

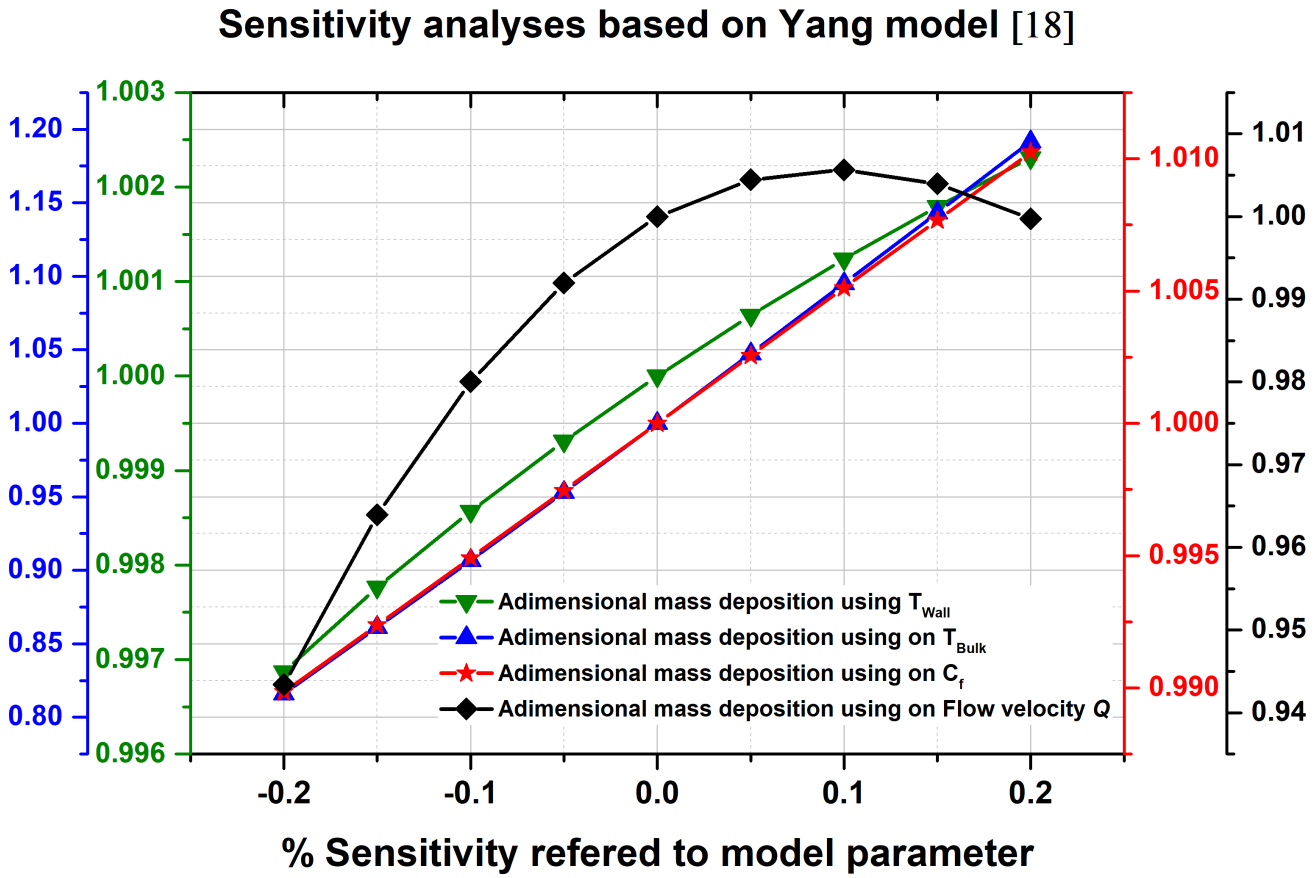

Figure 5.11: Sensitivity analyses using T_{Bulk},T_{wall}, C_F, Q.

As respect to the flow velocity, the curve shows that the parameter is one of the most complex of the four studied, this effect can be corroborated by the work of [38], which shows that the scale build-up can perform in this way depending on the flow regime, as the flow is closer with laminar regime the scale build-up can grow faster in comparison with a turbulent one.

Chapter 6

Conclusions and future work

An experimental mesoscale loop was made to study inlaying scale phenomena in lines; several attempts were studied to perform a controllable experiment, those attempts are registered at chapter four, with the main results and drawbacks to improve the experimental loop performance. In the case study in chapter five, four experiments were performed at a different time to get a rising curve which can describe the scale build-up comportment in time. The fourth attempt was the most controllable and gives good results in lesser time in comparison with the predecessors.

The importance of the loop system radicates in the dimensions used to generate scale build-up, the developed system was able to generate scale in a higher dimension in comparison with the literature predecessors.

Most of the predecessor scale investigation experiments focus on heat exchanger systems; here, the focus was in generate the scale in a pipeline with the use of electrical resistances.

Two types of adhesion formed inside the tube during the experiments;

Deposition; influenced by gravity effects, and Crystallization; influenced by diffusion effect.

Predominant adhesion was by deposition of particles and not due to the formation of crystals on the walls.

Heat transfer effects as fouling resistance R_f was not conclusive to predict mass deposition in the experimental system.

On the other handR_f was helpful to correlate that the fouling phenomena related to scale growth inside pipelines happens in the experimental system and can be detected by using these parameter.

Also two types of crystals were detected by XRD, Calcite and Aragonite as observed in figure 5.4.

In respect to the Case-study :

- A simple bypass system permitted to generate several experiments with con-

trollable parameters.

- The controlled experiments permitted to generate a curve to compare the mass deposition with several models.
- The best correlation was the Yang model, the model was able to describe scale build-up with a minimum difference at the first three experiments(1,2 and 4 hours long).
- All the proposed models, until now, never had been compared with experimental controlled variables and results.
- The experiments permites determinate which parameter can influence the models and could been correlated using the sensitivity analyses.
- Until now the models are only compared with particles transported in fluids, like Iron and even particles in air droplets, but never with particles of CaCO3 interacting in a pipeline system subjected to heat transfer phenomena in a pipeline, which is a realistic set-up to compare these models.

Also, there was no data in other bibliographical references that provide the evolution of the formation of scale build-up using non-destructive testing as the IR system used in this work.IR images were able to detect several phenomena in the pipeline:

- scale crystallization detected as the decrease of the wall temperature
- Scale deposition by gravity
- Bubbles generated by heat transfer
- Flow effects related to multi-phase flow

The pressure during the experiments was not able to describe the behaviour of the friction factor and in consequence, scale deposition evolution.

pH varies during case study experiments, but are not conclusive.

The experimental loop presented may become quite useful in future research projects related to test new coating materials , it is hoped to improve the system as new industry challenges are presented.

Recommendations for the optimization of the experimental system

Several mishaps demonstrated the need for constant system improvement, such as the following items:

- Extensive use of 316L stainless steel in the circuit and valves is recommended to prevent the formation of scale.
- Replace the flanked 150L system with a CLAMP type to facilitate the insertion of test bodies.
- Insert a transparent section to visualize the fluid in real time.

Recommendations for future work

The experimental system allows to:

Test different internal spare parts and materials found in real underwater systems (from Jumpers, wet X-mas trees, manifolds, valves, etc.)

Test new materials or coatings that can inhibit the formation of scale.

Experiment with new solutions composed of MEG (Mono ethylene Glycol) that has proven to generate problems in well injection systems by increasing the formation of calcium carbonate scale [100], [101], [102].

Increase the experiment pressures to evaluate the influence of this variable on the effects of scale formation.

The models could be improved by adding parameters such as pressure variation and diversifying the viscous characteristics of the fluids to be used in future experiments (MEG solutions, water and salts).

Regarding the infrared camera, possible analyzes using inverse problems [103] could be performed to evaluate the formation of scale inside the tube quantitatively.Also, the experimental apparatus presents a high potential to test chemical and physical scale inhibitors in kinetics deposition.

Bibliography

[1] GUAN, H., BOUAMRA, R., LINDVIG, T., et al. "Scale risk assessment and novel coating for smart completion: Scale simulation and CFD modelling approach", *Society of Petroleum Engineers - SPE International Oilfield Scale Conference and Exhibition 2018*, 2018.

[2] SHIPPEN, M., BAILEY, W. J. "Steady-state multiphase flow-past, present, and future, with a perspective on flow assurance", *Energy and Fuels*, v. 26, n. 7, pp. 4145–4157, 2012. ISSN: 08870624. doi: 10.1021/ef300301s.

[3] SHIRDEL, M., PAES, D., RIBEIRO, P., et al. "Evaluation and comparison of different models for asphaltene particle deposition in flow streams", *Journal of Petroleum Science and Engineering*, v. 84-85, pp. 57–71, 2012. ISSN: 09204105. doi: 10.1016/j.petrol.2012.02.005. Disponível em: <http://dx.doi.org/10.1016/j.petrol.2012.02.005>.

[4] PAES, D. M., RIBEIRO, P. R., SHIRDEL, M., et al. "Study of asphaltene deposition in wellbores during turbulent flow", *Journal of Petroleum Science and Engineering*, v. 129, pp. 77–87, 2015. ISSN: 09204105. doi: 10.1016/j.petrol.2015.02.010. Disponível em: <http://dx.doi.org/10.1016/j.petrol.2015.02.010>.

[5] MWABA, M. G. "CIP-DATA LIBRARY TECHNISCHE UNIVERSITEIT EINDHOVEN", .

[6] AWAD, M. M. "Fouling of heat transfer surfaces", *Chemical Engineering & Technology*, 2011. ISSN: 15214125. doi: 10.1002/ceat.270100115.

[7] GUDMUNDSSON, J. S. *Flow assurance solids in oil and gas production*. 2017. ISBN: 9781351733175. doi: 10.1201/9781315185118.

[8] CHUNG, J. S. *Offshore Pipelines.*, v. 107. 1985. ISBN: 075067847X.

[9] ROSTRON, P. "Critical Review of Pipeline Scale Measurement Technologies", v. 1, n. 1, pp. 1–14, 2018. doi: 10.15406/mojmm.2018.01.00004.

[10] LANE, W., CHARPENTIER, T. V. J., NEVILLE, A., et al. "Paper No. 7632", , n. 7632, pp. 1–13, 2016.

[11] GRAHAM, G. M., GOODWIN, N., ALBINO, E., et al. "Minimizing scale deposition through surface enhancement in downhole tools", *Society of Petroleum Engineers - SPE International Conference and Exhibition on Oilfield Scale 2014*, pp. 433–449, 2014. ISSN: 01603663.

[12] NAGI, M., WHITING, D. "Corrosion 2004", , n. 04326, pp. 1–37, 2004.

[13] API. "Flow Assurance Considerations in Subsea Production Systems", , n. January, 2015.

[14] CRABTREE, M., ESLINGER, D., FLETCHER, P., et al. "Fighting Scale — Removal and Prevention", *Oilfield Review*, pp. 30–45, 1999. Disponível em: <http://www.slb.com/{~}/media/Files/resources/oilfield{_}review/ors99/aut99/fighting.pdf>.

[15] MWABA, M. G., GU, J., GOLRIZ, M. R. "Effect of magnetic field on calcium sulfate crystal morphology", *Journal of Crystal Growth*, 2007. ISSN: 00220248. doi: 10.1016/j.jcrysgro.2006.10.256.

[16] EROINI, V., KAPUR, N., NEVILLE, A., et al. "Preventing Scale Formation Using Modified Surfaces", *Proceedings of NACE International Corrosion Conference & Expo 2011*, , n. 11344, pp. 1–15, 2011.

[17] HAMID, S., DE JESÚS, O., JACINTO, C., et al. "A practical method of predicting calcium carbonate scale formation in well completions", *SPE Production and Operations*, v. 31, n. 1, pp. 1–11, 2016. ISSN: 19301855.

[18] YANG, X., LI, W., GUO, L., et al. "Prediction of CaCO3 scaling in water injection wellbore", *Applied Thermal Engineering*, 2016. ISSN: 13594311. doi: 10.1016/j.applthermaleng.2015.12.048.

[19] PAKKONEN, T. M., RIIHIMAAKI, M., SIMONSON, C. J., et al. "Modeling CaCO3 crystallization fouling on a heat exchanger surface - Definition of fouling layer properties and model parameters", *International Journal of Heat and Mass Transfer*, v. 83, pp. 84–98, 2015. ISSN: 00179310. doi: 10.1016/j.ijheatmasstransfer.2014.11.073.

[20] BAI, Y., BAI, Q. "Subsea Engineering Handbook", 2012.

[21] MCCARTNEY, R. A., WATER, O., LIMITED, S., et al. "How accurate are scale prediction models ? An example from a gas condensate well ." , n. March, pp. 23–26, 2014.

[22] KAN, A. T., FU, G., TOMSON, M. B. "Mineral-Scale Control in Subsea Completion", 2014. doi: 10.4043/13236-ms.

[23] ZHAO, Q., LIU, Y., WANG, S. "Surface modification of water treatment equipment for reducing CaSO4 scale formation", *Desalination*, v. 180, n. 1-3, pp. 133–138, 2005. ISSN: 00119164. doi: 10.1016/j.desal.2005.01.002.

[24] CHILINGAR, G. V., MOURHATCH, R., AL-QAHTANI, G. D. "The Fundamentals of Corrosion and Scaling for Petroleum and Environmental Engineers", *America*, p. 296, 2008. doi: 10.1016/B978-1-933762-30-2.50015-X.

[25] OLAJIRE, A. A. "A review of oilfield scale management technology for oil and gas production", *Journal of Petroleum Science and Engineering*, v. 135, pp. 723–737, 2015. ISSN: 09204105. doi: 10.1016/j.petrol.2015.09.011. Disponível em: <http://dx.doi.org/10.1016/j.petrol.2015.09.011>.

[26] BOMBA, J., CHIN, D., KAK, A., et al. "Flow Assurance Engineering in Deepwater Offshore - Past, Present, and Future", 2018. doi: 10.4043/28704-ms.

[27] CHEONG, W. C., NEVILLE, A., GASKELL, P. H., et al. "Using nature to provide solutions to calcareous scale deposition", *Society of Petroleum Engineers - 9th International Conference on Oilfield Scale 2008 - "Managing Scale Through the Field Lifetime"*, pp. 368–378, 2008.

[28] CEYLAN, K., KELBALIYEV, G. "The roughness effects on friction and heat transfer in the fully developed turbulent flow in pipes", *Applied Thermal Engineering*, v. 23, n. 5, pp. 557–570, 2003. ISSN: 13594311. doi: 10.1016/S1359-4311(02)00225-9.

[29] LALOT, S., PÁLSSON, H. "Detection of fouling in a cross-flow heat exchanger using a neural network based technique", *International Journal of Thermal Sciences*, v. 49, n. 4, pp. 675–679, 2010. ISSN: 12900729. doi: 10.1016/j.ijthermalsci.2009.10.011.

[30] ALBERT, F., AUGUSTIN, W., SCHOLL, S. "Roughness and constriction effects on heat transfer in crystallization fouling", *Chemical Engineering Science*, v. 66, n. 3, pp. 499–509, 2011. ISSN: 00092509. doi: 10.1016/j.ces.2010.11.021. Disponível em: <http://dx.doi.org/10.1016/j.ces.2010.11.021>.

[31] DELROT, S., BUSAWON, K., DJEMAI, M., et al. "Fouling detection in heat exchangers", *IFAC Proceedings Volumes (IFAC-PapersOnline)*, v. 18, n. PART 1, pp. 13368–13373, 2011. ISSN: 14746670. doi: 10.3182/20110828-6-IT-1002.00581. Disponível em: <http://dx.doi.org/10.3182/20110828-6-IT-1002.00581>.

[32] YANG, M., YOUNG, A., NIYETKALIYEV, A., et al. "Modelling fouling induction periods", *International Journal of Thermal Sciences*, v. 51, n. 1, pp. 175–183, 2012. ISSN: 12900729. doi: 10.1016/j.ijthermalsci.2011.08.008. Disponível em: <http://dx.doi.org/10.1016/j.ijthermalsci.2011.08.008>.

[33] KUMAR, D., WELCH, J. C., XU, Z. "Reduction in scale build-up from sub-surface safety valve using hydrophobic material coating", *Proceedings - SPE Annual Technical Conference and Exhibition*, v. 3, n. 166218, pp. 1729–1743, 2013.

[34] ANDRITSOS, N., KONTOPOULOU, M., KARABELAS, A., et al. "Calcium Carbonate Deposit Formation under Isothermal Conditions", *Canadian Journal of Chemical Engineering*, v. 74, n. 6, pp. 911–919, 1996. ISSN: 00084034. doi: 10.1002/cjce.5450740614.

[35] KHAN, M. S., ZUBAIR, S. M., BUDAIR, M. O., et al. "Fouling resistance model for prediction of CaCO 3 scaling in AISI 316 tubes", *Heat and Mass Transfer*, v. 32, n. 1-2, pp. 73–79, 1996. ISSN: 0947-7411. doi: 10.1007/s002310050094. Disponível em: <http://link.springer.com/10.1007/s002310050094>.

[36] T.V.J CHARPENTLIER, NEVILLE, A. "Evaluation of Anti-fouling Surfaces for Prevention of Mineral Scaling in Sub-Surface Safety Valves", *SPE International Oilfield Scale Conference*, 2014.

[37] MAVREDAKI, E., NEVILLE, A. "Prediction and Evaluation of Calcium Carbonate Deposition at Surfaces", *Proceeding of SPE European Formation Damage Conference and Exihbition*, , n. 169796, pp. 14–15, 2014. doi: 10.2118/169796-ms.

[38] WANG, L. C., LI, S. F., WANG, L. B., et al. "Relationships between the characteristics of CaCO3 fouling and the flow velocity in smooth tube", *Experimental Thermal and Fluid Science*, v. 74, pp. 143–159, 2016. ISSN: 08941777. doi: 10.1016/j.expthermflusci.2015.12.001. Disponível em: <http://dx.doi.org/10.1016/j.expthermflusci.2015.12.001>.

[39] VAZIRIAN, M. M., CHARPENTIER, T. T. J., NEVILLE, A., et al. "Assessing Surface Engineering Solutions for Oilfield Scale; Correlating Laboratory Tests to Field Trials", *SPE International Oilfield Scale Conference and Exhibition*, pp. 1–14, 2016. doi: 10.2118/179862-MS. Disponível em: <https://www.onepetro.org/conference-paper/SPE-179862-MS>.

[40] PAZ, P. A., CAPRACE, J. D., CAJAIBA, J. F., et al. "Prediction of calcium carbonate scaling in pipes using artificial neural networks", *Proceedings of the International Conference on Offshore Mechanics and Arctic Engineering - OMAE*, v. 5A-2017, 2017. doi: 10.1115/OMAE2017-61233.

[41] EPSTEIN, N. "Fouling of Heat Exchangers." *Heat Exch Sourceb*, v. 13, n. 7, pp. 677–697, 1986.

[42] KERN, D. Q., SEATON, R. E. "A theoretical analysis of thermal surface fouling.pdf', *British Chemical Engineering*, v. 4, n. 5, pp. 258–262, 1959.

[43] CRITTENDEN, D. B., KOLACZKOWSKI, S. T., HOUT, S. A. "Modelling Hydrocarbon Fouling." *Chemical Engineering Research and Design*, v. 65, n. 2, pp. 171–179, 1987. ISSN: 02638762.

[44] EPSTEIN, N. "Particulate Fouling of Heat Transfer Surfaces: Mechanisms and Models", *Fouling Science and Technology*, v. 145, pp. 143–164, 1988. doi: 10.1007/978-94-009-2813-8_10.

[45] TAKEMOTO, T., CRITTENDEN, B. D., KOLACZKOWSKI, S. T. "Interpretation of fouling data in industrial shell and tube heat exchangers", *Chemical Engineering Research and Design*, v. 77, n. 8, pp. 769–778, 1999. ISSN: 02638762. doi: 10.1205/026387699526764.

[46] EBERT, W., PANCHAL, C. "Analysis of Exxon crude-oil-slip stream coking data", *Fouling mitigation of industrial heat exchangers*, pp. 18–23, 1995. doi: https://www.osti.gov/servlets/purl/453433. Disponível em: <https://www.osti.gov/biblio/453433>.

[47] SCARBOROUGH, C.E. CHERRINGTON, R. D., L.P.GOLAN. "Coking of crude oil at high heat flux levels", *Journal of Chemical Engineering Progress*, v. 75, pp. 41–47, 1979.

[48] POLLEY, G. T., WILSON, D. I., YEAP, B. L., et al. "Evaluation of laboratory crude oil threshold fouling data for application to refinery pre-heat trains", *Applied Thermal Engineering*, v. 22, n. 7, pp. 777–788, 2002. ISSN: 13594311. doi: 10.1016/S1359-4311(02)00023-6.

[49] KNUDSEN, J.G., LIN, D., EBERT, W. "The Determination of Threshold Curve for Crude Oil: Understanding Heat Exchanger Fouling and its Mitigation", *Proceedings of Fouling of Heat Exchangers Begell House, New York*, pp. 265–272, 1999.

[50] PATERSON, W. R., FRYER, P. J. "A reaction engineering approach to the analysis of fouling", *Chemical Engineering Science*, v. 43, n. 7, pp. 1714–1717, 1988. ISSN: 00092509. doi: 10.1016/0009-2509(88)85166-2.

[51] SALEH, Z., SHEIKHOLESSLAMI, R., WATIKNSON, A. "Heat Exchanger Fouling by a light Australian crude oil", *Proceedings in Heat Exchanger Fouling and Cleaning fundamentals and Aplications, Santa Fe*, 2003.

[52] AL-HADHRAMI, L. M., AHMAD, A., AL-QAHTANI, A. "Experimental Study of Fouling Resistance in Twisted Tube Heat Exchanger", v. 33, n. 12, pp. 1024–1032, 2012. doi: 10.1080/01457632.2012.659620.

[53] FOROUTAN, S., MOGHADASI, J. "A Neural Network Approach to Predict Formation Damage Due to Calcium Sulphate Precipitation", *Proceeding of SPE European Formation Damage Conference and Exihbition*, 2013.

[54] HARCHE, R., ABSI, R., MOUHEB, A. "Study of the fouling deposit in the heat exchangers of Algiers refinery", *International Journal of Industrial Chemistry*, v. 5, n. 2, pp. 16, 2014. ISSN: 2228-5970. doi: 10.1007/s40090-014-0016-6. Disponível em: <http://link.springer.com/10.1007/s40090-014-0016-6>.

[55] PÄÄKKÖNEN, T. M., RIIHIMÄKI, M., SIMONSON, C. J., et al. "Crystallization fouling of CaCO3 - Analysis of experimental thermal resistance and its uncertainty", *International Journal of Heat and Mass Transfer*, v. 55, n. 23-24, pp. 6927–6937, 2012. ISSN: 00179310. doi: 10.1016/j.ijheatmasstransfer.2012.07.006.

[56] AWAD, M. M. "Impact of Flow velocity on Surface Particulate Fouling - Theoretical Approach", *Journal of American Science*, v. 8, n. 9, 2012.

[57] MACIEL, R. S., COSMO, R. P., MACIEL, F. S., et al. "On the Hydrodynamic Aspects of the Carbonate Scale Formation Process in High Flow Rate Wells", , n. 2012, pp. 1–15, 2017. doi: 10.4043/28106-ms.

[58] KEOGH, W., NEVILLE, A., HUGGAN, M., et al. "Deposition of Inorganic Carbonate, Sulfate, and Sulfide Scales on Antifouling Surfaces in Multiphase Flow", *Energy and Fuels*, v. 31, n. 11, pp. 11838–11851, 2017. ISSN: 15205029. doi: 10.1021/acs.energyfuels.7b02165.

[59] RAHARJO, S., BAYUSENO, A., JAMARI, et al. "Calcium carbonate scale formation in copper pipes on laminar flow", *MATEC Web of Conferences*, v. 58, pp. 01029, 2016. ISSN: 2261236X. doi: 10.1051/matecconf/20165801029. Disponível em: <http://www.matec-conferences.org/10.1051/matecconf/20165801029>.

[60] JAFARI NASR, M. R., MAJIDI GIVI, M. "Modeling of crude oil fouling in preheat exchangers of refinery distillation units", *Applied Thermal Engineering*, v. 26, n. 14-15, pp. 1572–1577, 2006. ISSN: 13594311. doi: 10.1016/j.applthermaleng.2005.12.001.

[61] FALLIS, A. "Determinação Da Taxa De Incrustação Em Trocadores De Calor Com O Auxílio De Métodos De Otimização", *Journal of Chemical Information and Modeling*, v. 53, n. 9, pp. 1689–1699, 2013. ISSN: 1098-6596. doi: 10.1017/CBO9781107415324.004.

[62] GARCÍA, M., VEGA, J., PINEDA, Y., et al. "Development of an experimental methodology for assessing the growth of scale (CaCO ₃) in pipelines", *Journal of Physics: Conference Series*, v. 687, pp. 012002, 2016. ISSN: 1742-6588. doi: 10.1088/1742-6596/687/1/012002. Disponível em: <http://stacks.iop.org/1742-6596/687/i=1/a=012002?key=crossref.7c2f40a43a59670d4064f748a4d17496>.

[63] GIACCHETTA, G., MARCHETTI, B., LEPORINI, M., et al. "Pipeline wax deposition modeling: A sensitivity study on two commercial software", *Petroleum*, 2017. ISSN: 24056561. doi: 10.1016/j.petlm.2017.12.007. Disponível em: <http://linkinghub.elsevier.com/retrieve/pii/S2405656117301517>.

[64] AZIZI, N., HOMAYOON, R., HOJJATI, M. R. "Predicting the colebrook-white friction factor in the pipe flow by new explicit correlations", *Journal of Fluids Engineering, Transactions of the ASME*, v. 141, n. 5, pp. 051201, 2019. ISSN: 1528901X. doi: 10.1115/1.4041232.

[65] SETTA, F. A., NEVILLE, A. "Efficiency assessment of inhibitors on CaCO3 precipitation kinetics in the bulk and deposition on a stainless steel surface (316L)", *Desalination*, v. 281, n. 1, pp. 340–347, 2011. ISSN: 00119164. doi: 10.1016/j.desal.2011.08.021.

[66] SANNI, O., BUKUAGHANGIN, O., HUGGAN, M., et al. "Development of a novel once-Through flow visualization technique for kinetic study of bulk and surface scaling", *Review of Scientific Instruments*, v. 88, n. 10,

2017. ISSN: 10897623. doi: 10.1063/1.4991729. Disponível em: <http://dx.doi.org/10.1063/1.4991729>.

[67] MACIEL, R. S., COSMO, R. P., MACIEL, F. S., et al. "Study of asphaltene deposition in wellbores during turbulent flow", *Journal of Petroleum Science and Engineering*, v. 129, n. 1, pp. 1–14, 2016. ISSN: 09204105. doi: 10.1016/j.petrol.2015.02.010. Disponível em: <https://doi.org/10.1016/j.petrol.2018.01.071http://dx.doi.org/10.1016/j.petrol.2015.02.010http://dx.doi.org/10.1016/j.petrol.2015.11.005http://dx.doi.org/10.1063/1.4991729http://dx.doi.org/10.1007/978-981-13-3119-0{_}63http://www.ncbi.nlm.nih.gov/pubme>.

[68] ESCOBEDO, J., MANSOORI, G. A. "Prefouling behavior of suspended particles in petroleum fluid flow", *Scientia Iranica*, v. 17, n. 1 C, pp. 77–85, 2010. ISSN: 10263098. Disponível em: <https://search.proquest.com/openview/15b255891a32ff8df84f90dac803056c/1?pq-origsite=gscholar{&}cbl=54702{%}0Ahttp://www.sid.ir/en/VEWSSID/J{_}pdf/95520101C05.pdf>.

[69] PÄÄKKÖNEN, T. M., RIIHIMÄKI, M., SIMONSON, C. J., et al. "Crystallization fouling of CaCO3 - Analysis of experimental thermal resistance and its uncertainty", *International Journal of Heat and Mass Transfer*, v. 55, n. 23-24, pp. 6927–6937, 2012. ISSN: 00179310. doi: 10.1016/j.ijheatmasstransfer.2012.07.006.

[70] VAZIRIAN, M. M., CHARPENTIER, T. T. J., NEVILLE, A., et al. "Assessing Surface Engineering Solutions for Oilfield Scale; Correlating Laboratory Tests to Field Trials", *SPE International Oilfield Scale Conference and Exhibition*, pp. 1–14, 2016. doi: 10.2118/179862-MS. Disponível em: <https://www.onepetro.org/conference-paper/SPE-179862-MS>.

[71] HOSSAIN, A., NASER, J., IMTEAZ, M. A. "CFD Investigation of Particle Deposition in a Horizontal Looped Turbulent Pipe Flow", *Environmental Modeling and Assessment*, v. 16, n. 4, pp. 359–367, 2011. ISSN: 14202026. doi: 10.1007/s10666-011-9252-8.

[72] MARCHIOLI, C., PICCIOTTO, M., SOLDATI, A. "Influence of gravity and lift on particle velocity statistics and transfer rates in turbulent vertical channel flow", *International Journal of Multiphase Flow*, v. 33, n. 3, pp. 227–251, 2007. ISSN: 03019322. doi: 10.1016/j.ijmultiphaseflow.2006.09.005.

[73] WATKINSON, A. "Process Heat Transfer: Some Practical Problems", *J. Chem. Eng.*, v. 58, pp. 553–559, 1980.

[74] JACOBS, T. "The New Pathways of Multiphase Flow Modeling", *Journal of Petroleum Technology*, v. 67, n. 02, pp. 62–68, 2015. ISSN: 0149-2136. doi: 10.2118/0215-0062-jpt.

[75] ELFIL, H., ROQUESB, H. "Elfil 2001.pdf", v. 137, pp. 177–186, 2001.

[76] JAMIALAHMADI, M., SOLTANI, B., MÜLLER-STEINHAGEN, H., et al. "Measurement and prediction of the rate of deposition of flocculated asphaltene particles from oil", *International Journal of Heat and Mass Transfer*, v. 52, n. 19-20, pp. 4624–4634, 2009. ISSN: 00179310. doi: 10.1016/j.ijheatmasstransfer.2009.01.049. Disponível em: <http://dx.doi.org/10.1016/j.ijheatmasstransfer.2009.01.049>.

[77] YANG, J., SERRATOS, M. G. J., FARI-AROLE, D. S., et al. "Crude Oil Fouling: Fluid Dynamics, Reactions and Phase Change", *Procedia IUTAM*, v. 15, pp. 186–193, 2015. ISSN: 22109838. doi: 10.1016/j.piutam.2015.04.026. Disponível em: <http://www.sciencedirect.com/science/article/pii/S2210983815001376>.

[78] QUAN, Z., CHEN, Y., MA, C. "Experimental Study of Fouling on Heat Transfer Surface During Forced Convective Heat Transfer", *Chinese Journal of Chemical Engineering*, v. 16, n. 4, pp. 535–540, 2008. ISSN: 10049541. doi: 10.1016/S1004-9541(08)60117-2.

[79] BUSENBERG, L. N. P., EURYBIADES. "The solubilities of calcite, aragonite and vaterite in CO2-H2O solutions between 0 and 90C, and an evaluation of the aqueous model for the system CaCO3-CO2-H2O", *Geochimica et Cosmochimica Acta*, v. 46, pp. 1011–1040, 1982. doi: 10.1016/0016-7037(82)90056-4.

[80] BRAHIM, F., AUGUSTIN, W., BOHNET, M. "Numerical Simulation of the Fouling on Structured Heat Transfer Surfaces (Fouling)", *ECI Conf. on Heat Exchanger Fouling and Cleaning: Fundamentals and Applications*, v. RP1, pp. 121–129, 2003.

[81] FRIEDLANDER, S. K., JOHNSTONE, H. F. "Deposition of Suspended Particles from Turbulent Gas Streams", *Industrial & Engineering Chemistry*, v. 49, n. 7, pp. 1151–1156, 1957. ISSN: 0019-7866. doi: 10.1021/ie50571a039.

[82] ABRAHAM, J. P., SPARROW, E. M., GORMAN, J. M., et al. "Application of an intermittency model for laminar, transitional, and turbulent internal flows", *Journal of Fluids Engineering, Transactions of the ASME*, v. 141, n. 7, pp. 071204, 2019. ISSN: 1528901X. doi: 10.1115/1.4042664.

[83] KOR, P., KHARRAT, R. "Modeling of asphaltene particle deposition from turbulent oil flow in tubing: Model validation and a parametric study", *Petroleum*, v. 2, n. 4, pp. 393–398, 2016. ISSN: 24055816. doi: 10.1016/j.petlm.2016.08.010. Disponível em: <http://dx.doi.org/10.1016/j.petlm.2016.08.010>.

[84] DULCE, R. G., BALTAZAR, A. D., BAYON, F. E. B. "An Evaluation on the Applicability of Infrared Thermography in Identifying Silica Deposition in Geothermal Brine Lines", *World Geothermal Congress 2015*, , n. April, pp. 7, 2015.

[85] DA SILVA, J., LIMA, A., NEFF, F., et al. "Hammer impact test applied for fouling detection in pipelines", *Controle y Automacao*, v. 22, n. 6, pp. 620–630, 2011. ISSN: 01031759. doi: S01031759201100060007.

[86] SILVA, L. L. "Omae2014-23488 Acoustic Reflectometry for Blockage Detection in Pipeline", pp. 6–8, 2014. doi: 10.1115/OMAE2014-23488.

[87] KAKAC, S. *HEAT Exchangers: Selection,Rating and Thermal Design*. 2012. ISBN: 9781439849910.

[88] CHENG, L. *Frontiers and Progress in Multiphase Flow Frontiers and Progress in Multiphase Flow I*. ISBN: 9783319043579.

[89] GUDMUNDSSON, O., LALOT, S., THORSEN, J. "Comparison of Fouling Detection Methods", *Proceedings of International Conference on Heat Exchanger Fouling and Cleaning*, pp. 429–436, 2013.

[90] GUDMUNDSSON, O., LALOT, S., THORSEN, J. "Comparison of Fouling Detection Methods", *Proceedings of International Conference on Heat Exchanger Fouling and Cleaning*, pp. 429–436, 2013.

[91] KHALID, N. I., CHAN, K. W., AB AZIZ, N., et al. "Concentric tube-fouling rig for investigation of fouling deposit formation from pasteuriser of viscous food liquid", *Journal of Engineering Science and Technology*, v. 8, n. 1, pp. 16–26, 2013. ISSN: 18234690.

[92] ISHKOV, O., MACKAY, E., JORDAN, M., et al. "Magnesium depletion and impact on produced brine compositions in a waterflooded reservoir", *Proceedings - SPE International Symposium on Oilfield Chemistry*, v. 2019, 2019. ISSN: 10461779.

[93] VAZQUEZ, O., MCCARTNEY, R., WATER, O., et al. "SPE 164113 Produced Water Chemistry History Matching Using a 1D Reactive Injector Producer Reservoir Model", pp. 1–10, 2013.

[94] SAIFI, A., HALLOULA, H., ELAMIRI, A., et al. "Infrared thermography for detecting the deposit nature in steel water pipes", 2016. doi: 10.21611/qirt.2016.111.

[95] ENDO, H., KUSAKA, T. "Efficient inspection of gas pipes by infrared thermography", *R and D: Research and Development Kobe Steel Engineering Reports*, v. 64, n. 2, pp. 13–17, 2014. ISSN: 03738868.

[96] HAFEMANN, T. E., FEDERAL, U., CATARINA, D. S., et al. "Modeling of Fluid Flow and Heat Transfer in a Pre-Salt Oil Production Well", pp. 13–16, 2014.

[97] SANNI, O. S., BUKUAGHANGIN, O., CHARPENTIER, T. V., et al. "Evaluation of laboratory techniques for assessing scale inhibition efficiency", *Journal of Petroleum Science and Engineering*, p. 106347, 2019. ISSN: 09204105. doi: 10.1016/j.petrol.2019.106347. Disponível em: <https://linkinghub.elsevier.com/retrieve/pii/S0920410519307685>.

[98] MWABA, M. G., RINDT, C. C. M., VAN STEENHOVEN, A. A., et al. "Experimental Investigation of CaSO ₄ Crystallization on a Flat Plate", *Heat Transfer Engineering*, 2006. ISSN: 0145-7632. doi: 10.1080/01457630500458187.

[99] LI, G., GUO, S., ZHANG, J., et al. "Inhibition of scale buildup during produced-water reuse: Optimization of inhibitors and application in the field", *Desalination*, v. 351, pp. 213–219, 2014. ISSN: 00119164. doi: 10.1016/j.desal.2014.08.003. Disponível em: <http://dx.doi.org/10.1016/j.desal.2014.08.003>.

[100] JORDAN, M. M., FEASEY, N. D., JOHNSTON, C. J. "Inorganic scale control within MEG/methanol-treated produced fluids", *SPE Seventh International Symposium on Oilfield Scale 2005: Pushing the Boundaries of Scale Control, Proceedings*, pp. 93–105, 2005.

[101] BARAKA-LOKMANE, S., HURTEVENT, C., OHANESSIAN, J. L., et al. "Prediction of mineral scaling in a MEG loop system of a gas production offshore", *Society of Petroleum Engineers - SPE International Conference and Exhibition on Oilfield Scale 2012*, , n. November 2016, pp. 395–406, 2012. doi: 10.2118/155124-MS.

[102] KIM, H., YOO, W., LIM, Y., et al. "Economic evaluation of MEG injection and regeneration process for oil FPSO", *Journal of Petroleum Science and Engineering*, v. 164, n. September 2017, pp. 417–426, 2018. ISSN: 09204105. doi: 10.1016/j.petrol.2018.01.071. Disponível em: <https://doi.org/10.1016/j.petrol.2018.01.071>.

[103] TOUGRI, I., COLAÇO, M. J., BOZZOLI, F., et al. "Internal heat transfer coefficient estimation in three-dimensional ducts through the reciprocity functional approach – An analytical approach and validation with experimental data", *International Journal of Heat and Mass Transfer*, v. 122, pp. 587–601, 2018. ISSN: 00179310. doi: 10.1016/j.ijheatmasstransfer.2018.01.102. Disponível em: <https://doi.org/10.1016/j.ijheatmasstransfer.2018.01.102>.

Yang model code

```
%MODELO YANG
 %clc;    % Clear the command window.
% close all;  % Close all figures (except those of imtool.)
 clear;  % Erase all existing variables. Or clearvars if you want.


%-------------------------------------------------Constantes
Kb=1.38*(10^-23);%Constante de boltzman J/Kelvin
E=37143;%Energia activacion, J/mol
Kro=7.07;%Constante de la reaccion
kcaco =22;%W/m°K--->Conductividade térmica aço inox 316
CpAco=502;%Calor específico J/Kg°K
AcHo=-13.1;%-1206.9;%Entalpía de la solución
R=8.314472;%Constante de los gases J/mol*K
dp=0.0000173205;%0.000036;%%diametro partícula
roCaCO3=2710;%Densidade CaCO3 kg/m^3 Pakkonnen
delta=10^-6;%Coeficiente de expansion lineal K^-1 10.1 ~ 17.3
g=9.81;%Aceleracion de gravedad
a=0.035;%K/m gradiente geothermico
KCaCO3=0.97;%5.09;%Conductividade termica CaCO3 W/m*K
eD=2.2603*(10^-6);%input('Ripple height Rugosidad ducto en micrometros')
%E=147700;%J/mol
DeltaP=4218; %kgf/m^2
%rof=105;%Segun Pakkonen

%-----------------------------------------Variables de entrada---------
%-----------------------------------------Variables de entrada---------

    %=======Modelo 13
%     Tbulk=273+60.56;
%     Twall=(71.6+273);%input('Temperatura pared externa durante test en
Kelvin');
%     Cp=1.665;
%     CF=1.892;
%     h=4;%input('hours??');
%     Caudal=2.5;%input('Caudal')
    %Modelo 14
%     Tbulk=273+60.3;
%     Twall=(73.7+273);%input('Temperatura pared externa durante test en
Kelvin');
%     Cp=2.337;
%     CF=1.615;
    h=input('hours??');
    Tbulk=273+60.56;
    Twall=(71.6+273);%input('Temperatura pared externa durante test en
Kelvin');
    Sb=106.4;%106.4
    CF=2.3506;
    Caudal=input('Caudal');
%     %Modelo 16
%     Tbulk=273+57.4;
%     Twall=(66+273);%input('Temperatura pared externa durante test en
Kelvin');
%     Cp=2.407;
%     CF=2.407;
%     h=4;%input('hours??');
```

Figure 1: Yang model.

```
%     Caudal=2.5;%input('Caudal')


Tambiente=273+25.16;%Temp ambiente
%38.5;%370;%7.5;%input('Caudal estimado del loop
lts/min');%16.6;%370;%input('Caudal estimado del loop lts/min');
Diametro=0.0273;%input('Diametro');%0.1778;%0.14;%0.0273;%0.1778;%0.0273;
%input('Diametro interno loop en metros');
%input('Concentracion de la solución en kgs')
e=2.2603*(10^-6);%input('Ripple height Rugosidad ducto en micrometros')
%==================CaCl+NaHCO3=======Calc inicial
VolCaCl=120;%lts
CCaCl=1870;%grs CaCl
VolNaHCO3=50;%lts
CNaHCO3=800;%grs NaHCO3
pmCa=40.078;%gr/mol
pmCl=35.453;%gr/mol
pmNa=22.9897;
pmH=1;
pmCO3=60.0077;
pmCaCl=pmCl+pmCa;
%Calc ions Ca
PCaCl=CCaCl./pmCaCl;%CaCl em mol
PVCaCl=PCaCl./VolCaCl;%mol/lt
Ca=pmCa.*PVCaCl;%ions de Ca em Vol
%Cal ions Co3
pmNaHCO3=pmNa+pmCO3+pmH;
PNaHCO3=CNaHCO3./pmNaHCO3;
PVNaHCO3=PNaHCO3./VolNaHCO3;
CO3=PVNaHCO3.*pmCO3;
%-----------------------------------------Valores constantes durante

Xf=Diametro/2;
Xfo=0;
myang=0;
loop=0;
mo=0;
XfEP=0;%espessura Ebert e Panchal em t=0
ddf=0;
Rfd=0;
Rfk=0;
Xfk=0;
dmp=0;
dmc=0;
dmr=0;
Rf=0;
rf=0;
dm=0;
rof=1100;%Mean density of scaling layer stated by Pakkonen
ts=0:(3600*h);%902700, tiempo duración experimento en segundos 1584000
for t=ts

    do=Diametro-(2*Xfo);%Yang
    ed=(2.2603e-6)/do;
    ri=do./2;%Yang
    At=pi*(ri.^2);%
```

```
    Ai=2*pi*ri.*0.27;
    %Tbulk=(TEnt+TSal)/2;%Temperatura interna fluido loop
    %------------------------Calculo velocidad del fluido
    %Caudal en m^3/seg
    Qml=(Caudal)./1000;
    Qm=Qml./60;
    %----------------Velocidad del fluido interno en m/s
    Vel=Qm./At;%Yang

    %------------------------Calculo propiedades de densidad y viscosidad
    roh2o=((39*(380-Tbulk)/80)+1000);%Interpolando densidad
agua(corregido para Tb 20 hasta 90 agua
    kh2o=(1.1853*(Tbulk-273)+571.98)/1000;%(0.09*(Tbulk-
293)/80)+0.6804;%Interpolando Coef transf calor H2O agua
    Cph2o=(0.005*(Tbulk-273)/363)+4216;%Interpolando Calor específico
J/kg°K agua
    %Nu=0.0016*exp(-0.021*(Tbulk-273));%(0.0168*roh2o.*(Tbulk.^-
0.88))/1000;%Viscocidad dinamica
```

Figure 3: Yang model.

```
h45=(kh2o.*NuN)./do;%Coeficiente transf calor H2O + Sales
Tf=Twall-q.*(1.4e-4);

%Calculo Cs
ACs=AcHo./(2*3*R*Tf);
DeltaCp1=-3688200*(Tbulk.^(-3));
DeltaCp2=-184.79+(0.32322*Tbulk);
DeltaCp3=(-1.2974*(10^(-4)))*(Tbulk.^2);
DeltaCp4=3883.5*(Tbulk.^(-0.5));
DeltaCp=DeltaCp1+DeltaCp2+DeltaCp3+DeltaCp4;
Cs1=-AcHo./(2.3*R.*Tf);
Cs2=DeltaCp./R;
Cs3=log(Tf);
Cs4=Cs2*Cs3;
Cs5=Cs1+Cs4;
lammers=-84;
Cs6=lammers+Cs5;
Cs=e^Cs6;

DeltaC=CF-Cs;
%Diffusion coefficient
Dcoef=(Kb.*Tbulk)./(3*pi*knuw.*dp);%Stokes einstein equation
Sc=knuw./(Dcoef);%Schmidt number
%-------Número de Sherwood
Sh1=0.034*(Re.^(0.875));
Sh2=Sc.^0.333;
Sh=Sh1.*Sh2;%Numero de Sherwood
Beta=(Sh.*Dcoef)./do;
%Calculo Kr
Kr1=(R.*Tf);
Kr2=-E./Kr1;
Kr=Kro.*(exp(Kr2));
%------------CALCULO dmc/dt(deposition mass rate of crystalization)
dmc1=0.25*((Beta./Kr).^2);
dmc2=(Beta./Kr).*DeltaC;
dmc3=sqrt(dmc1+dmc2);
dmc5=(0.5*(Beta./Kr))+DeltaC;
dmc=(Beta.*(dmc5-dmc3));
%-----------Calculo dmp/dt
 %----------Calculo tiempo relaxation (tp)
```

Figure 4: Yang model.

```
    %============Stopping distance
    Sp=(Vp.*roCaCO3.*(dp.^2))./(Nu.*18);
    %============Stopping distance adimensional
    Spa=(Sp.*Vel.*(sqrt(f./2)))./Nu;
    %===========Calculo velocidad partícula
    Vp=0.9*Vel.*sqrt(f./2);%Particle velocity(Evaluation and comparison
of different models for asphaltene particle deposition in flow streams)


    %---------- tiempo relaxation (tp)
    tp=Sp./Vp;
    %----------Tiempo relajacion adimensional
    tpa=tp.*((f./2)*(Vel.^2)./knuw);

    %particle deposoition rate Vd m/s
    if tpa<0.02
                Vd=uf.*(0.07*(Sc.^(-2/3)));
    elseif (0.02<tpa)&& (tpa<=20)
                Vda=(uf.*(3.5*exp-4));
                Vd=Vda.*(tpa.^2);

    else
                Vd=0.18*uf;
    end
    %=======Calculo Sb usando Elfil
    kspb1C=-171.9-0.077993*Tbulk;
    kspb2C=2839./Tbulk;
    kspb3C=71.595*log(Tbulk);
    kspb4C=kspb1C+kspb2C+kspb3C;
    kspbC=log(kspb4C);
    %Aragonite proportion
    kspb1A=-171.9773-(0.077993*Tbulk);
    kspb2A=2903.973./Tbulk;
    kspb3A=71.595*log(Tbulk);
    kspb4A=kspb1A+kspb2A+kspb3A;
    kspbA=log(kspb4A);
    %Varetite proportion
    kspb1V=-172.1295-(0.077993*Tbulk);
    kspb2V=3074./Tbulk;
    kspb3V=71.595*log(Tbulk);
    kspb4V=kspb1V+kspb2V+kspb3V;
    kspbV=log(kspb4V);

    KspCalcite1=-1228.732 - (0.299444*Tbulk);
    KspCalcite2=(35512.75./Tbulk)+485.818*log(Tbulk);
```

Figure 5: Yang model.

```
Cp=-16.647+(1.667*Sb);%
dmp=(Vd.*Cp);%Taxa de deposição
%----------------DETERMINAÇÃO TAÇA DE REMOÇÃO dmr/dt

PsusK=83.2*(Vel.^(0.54));
KP=1./PsusK;
DeltaT=Rf.*q;
%=============Using Quan
Cr1=(0.00212*Vel.^(1.5));
Cr2=(KP.*sqrt(KCaCO3));
Cr=Cr1./Cr2;
dmr=Cr.*rof.*(Xfo.^1.5);

%---------Taxa incrustação
dm=(dmc+dmp)-dmr;

%---------masa segun Yang
myang=(2*dm.*pi*0.27*0.01365)+myang;

Xfo=Xfo+(dm./rof);
rof=myang./(Diametro.*Xfo.*pi*0.27);



%==================================================
loop=loop+1;



Xy(loop)=Xfo;%Modelo Yang
dmr1(loop)=dmr;
dmp1(loop)=dmp;
dmc1(loop)=dmc;
dmd(loop)=dmc+dmp;
dm1(loop)=dm;
massdep(loop)=myang;%    Modelo Yang
velocity(loop)=Vel;
Reynolds(loop)=Re;
vdep(loop)=Vd;
Friction(loop)=f;
Rfouling(loop)=Rf;
Schmidt(loop)=Sc;
rough(loop)=ed;
Rfouling(loop)=Rf;
 Peclet(loop)=Pecl;
tr(loop)=tpa;
Tfouling(loop)=Tf;
heatflux(loop)=q;
%sys=ss(dmc,dmp,dmr,Vely);%plot(Xv,'g','linewidth',3)
```


Figure 6: Yang model.

```
    massmodel=massdep(1:3600:end);
format long
    disp(max(massmodel));
    mass_exp=[0 0.004556 0.057354 0.00788 0.01388 0.01614];
 hold on
 plot(massdep,'b')
 % %plot(t,massmodel,'r');
% plot(t,massmodel,'b',t,mass_exp,'-rs')
% err=[0 0.000234 0.000273 0.000467 0.000934];
% %      hold on
% % %plot(t, massmodel,'r');
% %      plot(t, massmodel,'b',t,mass_exp,'-rs')%t,mass_exp,'-rs',
% %      grid
% %errorbar(t,massmodel)
% %
```

Figure 7: Yang model.